1994

Ionic Conductivity Of Rubidium Chloride

Marcia Lee Vernon

Ionic Conductivity of Rubidium Chloride

by
Marcia Lee Vernon

Department of Chemistry

Submitted in partial fulfilment
of the requirements for the degree of
Doctor of Philosophy

Faculty of Graduate Studies
The University of Western Ontario
London, Ontario
March 1994

ISBN 0-315-90548-4

Abstract

This investigation describes a theoretical and experimental examination of the defect properties of rubidium chloride. A theoretical study of the defect properties of RbBr and RbI is also presented.

Defect energy calculations were carried out on RbCl, RbBr and RbI using the HADES code and electron-gas potentials that were fitted to the crystal properties. Damping of the long-range dispersion energy was introduced during fitting of the potential and in the calculation of perfect lattice and defect properties.

In addition, defect energy calculations were done on Rb_2S using potentials developed for the $RbCl:S^{2-}$ system. These calculations represent the first theoretical study of the defect energies of Rb_2S.

Ionic conductivity measurements were made on pure, strontium-doped and sulphide-doped rubidium chloride using a new automated system. The data were analysed by means of a nonlinear least squares fitting routine. The analysis of the data suggested that both Schottky and anion Frenkel defects play a role in matter transport in RbCl. Cation interstitials were also found to be present in a small concentration. Vacancy pairs were found to contribute to diffusion, as had been indicated previously in diffusion studies of RbCl[1,2].

The calculated defect energies and the experimental enthalpies were in good agreement, suggesting the

reliability of both the data analysis and the calculation methods used.

Acknowledgements

I would like to thank Dr. P.W.M. Jacobs for his advice and support with this project.

I would also like to thank my husband, Tim Pope, for his help with the experimental work and for his constant support and encouragement.

Graduate life would not have been the same without the friendship of Vince Quiquero, Jabeen Ebrahim, and Harriet, Darrin, Katie and Sarah Rykse.

Table of Contents

List of Tables

Table

List of Figures

Figure

Chapter 1

Introduction

Matter transport in solids can occur through various processes, for example, ionic conductivity and diffusion. The study of these processes in crystalline solids requires an understanding of 'point' defects and their associated 'defect energies'. The term point defects refers to the vacant lattice sites, 'vacancies', and atoms occupying interstitial positions in the lattice, 'interstitials'. The term defect energies is a collective one, referring to the energies required to form these point defects or associated with their migration through the crystal. The energy of formation is the primary factor in determining the concentrations in which the defects are present at thermal equilibrium. The rates of defect migration through the crystal lattice are dependent on the activation energies needed for the ions to jump between lattice sites. Transport properties generally depend on the products of concentration and mobility of the different defects.

Two of the simplest examples of point defects are Frenkel and Schottky defects, both of which are present naturally in the crystal. Frenkel proposed that ions can receive enough energy from thermal vibrations to leave their lattice sites and are effectively pushed into the interstices of the lattice. Further thermal excitation causes the ion to jump between interstitial sites until a

vacant site is met and the ion drops back into a normal lattice position[3]. Schottky defects refer to vacancies that occur in stoichiometric proportions on both the cation and anion sub-lattices. Both defect types satisfy the condition of electroneutrality because the vacancy site carries an effective charge opposite to that of an occupied lattice site. A diagram of Schottky and Frenkel defects in the rock-salt structure of the rubidium halides is shown in Figure 1-1.

The primary motivation of this study was to provide a more complete picture of the ionic conductivity of the alkali halide group than existed previously. That is, the study of the alkali halides has focussed previously on the sodium and potassium halides but has not extended down the periodic table to rubidium.

Defects in the alkali halides have traditionally been assumed to be of the Schottky type, which has been found to be true in NaCl[4]. But work done on KCl[5], for example, has pointed to the presence of a small concentration of Frenkel defects on both sub-lattices. One would expect that Frenkel defects should exist in even greater concentrations in rubidium halides due to size considerations. That is, as the difference between the cation and anion radii decreases, the barriers to interstitial formation and migration should decrease relative to those of the vacancies. The rubidium halides, RbCl, RbBr, and RbI, should then provide an interesting counterpoint to the traditional Schottky model.

This study of the rubidium halides began with the calculation of their defect energies. Theoretical energies, when applied to new or imperfectly analyzed systems, can be useful in guiding interpretations of transport properties[6]. It should be kept in mind, however, that the defect energies, $u^v(0\ K)$, are calculated at constant volume in the harmonic approximation using the 0 K lattice parameter, and are thus independent of temperature. Conversely, the defect parameters determined from experiment are enthalpy changes at constant pressure and varying temperature, $h^p(T)$. The two quantities are related via the equation,

$$f^v = g^p \qquad (1\text{-}1)$$

where, for any defect process, f^v is the Helmholtz energy change at constant volume and g^p is the Gibbs energy change at constant pressure. This equation is valid to first order in the pressure change accompanying the defect process[7]. Thus, substitution of thermodynamic relations gives,

$$u^v - Ts^v = h^p - Ts^p \qquad (1\text{-}2)$$

where, for any defect process, u^v, s^v are the corresponding energy and entropy changes at constant volume, and h^p, s^p are the corresponding enthalpy and entropy changes at constant pressure.

The calculation of h^p from u^v then requires the

calculation of s^v. The information necessary to calculate s^v was not available and so a direct comparison of the calculated u^v and experimental h^p had to be made. The cancellation of some terms in $[h^p(T)-u^v(0\ K)]$, nevertheless, makes this comparison a useful one[7], and thus, the calculation of the defect energies could be used to direct the interpretation of the results of the second part of the study, the ionic conductivity.

The ionic conductivity of RbCl was studied using pure, cation-doped and anion-doped crystals. The idea behind the study of selectively doped crystals is that the conductivity of a particular defect type can be enhanced by the addition of aliovalent impurities. For example, the addition of a small amount of divalent cation impurity would also introduce an equal number of cation vacancies in order to conserve charge balance. That is, the virtual charge of -1 on the cation vacancy would balance the virtual charge of +1 on the impurity. The analogous effect would be observed with a divalent anion impurity. The increased contribution to conductivity of a particular defect species would then allow the determination of the associated enthalpy and entropy changes with greater accuracy than would be possible in study of the pure crystal only.

The theory involved in both parts of the study is only briefly outlined in the following chapters because detailed accounts exist elsewhere and are referenced appropriately. An excellent account of the theory of ionic conductivity is

given by Lidiard[3].

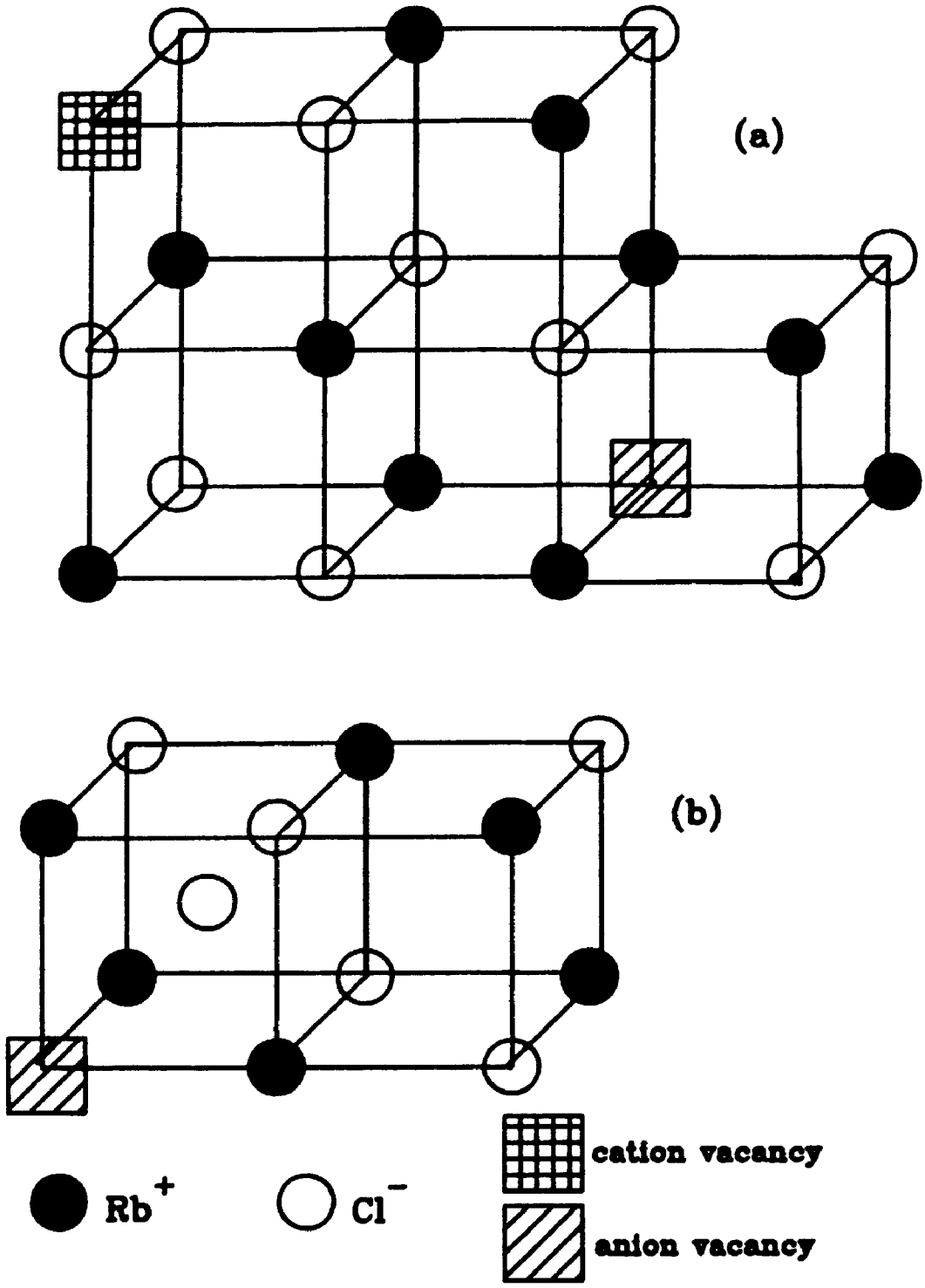

Figure 1–1: a) Schottky defect in RbCl
b) anion Frenkel defect in RbCl

Chapter 2

Interionic Potentials

The potential energy between the ions in an ionic crystal is dominated at long range by Coulombic forces but as ionic separations decrease, dispersion forces become important. These forces, which are attractive in nature, arise as a result of the interaction of mutually induced multipoles, the strongest of which is the dipole-dipole interaction, $\Phi^{DD}(r)$. As the ions move even closer, the charge densities start to overlap and a strong repulsion occurs. This repulsive energy, $\Phi^{R}(r)$, is commonly described by an exponential, or Born-Mayer, term. If many-body effects and angle-dependent forces are ignored, which is reasonable for alkali halide crystals[7], the potential energy can be described by pairwise interactions. At short range, the pair potential is then written as,

$$\Phi^{SR}(r) = \Phi^{R}(r) + \Phi^{DD}(r) = A_{ij} \exp(-r/\rho_{ij}) + \Phi^{DD}(r) \qquad (2\text{-}1)$$

where, A_{ij} is the repulsive parameter and ρ_{ij} is the hardness parameter.

The pair-potential model has been successfully incorporated into computer codes and the schematic for the development of an interionic potential is shown in Figure 2-1. The first step is to calculate the electron density of each ion in the crystal. The program used, **HFS**, is based on

Hartree-Fock self-consistent field calculations with the inclusion of an appropriate Madelung potential to account for the crystal environment[8]. These charge densities are then used in the program **WEDACT** to calculate the interaction energy, U(r), between all possible ion pairings as a function of their separation. The computational treatment of these interactions is based on the uniform gas approximation in which the ion is assumed to have a spherically symmetric charge distribution of finite radius. The densities of the two atoms are assumed to overlap in such a way that the overall density is the superimposable sum of the individual densities[9].

The interaction energies are fitted in **BORMAY** to a two-body potential (Equation 2-1) such that the differences between the calculated energies and those from the fitted potential are less than 1%. The dipole-dipole interaction includes a damping coefficient which removes the artificial net attraction in the potentials at small r, when $\phi^{DD} > \phi^{R}$ [7,8]. Thus,

$$\phi^{DD}(r) = \chi(r)\ (C_{ij}/\ r^6) \qquad (2\text{-}2)$$

where, C_{ij} is the van der Waals coefficient and $\chi(r)$ is the damping coefficient, given by[10],

$$\chi(r) = \exp[-((1.28\ R_M/\ r)\ -1)^2] \quad r < 1.28\ R_M$$
$$\chi(r) = 1 \quad r \geq 1.28\ R_M \qquad (2\text{-}3)$$

where R_M is the separation at the potential minimum.

The pair potentials are then refined by fitting them to the properties of the crystal in the **PLUTO** program[11]. That is, the cohesive energy and the elastic and dielectric constants are calculated and the potential parameters are adjusted until the calculated and experimental properties are in as close agreement as possible. In addition, the bulk lattice strain inherent in the crystal is calculated and minimized. The phonon dispersion is calculated in a separate program, **PHONON**, to further test the potential. The calculated frequencies are compared to available spectral data and the potentials are adjusted accordingly to obtain the best overall fit.

The calculation of the crystal properties requires the use of the shell model developed by Dick and Overhauser[12]. This simple mechanical model considers the ions as two components, a massless shell of charge Y displaced from a core of charge X. The core and shell are coupled by a harmonic spring with a force constant, K, such that the polarizability of the free ion is,

$$\alpha = Y^2 / K \qquad (2\text{-}4)$$

The parameters, Y and K, for each ion are obtained by fitting to the dielectric constants and the phonon dispersion. The shell model is represented schematically in Figure 2-2.

The development of interionic pair potentials is discussed in more detail by Catlow *et.al.*[13] and by Jacobs[7].

2-1 RbCl, RbBr and RbI Potentials

The pair potentials for the three rubidium halides were developed and fitted to 0 K crystal properties in the manner outlined above with adjustments made to the parameters such that they were in line with expected trends. That is, the Rb^+-Rb^+ potential for each halide was assumed to be similar with slight variations due to the different crystal environments. In addition, the C_{ij} coefficients for the Rb^+-halide interaction were adjusted such that the Rb^+-bromine coefficient lay midway between that of chlorine and that of iodine. A similar trend for the halide-halide van der Waals coefficient was allowed for in the fitting.

The resultant potentials are in Table 2-2 and the shell model parameters are in Table 2-3. The residual bulk lattice strain produced by the final potentials was zero for each crystal.

The calculated crystal lattice properties for the rubidium halides are compared with experimental values in Table 2-4. The calculated cohesive energies, static and high frequency dielectric constants, in each of the three cases, show excellent agreement with experiment. The gamma point frequencies are also in good agreement taking into account the difference in temperature, that is, the phonon dispersions were calculated at

0 K and determined experimentally at 80 K. The phonon dispersion curves for RbCl, RbBr and RbI are shown in Figures 2-3, 2-4 and 2-5.

The elastic constant, c_{11}, is in reasonable agreement with experiment, however, the effect of many-body forces is apparent in the observed differences between c_{12} and c_{44}. For a material with the rock-salt structure, such as the rubidium halides, in equilibrium under two-body type interactions, c_{12} and c_{44} must be equal. Since the calculated elastic constants are derived from pair potentials, they satisfy the Cauchy relation, $c_{12}=c_{44}$. Experimentally this is not the case and this failure emphasizes the role played by many-body interactions. Nonetheless, convincing arguments exist that the elastic constants may be used to give pair potentials that are not critically dependent on uncertainties about many-body forces[14].

2-2 Rb_2S Interionic Potential

The alkali chalcogenides are relatively unexplored and it was difficult to develop a reliable potential. Actual experimental data were unavailable but a few attempts have been made to calculate their cohesive energies[15,16] and a refractive index, where $n^2=\epsilon_\infty$, was available for Rb_2S[17]. The electron-gas potential was fitted using these two properties and by minimizing the bulk lattice strain to zero. The parameters are given in Table 2-5 and the calculated crystal properties are given in Table 2-6. Phonon dispersion curves

were calculated and are plotted in Figure 2-6.

2-3 $SrCl_2$ Interionic Potential

An initial 0 K potential for $SrCl_2$ was obtained from a previous study done in this laboratory[4] and, with the inclusion of damping, this was adjusted to reproduce crystal lattice properties. The potential parameters are given in Table 2-7 and the calculated lattice properties are compared with experimental values in Table 2-8. The calculated properties are in good agreement with experiment for all reported properties. The bulk lattice strain produced by the potential was zero. Phonon dispersion curves were plotted and compared to the experimental curves in Figure 2-7. The calculated curves show good agreement with the experimental points, although the calculated Raman dispersion is flatter than that found experimentally.

Some additional interionic potentials were required for the rubidium chloride system in order to calculate the relevant energies for the addition of impurity ions to the pure crystal. Potentials for the Sr^{+2}-Rb^{+} and the S^{-2}-Cl^{-} interactions were developed from electron-gas calculations and are given in Table 2-9.

The structures of $SrBr_2$ and SrI_2 are complicated and could not be incorporated into the **PLUTO**, **PHONON** and **HADES**[18] codes. Thus it was not possible to fit electron-gas potentials to crystal properties nor was it possible to calculate the defect energies.

Table 2-1: Symbols and units for potential parameters and physical properties.

Symbol	Definition	Units
Parameters		
A_{ij}	repulsive parameter	eV
ρ_{ij}	hardness parameter	Å
C_{ij}	van der Waals coefficient	eV Å^6
X_i	core charge	e
Y_i	shell charge	e
K_i	core-shell coupling constant	eV Å^{-2}
R_M	separation at potential minimum	Å
Properties		
a_0	lattice parameter	Å
c_{ij}	elastic constants	10^{-10}N m^{-2}
u_L	cohesive energy	eV
ϵ_∞	high frequency dielectric constant	
ϵ_s	static dielectric constant	
$\acute{\omega}_{LO}(\upsilon_{LO})$	longitudinal optic mode frequency	THz(cm^{-1})
$\acute{\omega}_{TO}(\upsilon_{TO})$	transverse optic mode frequency	THz(cm^{-1})
ω_R	Raman frequency	THz
$\omega_{LA}(\omega_{TA})$	longitudinal (transverse) acoustic mode frequencies	THz

Table 2-2: Potential parameters for RbCl, RbBr, and RbI.

Interaction	A_{ij}/eV	ρ_{ij}/Å	C_{ij}/eV Å^6	R_{min}/Å
RbCl				
Cl^--Cl^-	596.54	0.380	170.06	4.0
Rb^+-Cl^-	2050.94	0.348	108.87	4.1
Rb^+-Rb^+	4959.53	0.286	68.31	3.8
RbBr				
Br^--Br^-	1445.89	0.361	127.59	4.3
Rb^+-Br^-	5800.44	0.319	85.00	4.5
Rb^+-Rb^+	5020.49	0.285	70.02	3.8
RbI				
I^--I^-	1833.12	0.369	115.53	4.9
Rb^+-I^-	29540.18	0.287	27.00	5.6
Rb^+-Rb^+	5080.49	0.285	70.02	3.8

Table 2-3: Shell model parameters for RbCl, RbBr and RbI.

Ion	Y_i/eV	K_i/eV Å^{-2}
Cl^-	-2.485	29.5
Rb^+(RbCl)	5.0	171.0
Br^-	-3.205	34.7
Rb^+(RbBr)	5.0	175.0
I^-	-4.087	36.9
Rb^+(RbI)	5.0	185.0

Table 2-4: Experimental and calculated crystal lattice properties of RbCl, RbBr, and RbI.

Property	Calculated	Experimental
	RbCl	
a_0^* /Å		3.259[19]
u_L /eV	-7.02	-6.91[20]
c_{11} /10^{10} N m^{-2}	3.94	4.30[21]
c_{44} /10^{10} N m^{-2}	0.61	0.49[21]
c_{12} /10^{10} N m^{-2}	0.61	0.65[21]
ϵ_0	4.53	4.53[22]
ϵ_∞	2.21	2.20[23]
ω_{LO} /THz	5.00	5.17[23]
ω_{TO} /THz	3.34	3.72[23]
	RbBr	
a_0^* /Å		3.410[19]
u_L /eV	-6.71	-6.62[20]
c_{11} /10^{10} N m^{-2}	3.69	3.86[21]
c_{44} /10^{10} N m^{-2}	0.54	0.41[21]
c_{12} /10^{10} N m^{-2}	0.54	0.47[21]
ϵ_0	4.51	4.51[22]
ϵ_∞	2.36	2.36[23]
ω_{LO} /THz	3.79	3.88[23]
ω_{TO} /THz	2.70	2.81[23]
	RbI	
a_0^* /Å		3.628[19]
u_L /eV	-6.29	-6.2820
c_{11} /10^{10} N m^{-2}	3.34	3.21[21]
c_{44} /10^{10} N m^{-2}	0.43	0.29[21]
c_{12} /10^{10} N m^{-2}	0.43	0.36[21]
ϵ_0	4.55	4.55[22]
ϵ_∞	2.61	2.61[23]
ω_{LO} /THz	3.26	3.15[23]
ω_{TO} /THz	2.47	2.41[23]

*held constant at this value.

Table 2-5: Potential parameters for Rb_2S.

Interaction	A_{ij}/eV	ρ_{ij}/Å	C_{ij}/eV Å^6	R_{min}/Å
S^{2-}-S^{2-}	73.38	0.627	0.00	---
Rb^+-S^{2-}	1419.00	0.397	194.48	4.9
Rb^+-Rb^+	4793.04	0.289	54.96	4.1

Ion	Y/eV	K/eV Å^{-2}
S^{2-}	-3.7	28.5
Rb^+	5.0	128.35

Table 2-6: Calculated and experimental crystal lattice properties of Rb_2S.

Property	Calculated	Experimental
a_0^* /Å		3.825[24]
u_L /eV	-19.35	-19.55[16]
c_{11} /10^{10} N m^{-2}	3.79	
c_{44} /10^{10} N m^{-2}	0.42	
c_{12} /10^{10} N m^{-2}	1.44	
ϵ_0	7.90	
ϵ_∞	3.14	3.13[17]
ν_{LO} /cm^{-1}	215	
ν_R /cm^{-1}	125	
ν_{TO} /cm^{-1}	81	

Table 2-7: Potential parameters for $SrCl_2$.

Interaction	A_{ij}/eV	ρ_{ij}/Å	C_{ij}/eV Å^6	R_{min}/Å
Cl^--Cl^-	715.54	0.380	170.06	3.7
Sr^{2+}-Cl^-	4655.00	0.313	0.0	---
Sr^{2+}-Sr^{2+}	9949.10	0.245	0.0	---

Ion	Y/eV	K/eV Å^{-2}
Cl^-	-2.15	112.5
Sr^{2+}	9.6	198.5

Table 2-8: Calculated and experimental crystal lattice properties of $SrCl_2$.

Property	Calculated	Experimental[25]
a_0^* /Å		3.490
u_L /eV	-21.48	-21.40
c_{11} /10^{10} N m^{-2}	7.55	7.55
c_{44} /10^{10} N m^{-2}	1.73	1.03
c_{12} /10^{10} N m^{-2}	2.24	1.72
ϵ_0	6.94	6.94
ϵ_∞	2.74	2.70
υ_{LO} /cm^{-1}	230	248
υ_R /cm^{-1}	172	188
υ_{TO} /cm^{-1}	145	155

Table 2-9: Additional potentials

Interaction	A_{ij}/eV	ρ_{ij}/Å	C_{ij}/eV Å^6	R_{min}/Å
Sr^{2+}-Rb^{+}	16398.1	0.241	0.0	---
S^{2-}-Cl^{-}	277.00	0.444	0.0	---

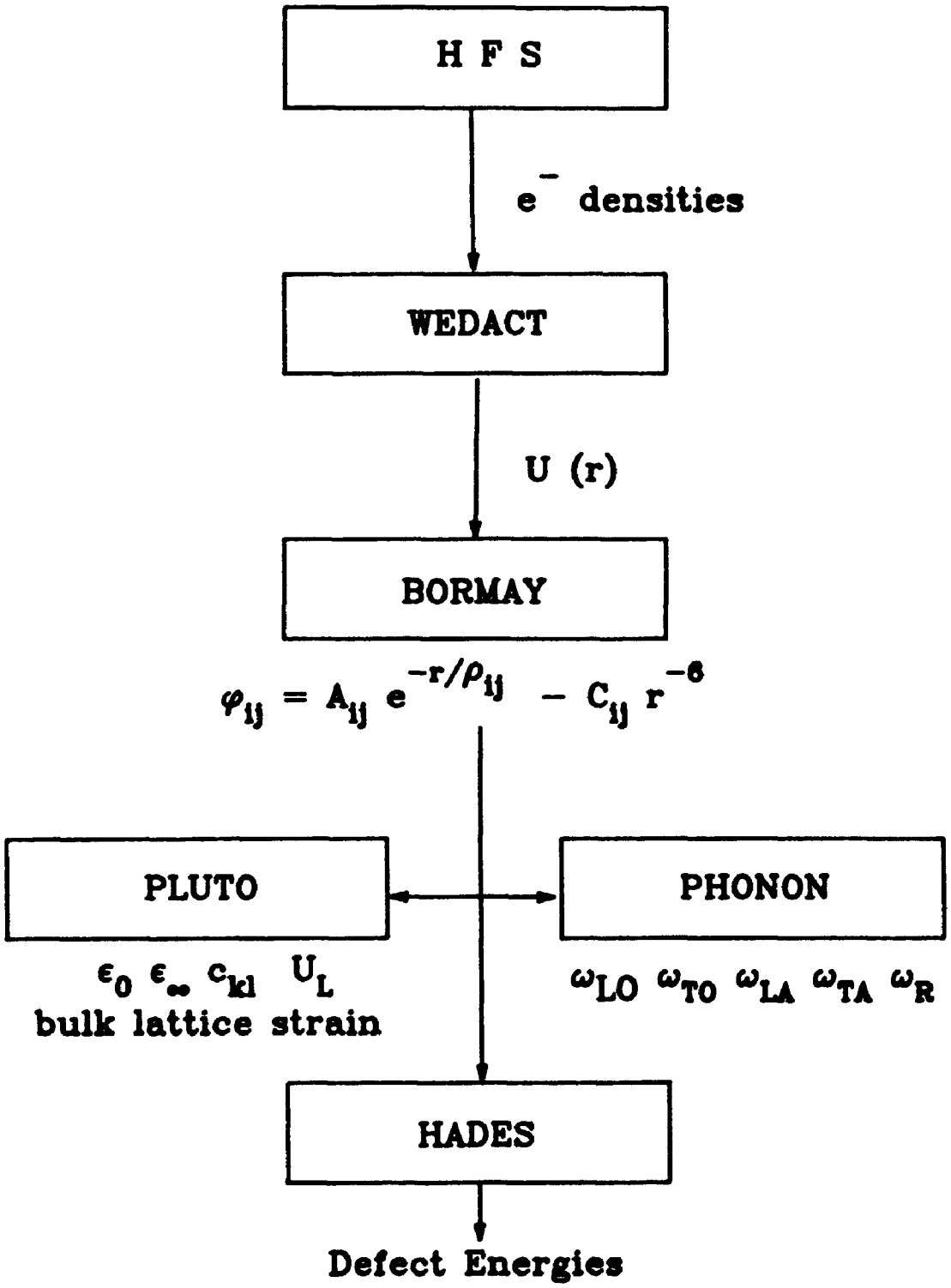

Figure 2–1: Schematic for the development of interionic potentials

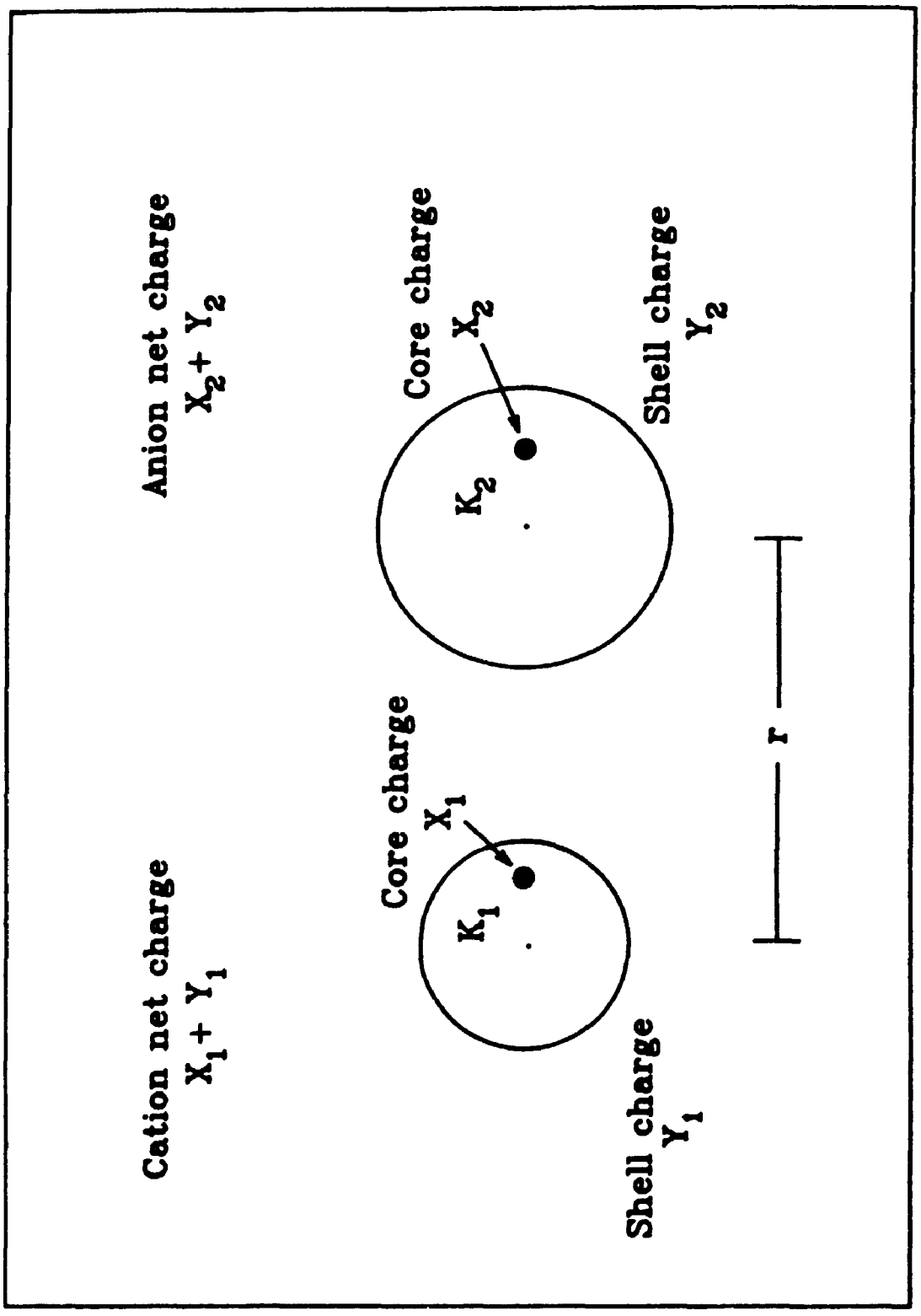

Figure 2–2: Simple shell model[12].

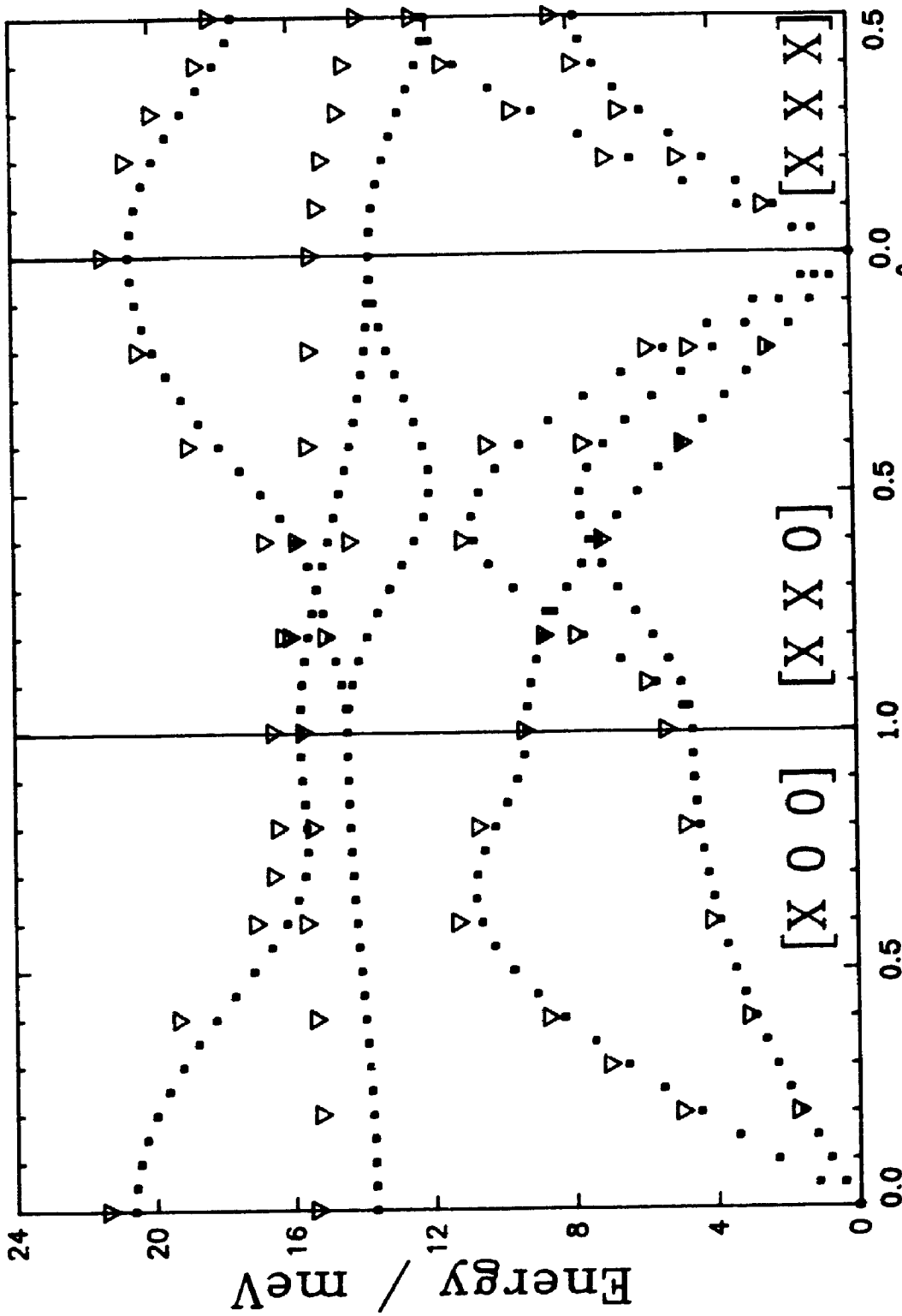

Figure 2–3: Phonon dispersion curves for RbCl, calculated (▪) and experimental (▵)[28].

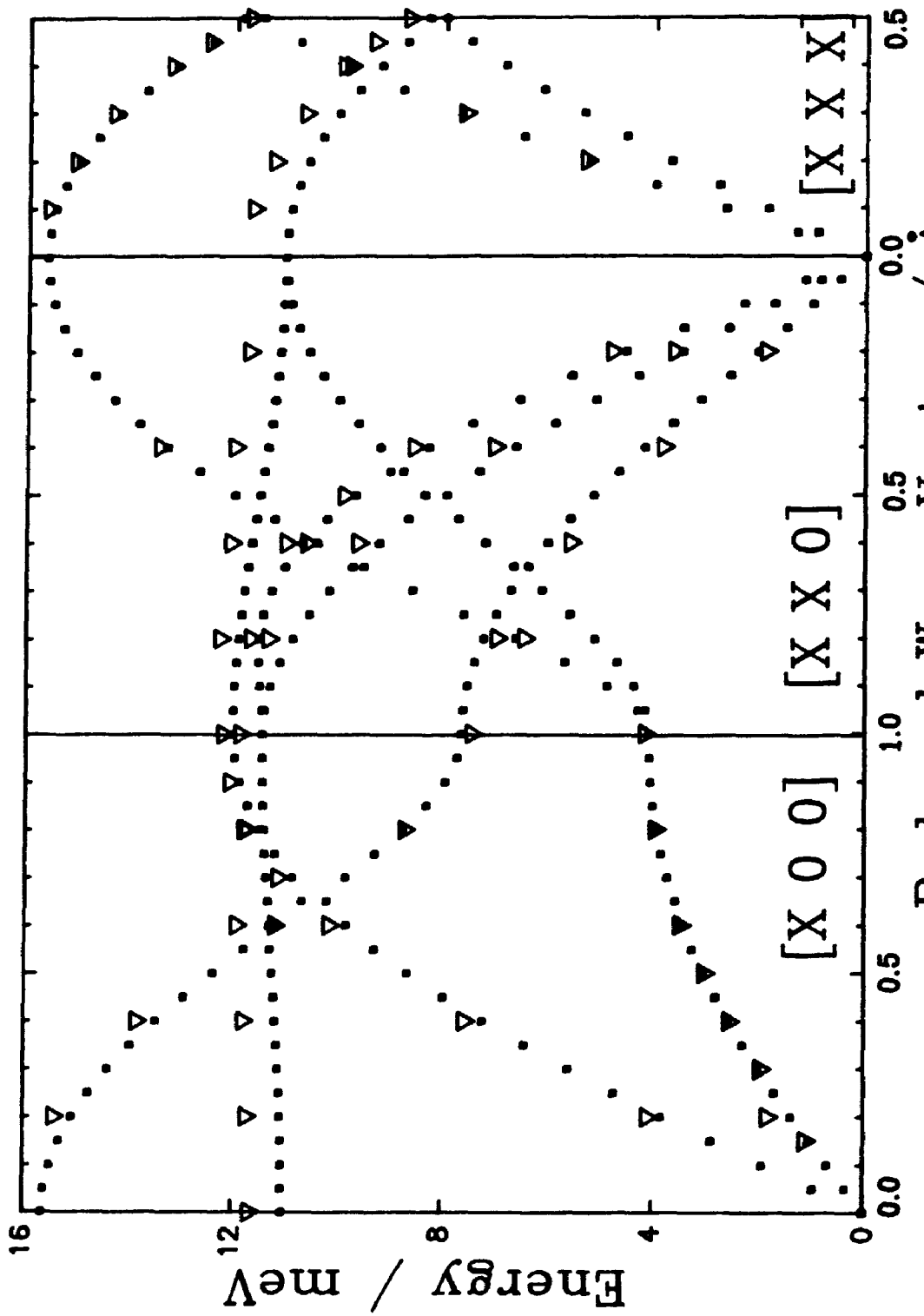

Figure 2–4: Phonon dispersion curves for RbBr, calculated (•) and experimental (▽)[27].

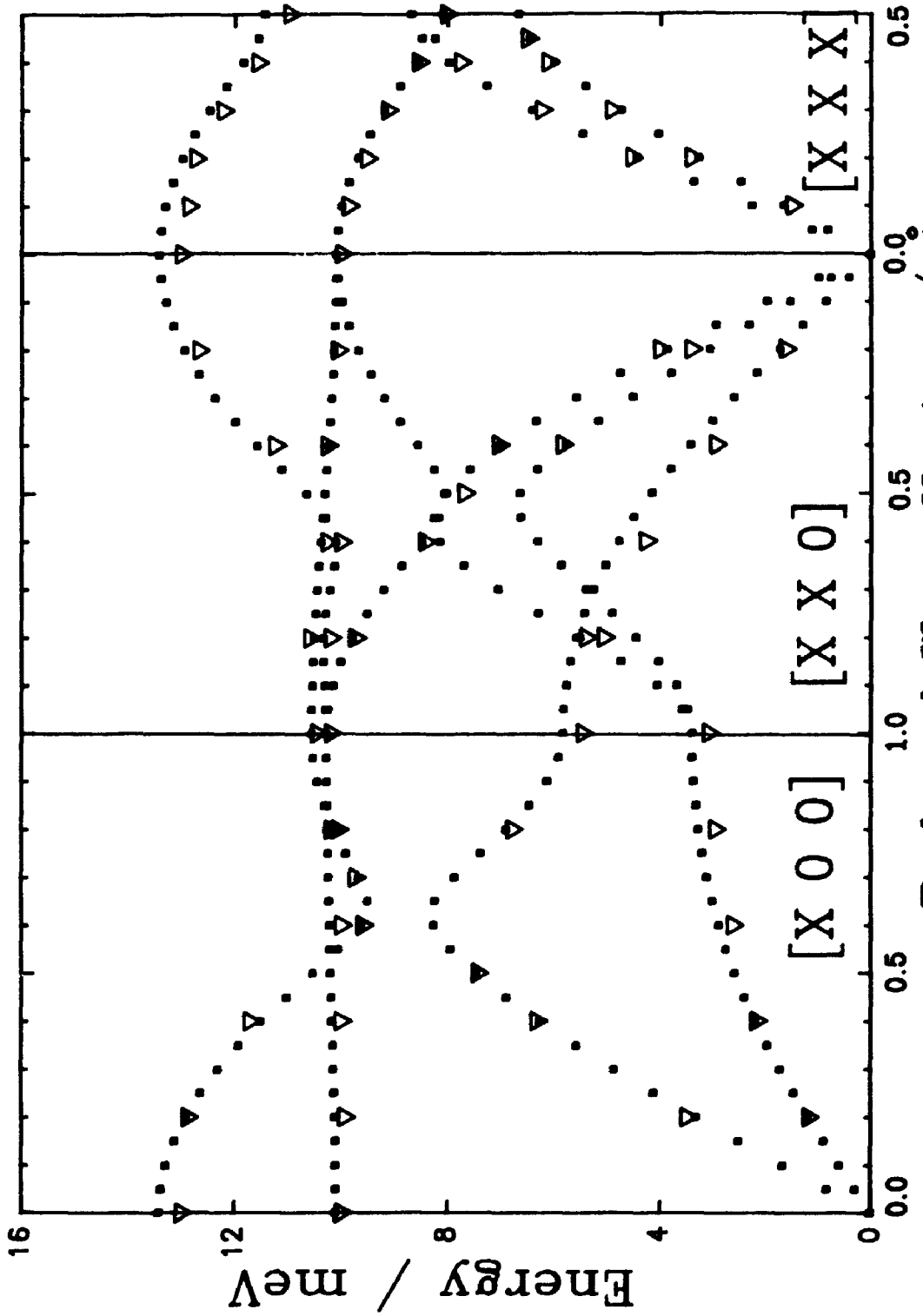

Figure 2–5: Phonon dispersion curves for RbI, calculated (•) and experimental (▽)[28].

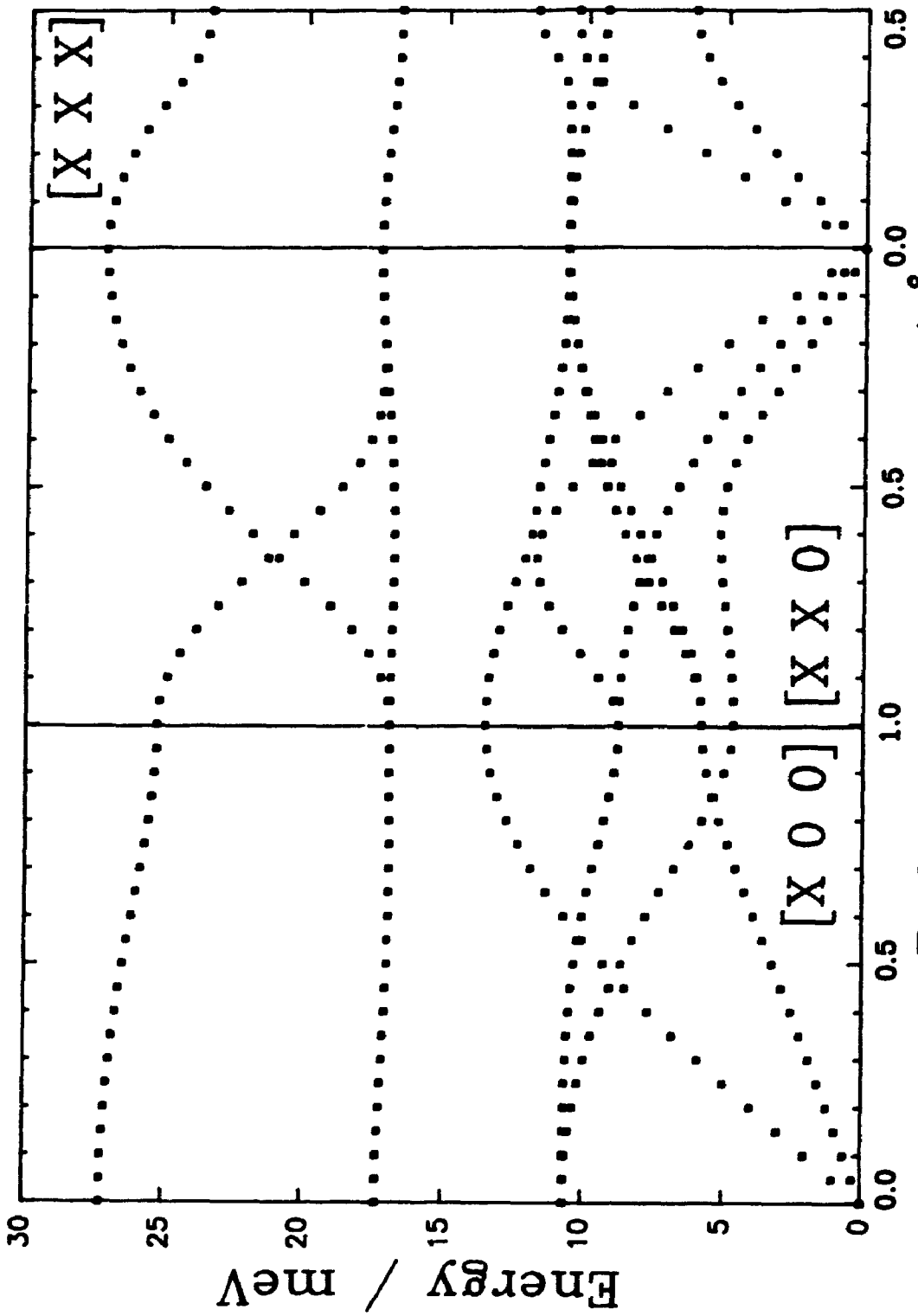

Figure 2–6: Calculated phonon dispersion curves for Rb_2S.

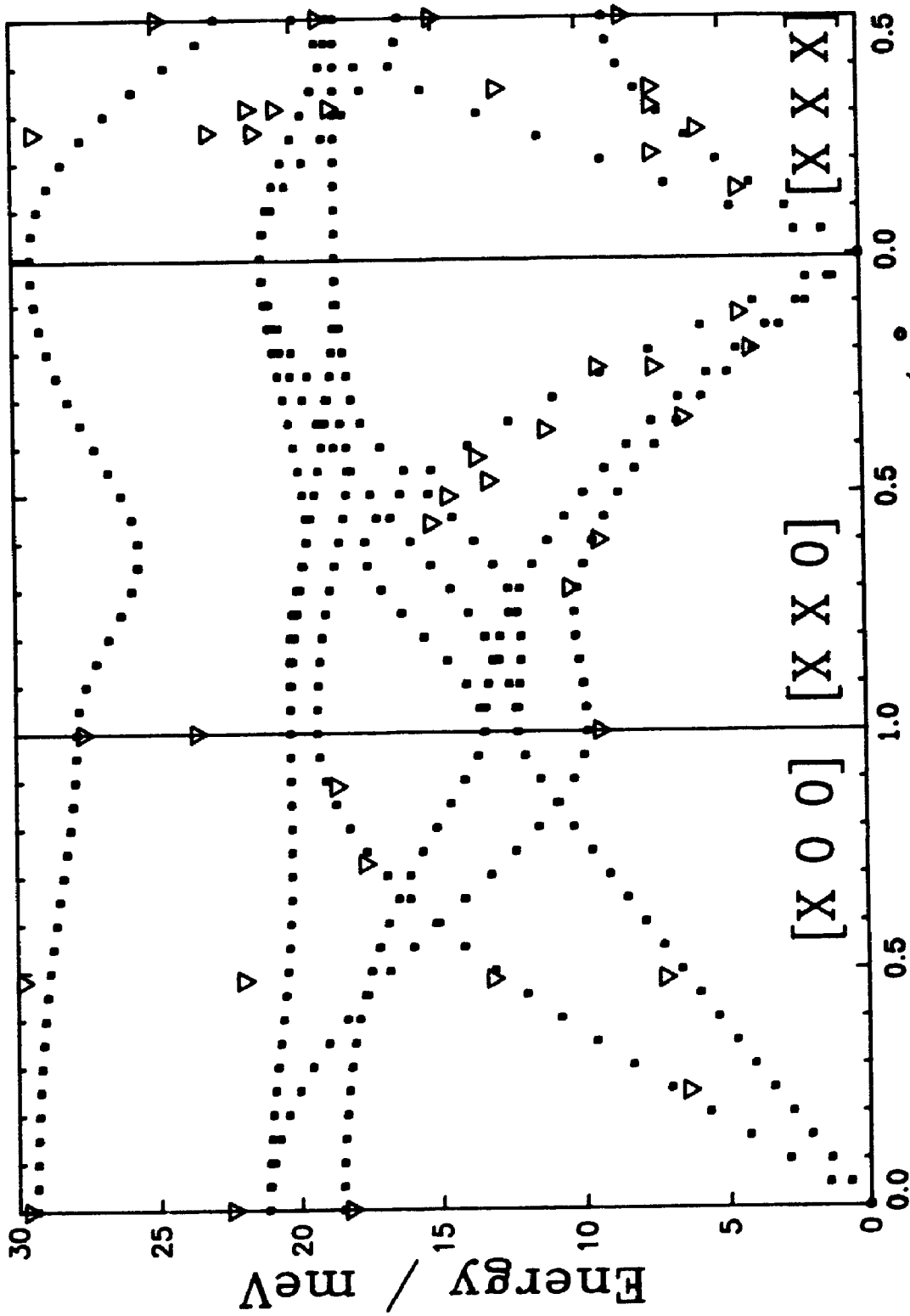

Figure 2.7: Phonon dispersion curves for $SrCl_2$,[29] calculated (•) and experimental (▽).

Chapter 3

Defect Energy Calculations

The general principle used in the calculation of defect energies is to partition the crystal into two regions, which are continuous at their boundary[30]. The inner region I immediately surrounds the defect and the interactions in this region are considered explicitly. That is, the lattice energy is calculated as a function of the ion coordinates and their equilibrium configurations are calculated by relaxing each ion until it is subject to zero net force. The outer region II is treated as a harmonic dielectric continuum with the dielectric, elastic and lattice dynamical properties of the crystal. The displacements of the ions are matched at the boundary between regions I and II to ensure continuity. The theory involved in these calculations has been described in detail in the literature[31,7].

The **HADES** program was used for the defect calculations[18] and required the input of the crystal potentials and structure. In addition, the region sizes needed to be specified, with the inner region generally consisting of 100 ions and the outer region of approximately 1000-1500 ions. The simulations are done at constant lattice parameter and thus generate defect energies, u^s, which are related to the corresponding energies at constant volume, u^v, by

$$u^v = u^s + P\ v^s \qquad (3\text{-}1)$$

where, v^a is the volume change associated with the defect process at constant lattice parameter, a. The term (Pv^a) is usually negligible at ordinary pressures and the distinction between the two energies can be ignored in the present study.

3-1 Defect Configuration and Energy Conventions

The definitions for the defect energy symbols and their units are given in Table 3-1. The defect energies were calculated using the convention that both the final position of an ion removed from the lattice to form a vacancy, and the initial position of an interstitial ion, are considered to be at infinity.

The energy required to form a Frenkel defect is the sum of the vacancy and interstitial formation energies. A Schottky defect ultimately places the electrically neutral set of ions at the crystal surface so that the formation energy is the difference between the sum of the vacancy formation energies and the cohesive energy of the crystal. The configurations of these defects are shown in Figure 1-1.

The vacancy migration energy is essentially the energy barrier, or saddlepoint energy, that an ion in a lattice site must overcome in order to migrate to a vacant site along a direct path. The migration of an interstitial by the interstitialcy mechanism is such that as it moves towards an occupied lattice site, the ion occupying the site is forced out by repulsive interactions towards an empty

interstitial site. This can occur along a collinear or a non-collinear path. The interstitial may also jump directly to the next interstitial site (see Figure 3-1).

The vacancy pair formation energy is the difference between the formation energy of associated anion and cation vacancies and the formation energies of the unassociated vacancies. It would be expected to be a negative quantity because of the Coulomb attraction between the vacancies. The migration of the vacancy pair is achieved via cation or anion jumps into the pair. The saddlepoint configuration for these jumps is shown in Figure 3-2.

The contribution of a defect type to transport depends on its Arrhenius energy, which derives from the logarithmic nature of the conductivity plots (see Chapter 5). Thus for cations, the Arrhenius energies are,

$$E^S_{cv} = u_S/2 + \Delta u_{cv} \qquad E^F_{cv} = u_{Fc}/2 + \Delta u_{cv} \tag{3-2}$$

$$E^F_{ci} = u_{Fc}/2 + \Delta u_{ci} \tag{3-3}$$

where, the superscript refers to the dominant formation process, Schottky or Frenkel.

For a cation jump into the vacancy pair, the Arrhenius energy is,

$$E_{cp} = u_S + u_{vp} + \Delta u_{cp} \tag{3-4}$$

Corresponding equations for the anion were used.

3-2 RbCl, RbBr and RbI Defect Calculations

The defect energies calculated for the three rubidium halides are summarized in Table 3-2. Previous theoretical

values are listed in Table 3-3. The discrepancy between calculations, which use various region sizes and model types, is indicative of the difficulty in comparing theoretical results between different methods. Even within the same method care must be taken; for example, the results of Rowell *et.al.*[32] were intended to augment the Uppal *et.al.* calculations[33] and used the same potentials and models. However, the calculated energies differed by up to 0.2 eV, which the authors attributed to a difference in the short-range potential cutoff used in their respective defect calculations.

With this in mind, the values calculated in the present work are within the range established in previous work. The best test of theoretical energies is a comparison with experiment, which is done in Chapter 6 for RbCl.

For RbBr, an ionic conductivity and diffusion study has been done on pure crystals in the high temperature region by Downing and Friauf[34]. The conductivity and diffusion parameters were determined by a least-squares straight-line fit of the results, considering only cation and anion vacancies. They found the Arrhenius energies of activation for rubidium and bromine to be 2.01 eV and 1.99 eV, respectively, from the diffusion results and the Arrhenius activation energy from the conductivity measurements to be 2.017 eV. However, the observed curvature in the conductivity data could not be fitted significantly to a straight line using equal activation energies for cations

and anions. They also concluded that vacancy pairs made a significant contribution to diffusion.

These results compare favourably with the Arrhenius energies for RbBr (Table 3-4). The activation energies for Schottky defects were found to be nearly equal for both kinds of vacancies and in close agreement with the results of Downing *et.al.*. But the cation activation energy for Frenkel defects is smaller than that for the anion, which would mean a greater contribution from cation vacancies to transport. This would account for some of the curvature in the conductivity plots. In addition, the Arrhenius energies for the interstitials and vacancy pairs would indicate the participation of both in transport processes.

The ionic conductivity of pure and strontium-doped RbI was measured by Chandra and Rolfe[35] and their Schottky enthalpy of 2.1 eV is in excellent agreement with our calculated result of 2.14 eV. As a result of the insolubility of $RbCO_3$ in RbI, the conductivity of anion-doped crystals could not be measured and the anion parameters were less accurately determined than the others. This would account for their high anion migration enthalpy of 1.6 eV. The cation vacancy migration enthalpy of 0.60 eV agrees moderately well with our value of 0.706 eV. However, their analysis did not include the contribution of interstitials, which should play a role if their Arrhenius energies are considered (Table 3-4).

A comparison of the defect energies for the three

rubidium halides indicates that while it is easier to form defects in RbI, they are more mobile in RbCl. It would appear that the decreasing difference in ionic radii (0.32 Å-RbI, 0.13 Å-RbBr, 0.01 Å-RbCl,)[36] has the effect of lowering the relative saddlepoint energies and thus the defects are opposed by a lower barrier in RbCl than in RbI. The cohesive energy for the perfect lattice (Table 2-4) is greater in RbCl than in RbI which would make it more difficult to form lattice defects in the former. The collinear interstitialcy mechanism predominates for interstitial migration in all three halides.

3-3 RbCl:Sr^{2+} and RbCl:S^{2-} Defect Calculations

The effect of divalent impurities is of interest in the study of transport processes (Chapter 5) and point defect calculations can be used to calculate the energies required for impurity migration. An impurity ion on a normal lattice site can migrate by jumping into an interstitial position or by exchanging lattice sites with an adjacent vacancy. The mobility of the impurity, in the latter case, will then depend on the jump frequencies of the vacancy towards, w_3, and away, w_4, from the impurity. It will also depend on the frequency of site exchange between the vacancy and the impurity, w_2, and the frequency that the vacancy will jump from nearest-neighbour (nn) to nn site, w_1. Diagrams of these jumps are shown in Figure 3-3. The complexes involving an impurity-vacancy pair on a nn or next nearest-

neighbour (nnn) site are also shown.

Unfortunately, there are no previous experimental or theoretical results with which to compare the calculated activation energies, shown in Table 3-5. The binding energies for the nn and nnn complexes are similar for the cation-impurity and so both species will exist in equilibrium. The S^{2-}-nn complex is energetically more favourable, but the energy difference is not large enough to rule out the formation of nnn complexes.

The activation energies for the jumps which involve the movement of a host ion, w_1, w_3 and w_4, are quite similar for the $RbCl:Sr^{2+}$ system due to the energetic equivalence of the nn and nnn complexes. This has been observed in other studies of alkaline earth impurities in alkali halides[37]. In the $RbCl:S^{2-}$ system, the w_4 jump has a higher activation energy than w_3 because the former involves a jump into the less stable nnn configuration. This ordering was also observed in calculations on $NaCl:S^{2-}$ [4].

The activation energy for the w_2 jump is higher than that for the other jumps which is typical for calculations done on divalent impurities in alkali halides[37].

3-4 Rb_2S Defect Calculations

The primary purpose of this study was to develop a Rb^+-S^{2-} potential for the impurity calculations of the previous section, however, the availability of this potential meant that defect calculations could be made on Rb_2S. Previous

work on Rb_2S in this respect has not been done so comparisons are limited to a similar study on Na_2S[4] (see Table 3-6).

Rubidium sulphide has the anti-fluorite structure where the rubidium ions occupy the corners of cubes and sulphur ions are positioned at the centre of every other cube (Figure 3-4)

The formation energy of cation Frenkel defects is less than the Schottky formation energy which would indicate that the former are the predominant defects. However, the cation interstitial migration energy is much higher than that for cation vacancies indicating that the main carriers are cation vacancies. The anion parameters are all much higher than those for the cation because of the relative size and charge difference. These patterns were also observed in the sodium sulphide study[4].

Table 3-1: Defect energy symbols

Symbol	Defect Process
u_s	Schottky formation
Δu_{cv}	cation vacancy migration
Δu_{av}	anion vacancy migration
u_{Fc}	cation Frenkel formation
u_{Fa}	anion Frenkel formation
Δu_{cid}	cation interstitial migration, direct
Δu_{cic}	collinear
Δu_{cinc}	non-collinear
Δu_{aid}	anion interstitial migration, direct
Δu_{aic}	collinear
Δu_{ainc}	non-collinear
u_{vp}	vacancy pair association
Δu_{cp}	cation jump into pair
Δu_{ap}	anion jump into pair
u_1	impurity-vacancy nn complex
u_2	impurity-vacancy nnn complex
Δu_1	w_1 jump
Δu_2	w_2 jump
Δu_3	w_3 jump
Δu_4	w_4 jump
E'_z	Arrhenius energy, with subscript indicating mobile defect and superscript indicating the origin of the defect

Table 3-2: Calculated defect energies in eV at 0 K for RbCl, RbBr, and RbI.

Defect	RbCl	RbBr	RbI
u_s	2.520	2.365	2.139
Δu_{cv}	0.661	0.684	0.706
Δu_{av}	0.667	0.699	0.723
u_{Fc}	3.457	3.290	3.062
u_{Fa}	3.480	3.542	3.439
Δu_{cid}	0.264	0.303	0.335
Δu_{cic}	0.208	0.249	0.291
Δu_{cinc}	0.252	0.287	0.314
Δu_{aid}	0.241	0.265	0.330
Δu_{aic}	0.188	0.194	0.237
Δu_{ainc}	0.226	0.258	0.325
u_{vp}	-0.940	-0.908	-0.851
Δu_{cp}	0.795	0.806	0.803
Δu_{ap}	0.808	0.800	0.765

Table 3-3: Calculated defect energies from previous work.

Defect	reference	RbCl	RbBr	RbI
u_s	33	2.52	2.51	2.47
	38	2.36,2.42		
	32	2.62	2.69	2.66
	39	2.16,2.43	2.20,2.37	2.07,2.28
	40	2.37,2.44	2.34,2.46	2.16,2.30
	41	2.46-2.52	2.41-2.47	2.29-2.35
Δu_{cv}	33	0.76	0.74	0.74
	38	0.65,0.68		
	32	0.80	0.81	0.82
	40	0.63	0.62,0.64	0.58,0.62
Δu_{av}	33	0.79	0.76	0.79
	38	0.64,0.66		
	32	0.84	0.86	0.89
	40	0.63	0.64	0.62,0.64
u_{Fc}	38	2.96,3.25		
	32	3.21	3.13	2.97
u_{Fa}	38	3.94,4.54		
	32	3.94	4.10	4.23
Δu_{ci}	38	0.46		
	32	0.41	0.45	0.44
Δu_{ai}	38	0.10		
	32	0.15	0.14	0.12
u_{vp}	40	1.49,1.52	1.46,1.52	1.37,1.45
Δu_{cp}	40	0.70	0.68	0.64
Δu_{ap}	40	0.72	0.69	0.61

Table 3-4: Arrhenius energies for RbCl, RbBr and RbI.

Energy / eV	**RbCl**	**RbBr**	**RbI**
E^{S}_{cv}	1.92	1.87	1.78
E^{F}_{cv}	2.39	2.33	2.34
E^{S}_{av}	1.93	1.88	1.79
E^{F}_{av}	2.41	2.47	2.44
E_{ci}	1.94	1.89	1.82
E_{ai}	1.93	1.92	1.96
E_{cp}	2.38	2.42	2.47
E_{ap}	2.39	2.41	2.43

Table 3-5: RbCl:Sr^{2+} and RbCl:S^{2-} binding and vacancy jump energies in eV.

Defect	**RbCl:Sr^{2+}**	**RbCl:S^{2-}**
u_1	-0.596	-0.650
u_2	-0.583	-0.515
Δu_1	0.642	0.712
Δu_2	1.25	0.937
Δu_3	0.624	0.634
Δu_4	0.637	0.770

Table 3-6: Calculated defect energies at 0 K for Rb_2S and at 50 K for Na_2S[4].

Defect	Na_2S	Rb_2S
u_S	4.78	3.745
Δu_{cv}	0.23	0.273
Δu_{av}	2.11	1.588
u_{Fc}	1.87	1.687
u_{Fa}	6.09	5.327
Δu_{cic}	0.56	0.396
Δu_{aic}	2.83	2.810

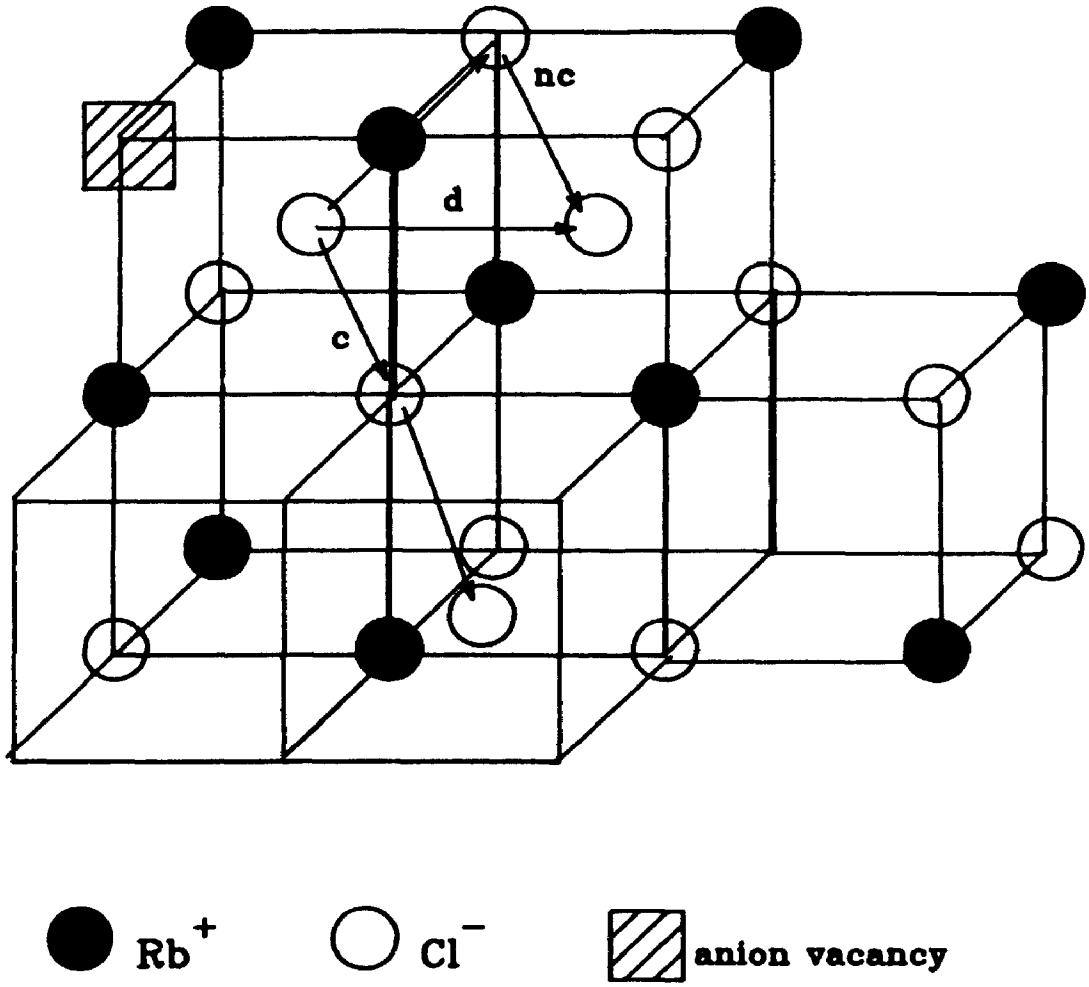

Figure 3−1: Interstitial migration mechanisms

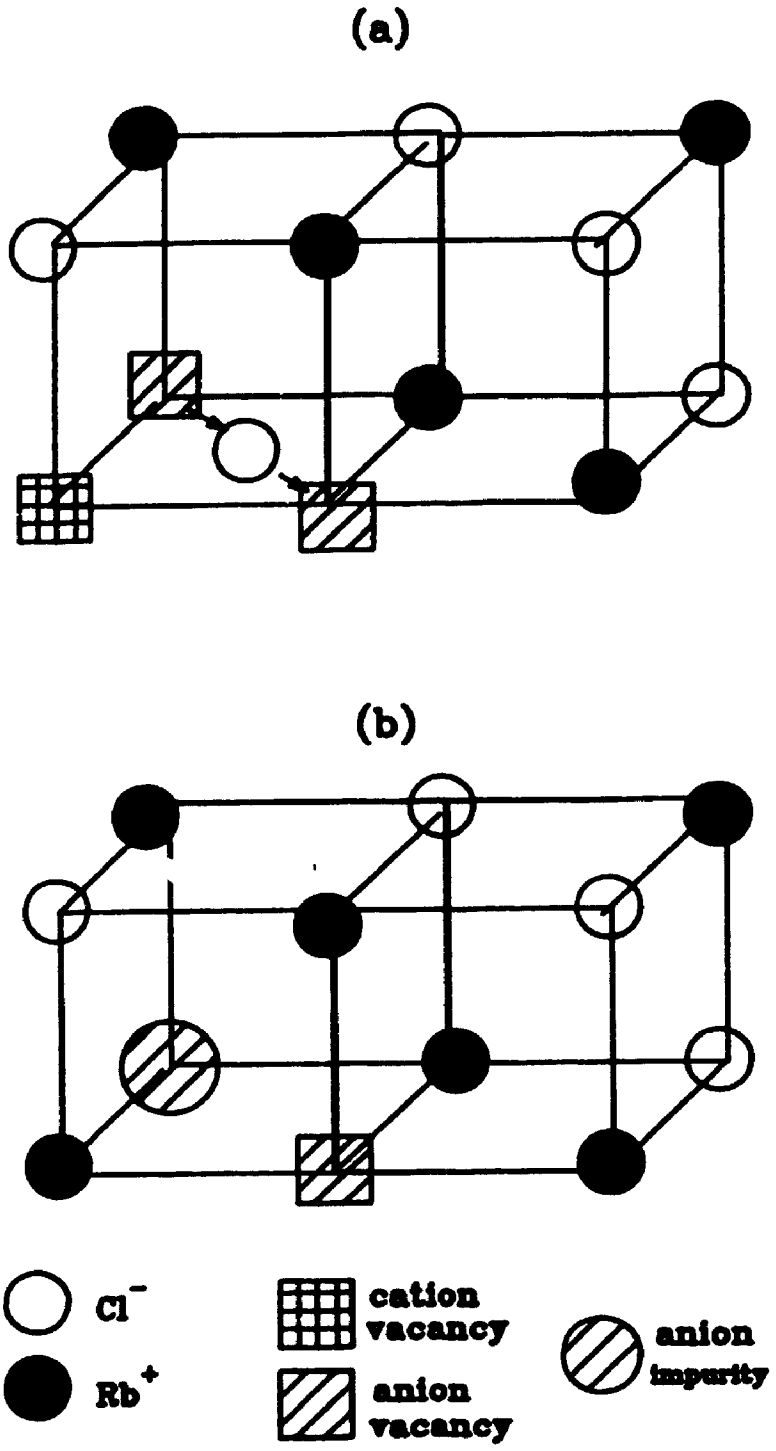

Figure 3–2: a) anion jump into vacancy pair
b) impurity–vacancy complex

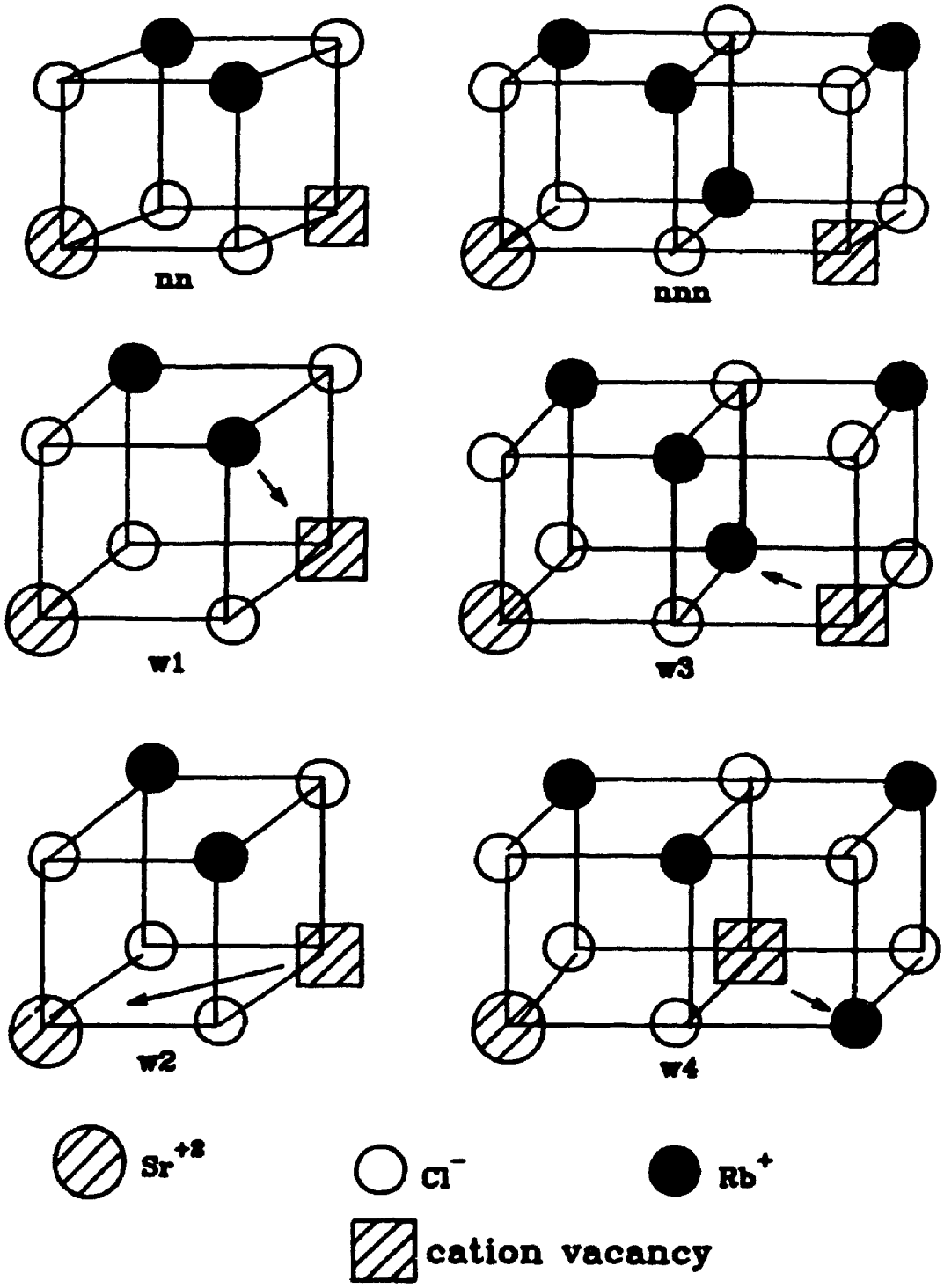

Figure 3–3: RbCl:Sr^{+2} complexes and vacancy jumps

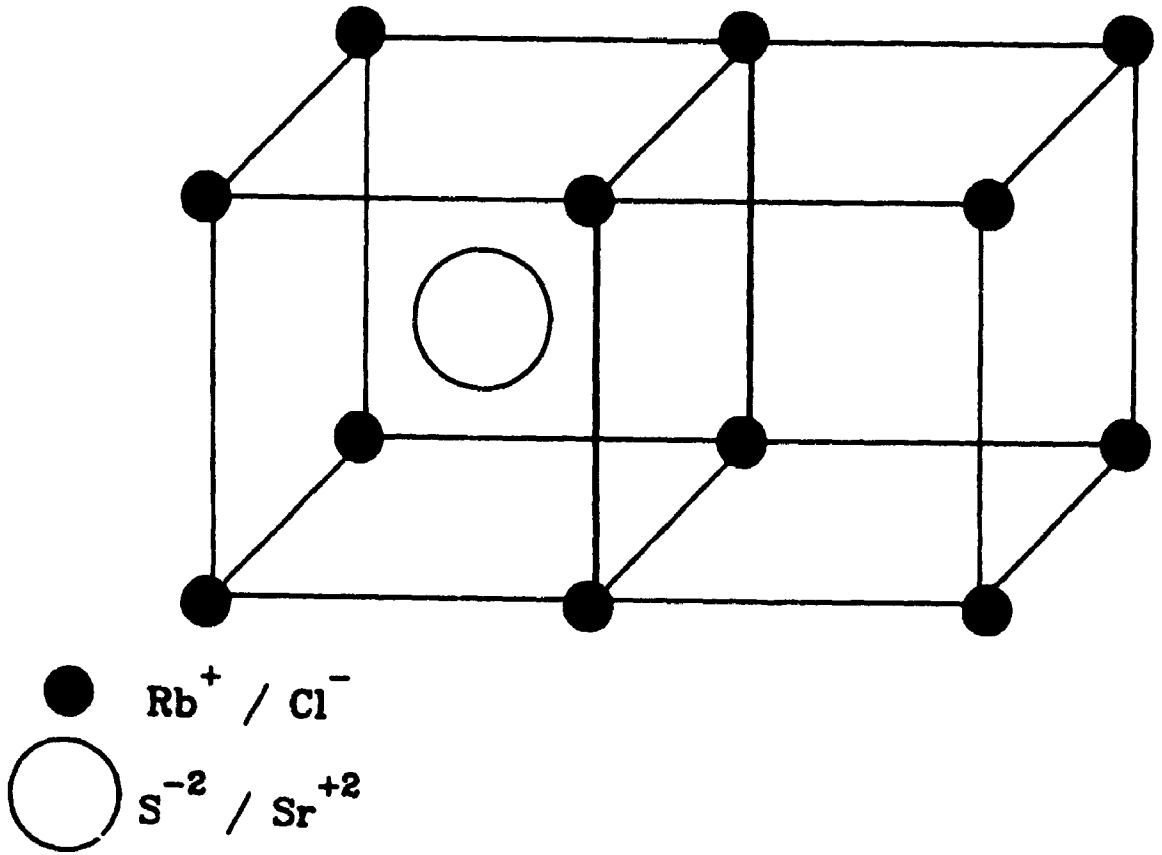

Figure 3–4: The anti–fluorite/fluorite structure of $Rb_2S/SrCl_2$.

Chapter 4

Experimental Measurement of Ionic Conductivity

The conductivity of a crystal is given by

$$\sigma(T) = G(T)\ h(T)/A(T) \qquad (4\text{-}1)$$

where $\sigma(T)$ is the conductivity, G(T) is the measured conductance, A(T) is the area of the crystal, and h(T) is the thickness of the crystal. Thus, the accurate measurement of ionic conductivity is dependent on the individual accuracy of three measurements--conductance, temperature and the geometrical factor, h(T)/A(T). The experimental apparatus and its arrangement, the sample preparation and the method used to execute the experiment were all designed to reduce the uncertainty in each of these factors.

4-1 The Apparatus

A schematic diagram of the apparatus used for conductivity measurements is shown in Hooton's work on NaCl[4]. The apparatus consists of several components. One component is the electrode system into which the crystals are mounted and which is designed to measure the temperature and conductivity. Another component is the surrounding conductivity cell which provides the mechanical support for the electrode system and holds the appropriate atmosphere

for the conductivity runs. A third element is the furnace which is designed to provide the thermal environment for the experiments. The appropriate pressure and atmosphere are achieved and maintained by the final element, the vacuum line.

4-1.1 The Electrode System

The electrodes are arranged in a configuration that allows for the simultaneous measurement of two crystals (Figure 4-1). Each crystal is positioned between two sheets of 0.25 mm thick Pt foil in a stacked arrangement. The crystals are separated by a centre foil folded in half, with the two halves isolated from contact by mica (see Figure 4-1). Pt wires are spot-welded on to the corner of each foil and Pt-13%Rh wires are spot-welded to the centre of each. The Pt and Pt-13%Rh wires form Type-R thermocouples which are used to measure the temperature at each face of the crystal. The conductivity of each crystal is measured between the Pt electrodes.

The upper and lower Pt-13%Rh wires are isolated from the electrodes by alumina discs through which they are threaded. Slits in the quartz and alumina discs prevent the wires from protruding and thus deforming the crystals at high temperatures. The middle Pt-13%Rh wire is isolated from the Pt foil by the mica. This arrangement ensures that the temperature is measured at the centre of the crystal faces.

4-1.2 The Conductivity Cell

The crystals and the electrodes are mounted in a quartz holder which is supported by a stainless steel holder welded on to a flange. Two quartz discs hold the crystal/electrode system in place. The bottom disc is attached to a rod which sits on a spring. The pressure of the rod and thus the force on the crystals is controlled by a linear motion feedthrough. This feature is important because at high temperatures the crystals are soft and prone to deformation. The electrode leads are threaded through quartz tubes to the flange where they are connected to thermocouple feedthroughs. Shielded copper wires connect the leads to the switching box. A diagram of the complete cell is shown in Hooton's thesis[4].

4-1.3 The Furnace

The cell is fitted into an outer quartz jacket sealed to a stainless steel flange. This jacket is surrounded by a three-zone furnace built from Lindberg windings. The furnace consists of three windings or zones in order to maintain an even temperature profile. The height of the inner quartz holder is such that the crystals are in the middle of the furnace. The temperature of the furnace is monitored by a Type-K thermocouple inserted between the cell jacket and the furnace, at its centre. Quartz wool and aluminum foil are arranged around the furnace to provide

extra insulation.

4-1.4 The Vacuum Line

The cell and jacket flanges are sealed using a copper gasket and the cell is connected to a metal vacuum line. An Edwards diffusion pump and a Leybold-Heraeus roughing pump are used to evacuate the system. The pressure is measured using an Edwards Penning 8 gauge. Experiments are carried out under an atmosphere of pre-purified argon to prevent large changes in the geometrical factor caused by sublimation. The gas is passed through a leak valve and several feet of stainless steel capillary tubing to ensure a slow flow rate through the cell. The argon enters at the top of the jacket through a quartz tube and exits at the bottom, passing through a system of molecular sieves, charcoal and a bubbler containing Santovac 5 pump oil.

4-2 Automated Control

In previous work, the temperatures of the furnace zones had been regulated by three temperature controllers, which were set manually. Furnace temperatures were difficult to regulate as they were influenced by fluctuating line voltages and varying room temperatures. The large thermal lag of the furnace made manual adjustments difficult and time-consuming. These conditions also made specific temperatures difficult to reproduce. In addition, the measurement of conductance and temperature had previously

been done manually. All of these factors resulted in samples sitting at elevated temperatures for extended periods of time due to human time constraints. We felt that by automating both the temperature regulation and the acquisition of data, these difficulties could be significantly reduced.

The experiment is controlled at all stages by a Zenith EasyPC. The COM1 port connects the temperature controller and the COM2 port connects the conductivity bridge. The crystal temperature is read by using a combined A/D and I/O board, which is also responsible for switching between temperature and conductance measurements.

We decided to regulate the furnace temperature with a Watlow 945 digital controller selected for proportional-integral-differential (PID) control. The PID parameters that the Watlow uses are dependent on the thermal response of the system and must be determined for each temperature. A program was written, using the controller's autotuning feature, which could tune the response at each temperature setpoint and thus create a file containing these parameters. These parameters are sent to the Watlow from the computer during conductivity runs. The temperature setpoint is maintained via three Crydom D1225 solid state relays, one for each zone of the furnace.

The temperature is measured at the top and bottom faces of each crystal using the Type-R thermocouples, which constitute the electrode system described in 4-1.1,

connected to OMEGA OM5-ITC-R thermocouple conditioning modules with cold junction compensation. The 0-5 V signal output is dropped to a 0-2 V signal via two resistors in series. This signal can then be read by an OMEGA WB-800 A/D I/O board. Each OM5-module has a different ice-point compensation which was determined using a constant voltage source. The modules are periodically recalibrated.

The conductance is measured with a Wayne Kerr Autobalance Bridge (B905). The switching between the three temperature and two conductance measurements is done via a digital output from the WB-800 board to a set of five Potter and Brumfield relays. All lead resistances were measured and found to be negligible.

The complete layout of the automated system is shown in Figure 4-2.

The computer control program was written using Microsoft QuickBasic and is included in Appendix 1.

4-3 Sample Preparation

Crystals of RbCl, RbCl:Sr^{2+} and RbCl:S^{2-} were prepared for us by Dr. Jaanson of the Institute of Physics, Estonian Academy of Sciences. The RbCl used for these crystals was purified using zone-refining.

Samples for the experiments are cleaved from these crystals and microtomed into parallelepipeds. Powdered graphite is rubbed onto the large microtomed faces until a highly conductive surface is obtained in order to assist

perfect contact, i.e. zero resistance, between the external electrodes and the crystal faces. The crystal edges are cleaved to remove any excess graphite.

The geometrical factor is determined by room temperature measurement of the crystal dimensions using a Mitutoyo Profile Projector Type PJ-250. This measurement is repeated after the experiment. Thermal expansion is corrected for during data analysis. In addition, samples are weighed before and after the experiment to check for sublimation and the difference between these weights was never greater than two percent.

4-4 Procedure

After the crystals are placed in the sample holder and the cell is fitted into the furnace, the system is pumped down to a pressure of 1-2 $x10^{-5}$ mbar. The cell is then heated to 200 °C in order to dry the system. Once the pressure has stabilized at a minimum pressure of 1-1.5 $x10^{-5}$ mbar, the cell is isolated from vacuum, filled with argon and heated to 600 °C over a period of eight hours. After a short annealing period at 600 °C of two hours, the system is cycled between 600 and 630 °C over a period of three hours. If the temperature and conductance readings are reproducible, then the crystals have equilibrated and the experiment is started.

The crystals are heated to 716 °C and the temperature is allowed to stabilize for a further 15 minutes. The

thermocouple and bridge readings are then taken, in the sequence temperature-conductance-temperature-conductance-temperature. The furnace setpoint is then decreased and the crystals are allowed to equilibrate over a 15 minute period. Temperature and conductance are again read and this pattern is repeated over the desired temperature range. The furnace temperature is decreased in decrements of 2 °C until 600 °C is reached. Below 600 °C it is decreased by 5 °C decrements. The data is plotted continuously on the computer screen in the form log σT versus 1/T in order to monitor the progress of the experiment.

The temperature was measured at each face of the crystals and the gradient was never greater than 0.1%. The conductance measurements were made at 120 Hz, 300 Hz and 1.02 kHz, 10.2 kHz. These four measurements were made to check for frequency dependence. The variation in conductance readings with frequency was never greater than 0.2% and it was concluded that the conductivity due to relaxation effects was not important.

In order to reduce noise effects and increase resolution, the conductance measurements are averages of thirty-two measurements made over a period of nine seconds. The criteria for acceptable temperature readings is that two consecutive averages of ten measurements each must lie within 0.1 K of each other. In addition, there is a delay of two minutes after switching to allow time for the reading to settle.

Once the system has cooled to room temperature, the crystals were removed from the cell and examined for any possible cracks and damage. If the crystal showed macroscopic damage then the run was rejected. The crystal dimensions were also re-measured.

4-5 Analysis of Concentration

The dopant concentration of the RbCl:Sr^{2+} crystals was measured using a Dionex DX-100 ion chromatograph (I.C.) and an IonPac CS10 cation exchange column. The I.C. was controlled by Dionex AI-450 Chromatography Software. Standards covering the range of possible concentration levels in the crystals were prepared using ultrapure H_2O and Fisher Scientific Atomic Absorption standard 1000 ppm Sr^{2+}. A calibration curve was generated using the peak height of 1, 2, 6, 10 and 20 ppm standard solutions. The crystals were dissolved in ultrapure H_2O and the concentrations of Sr^{2+} were determined from the height of the peak generated. An I.C. was run using 1 ml ultrapure H_2O and 50μl of 1000 ppm Sr^{2+}. This was compared with another I.C. run with 1 ml of a crystal solution and 50 μl of 1000 ppm Sr^{2+}. The retention times were identical and the peak heights were the same within the constraints of the equipment. These two ion chromatographs demonstrated that it was the Sr^{2+} concentration that was measured in the crystal solutions, and that the large excess of Rb^{+} did not interfere with the Sr^{2+} peak. The detection limits were determined using a

1 ppm solution of Sr^{2+} run at 0.3 μS full scale. The signal-to-noise ratio gave a detection limit of 0.36 ppm. All three crystal solutions were well above that limit.

The pure crystals were not analysed for Ca^{2+} concentration because the dopant level would have been below the detection limits. The anion doped crystals were not analysed for S^{2-} concentration because a suitable method was not available for the low levels present in these crystals. However, in such cases the impurity concentration can be determined from the data analysis (Chapter 5).

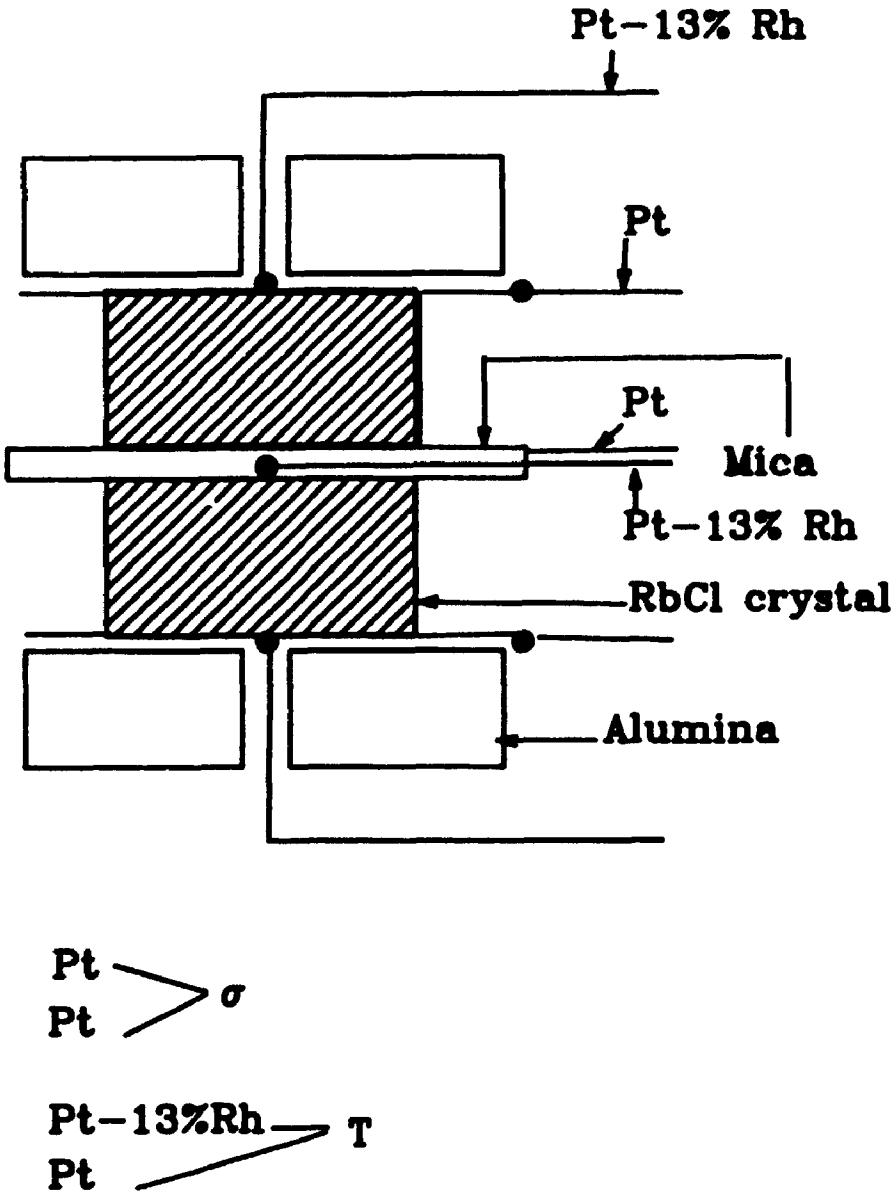

Figure 4–1: Electrode system

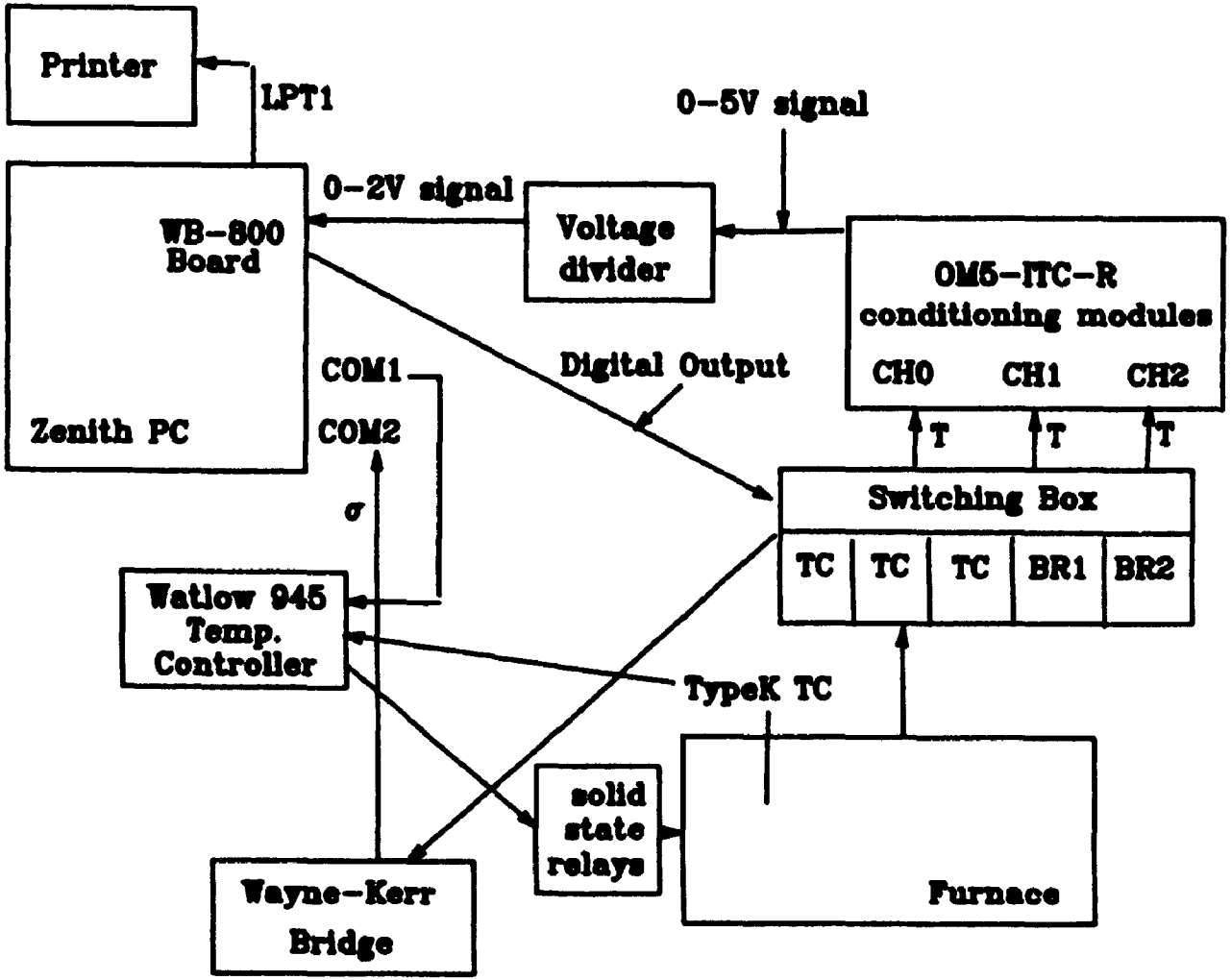

TC = thermocouple
BR = bridge

Figure 4–2: Schematic of automated experimental apparatus.

Chapter 5

Results and Analysis

5-1 Characterization of Conductivity Experiments

The ionic conductivity is a function of the concentrations and mobilities of the contributing defect species. The concentration is exponentially dependent on the inverse temperature. The mobility depends exponentially on the inverse temperature and is also inversely dependent on the temperature. The conductivity may therefore be written,

$$\sigma = \sum_r (A_r / T) \exp(-g_r / k_B T) \qquad (5\text{-}1)$$

where, g_r is the Gibbs energy for species r and A_r is a pre-exponential factor[6]. Thus, the results of ionic conductivity experiments are typically plotted in Arrhenius form, $\log(\sigma T)$ versus $1/T$. This type of plot is generally characterized by two curves separated by a region of much greater curvature called the 'knee'. In the upper region, the magnitude of the conductivity is determined by thermally generated defects and is dependent on the properties of the crystal. This high temperature 'intrinsic' portion should therefore be reproducible in different crystal specimens. The shape of the lower region is specific to the sample chosen. That is, the low temperature 'extrinsic' conductivity is dependent on the nature and concentration of

the impurities in the crystal.

5-1 Crystal Samples

Conductivity data from nine crystals were selected for analysis and fitting--three pure, three cation-doped and three anion-doped. Two of the pure crystals (#4-1, #4-2) were run together and the third (#2-1) was run with a sulphide-doped crystal (#3-1). The other two RbCl:S^{2-} crystals chosen were run at the same time (#1-3, #5). Two of the strontium-doped crystals were from the same crystal section (#1-1, #1-2). The third Sr^{2+}-doped crystal was from a different crystal section (#6-1). The first number in the sample code is the section of the zone-refined crystal. The second number indicates the cleaved sample of the section.

The first criterion for selection was an absence of apparent damage to the crystal, for example, cracks or crystal deformation. The second criterion was that the change in the cell constant be within one percent The final criterion is that the Arrhenius plot of $\log(\sigma T)$ versus $1/T$ be smooth and continuous. In addition, the Arrhenius plot of each type must resemble others of the same type with regards to its general shape.

5-1.2 RbCl:pure

The Arrhenius curves of the pure crystals are shown in Figure 5-1. The curves for the two samples of section 4 are superimposed which is indicative of the good reproducibility

of the measurements. The curve for sample 2-1 reproduces the other two at high temperatures and lies below them in the extrinsic region. This is reasonable if one considers that pure crystals commonly have residual impurities and that these impurities may be present in varying amounts. The impurities are unidentified but are likely Ca^{2+} and are referred to as such for convenience. The concentrations determined in the data analysis are consistent with this argument--sample 2-1 has a concentration of 1.3 ppm while #4-1 has a level of 1.7 ppm and #4-2 has a level of 1.9 ppm. The slightly higher concentration of Ca^{2+} in samples 4-1 and 4-2 would result in more cation vacancies and thus a slightly higher conductivity in the extrinsic region.

The upper limit of the extrinsic region may be considered to be the temperature at which the intrinsic disorder and the impurity concentration are equal[Lid]. Thus the long curved knee exhibited by all three pure samples indicates a large transition region.

5-1.3 RbCl:Sr^{2+}

The Arrhenius plots for the strontium-doped crystals are shown in Figure 5-2. The difference in conductivity due to the small concentration differences between the crystals is not readily apparent from their conductivity curves on this scale. This would indicate that the enhancement of conductivity due to the greater Sr^{2+} doping is not sensitive to small concentration differences.

In all three cases, at the highest temperatures there is an upwards curvature which signifies the transition region or knee as the temperature of the samples move towards the intrinsic region. The long extrinsic region has a downward curvature which is due to formation of Sr^{2+}-cation vacancy complexes. The precipitation of $SrCl_2$ is generally characterized by a sudden drop in conductivity at the lowest temperatures. This effect is not apparent from the Arrhenius plots, however, in all three cases, the fitting fails at the lowest temperatures, which is probably the result of $SrCl_2$ formation.

The ratio of the conductivities of the doped crystals to pure crystal 2-1, σ/σ_0, were plotted against 1/T, over the temperature region analysed, in order to illustrate the enhancement in conductivity due to doping (Figures 5-3, 5-4, 5-5). The ratio at the highest temperatures analysed was approximately 1.3 for each sample, indicating extrinsic behaviour. σ/σ_0 increases to a maximum after which the association of impurities with cation vacancies becomes important and the conductivity ratio falls.

5-1.4 RbCl:S^{2-}

The Arrhenius plots for the sulphide-doped samples are shown in Figure 5-6. The curve for sample 1-3 includes points in the region 800-690 K that were interpolated from the experimental data. This was necessary because the electrodes shorted out in this region. The high temperature

region for sample 5 demonstrated some interesting features that were not apparent in the slightly more doped samples 1-3 and 3-1. This region is compared to that for the pure 2-1 in Figure 5-8 (967-909 K) and in Figure 5-7 (967-467 K). The differences between the pure and the S^{2-}-doped samples are small but are significant within the precision of the measurements. The ratios, σ/σ_0, were plotted for each sample in the temperature region of the data analysis and the results are shown in Figures 5-9, 5-10, 5-11.

At the highest temperatures, the Arrhenius curve for #5 shows a conductivity that is slightly greater than that of the pure crystal (Figure 5-8). This small enhancement is expected and is due to the higher mobility of the anion vacancies relative to the cation vacancies at high temperatures. This continues until, at approximately 936 K ($1.068*10^{-3}$ K^{-1}), the conductivity of the S^{2-}-doped sample decreases slightly to become equal to that of the pure. The conductivity moves below that of the pure at approximately 923 K ($1.083*10^{-3}$ K^{-1}). This effect is emphasized in the ratio plot where σ/σ_0 is less than one and is a result of the presence of a smaller Ca^{2+} concentration in the doped sample without a compensating increase in the sulphide concentration (see Table 5-2).

At 768 K ($1.302*10^{-3}$ K^{-1}), the cation vacancy concentration is still lower than in the pure but the anion vacancy concentration has risen above that in a pure crystal at the same temperature and this effect results in a σ/σ_0

ratio of one. The conductivity continues to rise relative to the pure as the anion vacancies created by the presence of S^{2-} impurities become increasingly important. σ/σ_0 then goes through a maximum at 654 K ($1.529*10^{-3}$ K^{-1}), also seen in the downward curvature of the Arrhenius plot at this point, and starts to decrease. This is due to the influence of anion association and continues until the sulphide is either associated or has precipitated as Rb_2S. At this point the conductivity is due to the residual Ca^{2+}. As the temperature further decreases, the sample appears to be spuriously pure due to the precipitation of a small amount of the Ca^{2+} which is naturally present in the samples.

The intrinsic region for sample 3-1 was displaced by a constant amount which was in excess of the measurement error. This amount was inconsistent with the small enhancement expected due to the greater anion vacancy mobility and was manifested in the fitting by a higher anion vacancy migration entropy. In order to compensate for this unexplained displacement, the curve for sample 3-1 was shifted by a constant factor that allowed for the overlay of the pure 2-1 and S^{2-} 3-1 intrinsic regions and the data refitted. The resultant Arrhenius curve follows the same pattern as that observed for sample 5 in the extrinsic region, with the σ/σ_0 ratio reaching a maximum at approximately the same temperature.

The Arrhenius curve for sample 1-3 is slightly higher than that of the pure at the highest temperatures and

remains so throughout the experiment. The concentration of the sulphide was determined to be 1.2 ppm, which is the highest concentration of the three samples, and the Ca^{2+} concentration is 0 ppm. This means that all the Ca^{2+} is paired or precipitated by the S^{2-}. This sample therefore contains a higher c_{av}/c_{cv} ratio than does the pure crystal and, because of the higher anion mobility, σ/σ_0 is therefore greater than one. The conductivity at the lowest temperatures is the highest of the three sulphide-doped crystals due to the greater S^{2-} concentration.

5-2 Analysis of the Data

The aim of the analysis of the conductivity data was to determine a self-consistent set of defect parameters. That is, a set of parameters that would describe the formation, migration and association of defects in the pure, cation-doped and anion-doped crystals studied. The determination of an accurate set of values requires an appropriate defect model and the application of a non-linear least squares fitting routine. The data can then be fitted to the theoretical expression for conductivity, initially using estimates for the parameters. A parameter set is determined for each crystal specimen by minimizing the residual sum of squares, RSS, and maximizing the number of sign changes of the residuals.

$$RSS = \sum ((\sigma_{exp} - \sigma_{calc}) / \sigma_{calc})^2 \qquad (5\text{-}2)$$

The final parameter set is the average of the individual sets.

5-2.1 Theoretical Conductivity Model

The defect model that best described the conductivity data was one which, in addition to Schottky defects, also included Frenkel defects on both the cation and anion sublattices. The model assumed that both anion and cation impurities would form vacancy-impurity complexes.

Using initial estimates of the defect parameters, the equilibrium constants for each species, K'_r, were calculated using the Gibbs energy of defects, $g_r = h_r - Ts_r$. The equilibrium constants are also given in terms of the activities of each species, a_r, for later reference

$$K'_S = a_{cv}\, a_{av} = K_S\, f_{cv}\, f_{av} = \exp(-g_S/k_BT) \qquad (5\text{-}3)$$

$$K'_{Fc} = a_{cv}\, a_{ci} = K_{Fc}\, f_{cv}\, f_{ci} = 2\, \exp(-g_{Fc}/k_BT) \qquad (5\text{-}4)$$

$$K'_{Fa} = a_{av}\, a_{ai} = K_{Fa}\, f_{av}\, f_{ai} = 2\, \exp(-g_{Fa}/k_BT) \qquad (5\text{-}5)$$

where f_r is the activity coefficient of species r, k_B is the Boltzmann constant and T is the temperature in Kelvin. There is a factor 2 in (5-4) and (5-5) because there are two interstitial sites per lattice site available in the fcc lattice.

If association is neglected and the activity coefficients are set equal to unity initially, the mole fractions of each species, $n_r = a_r/f_r$, can then be substituted

into the expression for charge neutrality,

$$n_{ci} + n_{av} + c_M = n_{ai} + n_{cv} + c_X \qquad (5\text{-}6)$$

where c_M is the concentration of divalent cation impurity, and c_X is the concentration of divalent anion impurity. Substituting Equations (5-3), (5-4) and (5-5) into (5-6) yields a quadratic in n_{cv}, which can then be solved to give an initial estimate of the concentration of cation vacancies.

The equilibrium constants for impurity-vacancy complexes were next calculated using the Gibbs energies of association,

$$K'_{ck} = K_{ck}/f_{cv}\ f_M = 12\ \exp(-g_{ck}/k_BT) \qquad (5\text{-}7)$$

$$K'_{ak} = K_{ak}/f_{av}\ f_X = 12\ \exp(-g_{ak}/k_BT) \qquad (5\text{-}8)$$

where the factor 12 is the number of distinct complex configurations.

The Debye-Hückel screening constant, κ, was then calculated from the equation,

$$\kappa^2 = (8\ \pi\ q^2\ n_{cv})\ /\ ((2a^3)\ \epsilon_s\ k_BT) \qquad (5\text{-}9)$$

where q is the ionic charge, a is the lattice parameter and ϵ_s is the static dielectric constant. The lattice parameter was calculated from thermal expansion data[42],

$$a = a_0(1 + (-0.886 + 2.292*10^{-3}T + 2.709*10^{-6}T^2 - 9.101*10^{-10}T^3)/100) \qquad (5\text{-}10)$$

where, $a_0 = 3.284*10^{-10}$m and T is the temperature in Kelvin.

The dielectric constant was calculated from equation (5-11), which was obtained by fitting the data of Lowndes and Martin[23] and Chandra *et.al.*[43],

$$\epsilon_s = 4.65258 + 1.19*10^{-3}\,T + 1.00*10^{-5}\,T^2 - 9.66*10^{-8}\,T^3 + 3.17*10^{-10}\,T^4 - 4.33*10^{-13}\,T^5 + 2.16*10^{-16}\,T^6 \qquad (5\text{-}11)$$

κ could then be used to calculate the activity coefficients using Lidiard's adaptation of the Debye-Hückel theory of electrolytes[3]. The activity coefficients are written as

$$\log f_r = -(q^2 / 2\epsilon_s k_B T) * (\kappa / (1 + \kappa R_r)) \qquad (5\text{-}12)$$

where R_r is the distance of closest approach for separate ionic species. The values of R_r used were $\sqrt{3}a$ for Schottky defects, $(\sqrt{11}/2)a$ for Frenkel defects, and 2a for vacancy-divalent impurity complexes.

Once the activity coefficients were calculated from (5-12), they could then be used to calculate the 'unprimed' equilibrium constants from equations (5-3), (5-4), (5-5), (5-7) and (5-8). Then, using these values and equation (5-6) modified to include impurity-vacancy complexes

$$n_{ci} + n_{av} + c_M + n_{ck} = n_{ai} + n_{cv} + c_X + n_{ak} \qquad (5\text{-}6')$$

fourth-order equations in terms of either n_{cv} or n_{av} were obtained. These equations were solved numerically using Newton's method and the concentrations of the other defect species were calculated from the equilibrium expressions.

The conductivity of a defect species is a function of its mobility and the total conductivity is the sum of the individual contributions, that is

$$\sigma = \sum_r \sigma_r = \sum_r n_r u_r |q_r| \qquad (5\text{-}13)$$

where n_r is the number of species r per unit volume, u_r is the mobility of species r and q_r is the effective charge of species r.

The mobilities were calculated using

$$u_r = u S_r |q_r| a_r^2 \omega_r / k_B T \qquad (5\text{-}14)$$

where the Onsager-Pitts correction factor, u, is given by

$$u = 1 - (e^2\kappa / 3\epsilon_s k_B T(\sqrt{2} + 1)(\sqrt{2} + \kappa R_r)(1 + \kappa R_r)) \qquad (5\text{-}15)$$

and, S_r is the number of equivalent sites into which the defect can jump (S_r=4 for vacancies, and S_r=2 for interstitials). The component of the jump distance along the direction of the electric field is a_r. The jump probability, ω_r, is the fraction of jump attempts that result in the ion surmounting the energy barrier separating

initial and final positions. Thus

$$\omega_t = \upsilon_0 \exp(-\Delta g_t / k_B T) \qquad (5\text{-}16)$$

where υ_0 is the Debye frequency of RbCl, $3.96*10^{12} s^{-1}$.

5-2.2 Fitting Method

The initial estimates of the defect enthalpies were the calculated Hades energies (Chapter 3) and the defect entropies were from Acūna's work on KCl[5]. It was assumed that a small amount of divalent cation impurity was present in the pure crystal samples and that this level of impurity was also present in the sulphide-doped samples. In both cases the concentration of cation impurity was allowed to vary, as was the S^{2-} concentration in the anion-doped crystals. The concentration of Sr^{2+} was held constant at the experimentally determined values in the cation-doped samples.

The cation vacancy migration and association parameters were allowed to vary in one cation-doped sample, with all other parameters fixed, until the root-mean-square of the residuals was minimized over as large a temperature range as possible. The values were then used as starting parameters for a second cation-doped sample and again allowed to vary in the same manner. Once minimized values were obtained, they were used as starting parameters for the third sample, and again allowed to vary. This procedure was repeated

iteratively until the same values were obtained for each sample.

These cation vacancy parameters were then held constant during the analysis of the data for the anion-doped samples. The iterative procedure detailed above was repeated with the sulphide-doped crystals, but now the concentration of anion and cation impurity as well as the anion vacancy parameters were allowed to vary.

The vacancy parameters thus determined were then held constant in the analysis of the data for the pure samples. The Schottky parameters and cation impurity concentration were allowed to vary in the manner described for the cation-doped crystals. The values for the Schottky parameters were then used in the analysis of the data for the cation-doped crystals, and the entire procedure was repeated.

Each time the procedure was repeated different parameters were allowed to vary in order to satisfy the fitting criterion. That is, the root mean square of the residuals must be minimized and the number of sign changes be maximized. This latter condition is simply to ensure that the fitting is random. The third criterion is that the fitting is done over as large a temperature range as possible. Finally, the parameter set must correspond to values that are physically reasonable with respect to calculated values and values determined for other alkali halides. The ideal would be to meet these criteria within the framework of a parameter set that described all the

experimental data equally well. This is impossible to achieve, so the goal was to meet the criteria with individual parameter sets, between which the variation was a minimum.

5-2.3 Results of the Fitting

The defect parameter sets for each crystal specimen are contained in Tables 5-3, 5-4 and 5-5. The final averaged parameter set is contained in Table 5-6. The values that were held constant in a particular sample are marked with an asterisk. The rcot mean square of the residuals and the temperature range over which the data was fitted are also given in these tables.

Examples of the residuals for the final individual fittings are plotted in Figures 5-12, 5-13, 5-14. The deviations between experimental and calculated points were generally less than 1% for the RbCl:Sr^{2+} samples, generally less than 1.5% for the RbCl:S^{2-} samples, and less than 2% for the pure. The deviations in all cases were always less than 2%. The randomness, although not ideal, converged at the same time as the other fitting criteria and could not be further maximized.

The calculated ratios, σ_c/σ_0, were plotted for the six doped samples and compared with the experimental ratios, σ_e/σ_0 (Figures 5-3, 5-4, 5-5 and 5-9, 5-10, 5-11). The agreement with experiment is excellent, in particular for the strontium-doped samples.

It was found that although it was necessary to include cation Frenkel defects in the model, the fitting was not sensitive to small variations in their thermodynamic parameters and it could then be assumed that their concentrations were low. The cation association parameters were allowed to differ in the pure from the values found in the cation-doped samples. This was necessary in order to achieve a good fit to the experimental data and was thought to be a result of the differing nature of the impurities-- Ca^{2+} in the pure and Sr^{2+} in the cation-doped.

5-2.4 Discussion of Conductivity Model and Parameters

The conductivity model traditionally applied to alkali halides is one in which Schottky defects are considered to be the only contributors to matter transport. In NaCl this simple Schottky model was found to be sufficient to describe matter transport properties[4] but in Acuna's[5] work on KCl, it was found that the inclusion of cation and anion Frenkel defects was necessary to explain the observed properties successfully.

The conductivity data for RbCl were analysed using only one model because it became apparent very early in the fitting that anion Frenkel defects were important. This is reasonable if one considers the Arrhenius energies for RbCl from Table 5-7. Using the calculated energies as a guide to the enthalpies, it is apparent that cation and anion interstitials should contribute to matter transport. The

inclusion of Frenkel defects on the cation sub-lattice was necessary in order to effect a better fit to the data. However, as was stated previously, the concentrations of cation Frenkel defects are considered to be low.

The ionic conductivity of RbCl has not been examined to any large extent and so experimental comparison is limited to a few studies. Fuller and Reilly[44] measured the conductivity of pure RbCl in the intrinsic region and evaluated the cationic and anionic migration contributions. They found the enthalpies of cation and anion migration to be 0.54 eV and 1.45 eV, respectively, and observed that for alkali-metal chlorides, as the difference in ionic radii decreases, the difference between cation and anion activation enthalpies increases. This observation is in contradiction to the general trend in the alkali halides that the difference in activation enthalpies decreases with decreasing ionic radii[6]. In RbCl, the cation and anion are similar in size, with a difference of 1.00*10-12 m [36]. It may be that the model chosen for the least squares analysis was not entirely correct.

Shukla and Rao[45] also studied the ionic conductivity of pure RbCl. They equated the cation migration energy with the activation energy for the extrinsic region which they found from the slope to be 0.93 eV. The Schottky energy was estimated to be 2.12 eV using the Arrhenius energy determined from the slope of the intrinsic region. The Arrhenius energies found from the slope can only serve as an

approximation because of the non-linearity of the Arrhenius plots (Figures 5-1, 5-2 and 5-6). This curvature is due to the presence of more than one transport mechanism. Thus, their values can only be used as a rough guide to the actual defect parameters.

Jurczak and Whitmore[46] measured the ionic conductivity of pure and Ba^{+2}-doped RbCl in the temperature range 523-963 K. The data was fitted using the Schottky model and allowed for the association of cation vacancies with divalent cation impurities on nn cation sites. Their Schottky formation enthalpy was 2.24 eV and the corresponding entropy was 8.47 k. The cation vacancy migration enthalpy was determined to be 0.44 eV and the entropy was 0.12 k. The anion vacancy migration enthalpy and entropy were 1.31 eV and 10.44 k, respectively. The difference between cation and anion activation enthalpies was considered to be anomalously high but was not explained. As in the case of Fuller *et al.*, this is most likely due to an incorrect choice of the defect model used.

In addition, the determination of defect parameters is best done by fitting data from systems in which that defect is the main carrier. This is achieved by doping the crystal with aliovalent impurities and thus enhancing the contribution from a particular kind of defect. The results of Jurczak *et.al.* then cannot be considered to be completely reliable without the measurement of an anion-doped system which would enhance the anion contributions.

This is also a problem in the first two studies mentioned where the conductivity was measured in the pure crystals only and in the case of the Fuller's study[44], only the intrinsic conductivity was measured.

The diffusion of Na^+ in RbCl was studied by Peterson and Rothman[47]. They estimated the Schottky parameter to be 2.44 eV and the activation energy for cation migration to be 0.55 eV, using a theoretical value for the Na^+-vacancy binding energy. In earlier conductivity experiments[48], they found the Schottky energy to be 2.36 eV and the cation migration to be 0.78 eV. Here again the Arrhenius energies are found from the slopes of the Arrhenius plots and thus, their values are only an approximation.

In view of the lack of properly analysed experimental data for RbCl, it was decided to use a vertical comparison. The work done by Hooton[4] on NaCl and by Acūna[5] on KCl was used for this purpose (Table 5-6). The defect parameters for the three alkali halides were expected to have similar values.

The Schottky enthalpy parameter was initially held constant at the calculated value of 2.52 eV in order to determine a reasonable Schottky entropy. The Schottky enthalpy eventually minimized back to 2.52 eV. This is reasonable in comparison to the value for NaCl of 2.41 eV and the value for KCl of 2.50 eV, as h_s in the alkali halides is typically ~2 eV[6]. The entropy parameter, 8.87 k_B, was also in line with the NaCl value, 8.896 k_B, and

slightly higher than the KCl range, 7.0-7.5 k_B.

The cation and anion vacancy parameters also compare favourably with NaCl and KCl, in particular if one considers the Gibbs energies of migration, $\Delta g=(\Delta h-T\Delta s)$. The difference between the cation and anion migration energies is much less in RbCl and in fact, is negative. This is reasonable if the similarity in ionic radii is considered.

The anion Frenkel formation and migration enthalpies were lower in RbCl than in KCl due to the different nature of the impurity, SO_4^{-2}, and the greater role of the anion interstitial in matter transport in the former material. The formation entropy was higher than expected but this was necessary in order to achieve a good fit and was compensated for by the higher mobility of the anion interstitial. Hooton[4] found that the Schottky model best described NaCl and so did not fit anion Frenkel parameters.

The cation association parameters were less satisfactorily determined. The entropies for Ca^{2+} and Sr^{2+} are not too dissimilar and are believable in comparison with KCl and NaCl values. However, the Ca^{2+} association enthalpy is lower than expected in comparison to the other enthalpies. Unfortunately, this value was necessary in order to achieve any sort of reasonable fit for the pure crystal data. The anion association enthalpy compares well with the value for S^{2-} found in NaCl but the entropy was less easily fitted.

The Arrhenius energies, $E_r= 1/2\ h_r+ \Delta h_r$, found

experimentally for RbCl are in agreement with the calculated values (Table 5-7) and with the values found for NaCl and KCl.

5-2.5 Transport Numbers and Complex Concentrations

Transport numbers, t_r, i.e. the fraction of the total conductivity that the defect species r carries, were calculated for each of the specimens. The cation vacancy transport numbers are shown in Figure 5-15.

In the pure crystals, as the conductivity becomes extrinsic, t_{cv} approaches unity and cation vacancies can be considered to be the dominant charge carrier. However, as the temperature increases, the fraction of current carried by the cation vacancies decreases rapidly as anion vacancies and anion interstitials increase in importance. The proportion of conductivity carried by each of cation vacancies, anion vacancies and anion interstitials levels off at approximately one-third.

The transport number for the cation vacancy in the strontium-doped samples indicates that it is the only charge carrier of note in the lengthy extrinsic region. Transport by anion vacancies and anion interstitials becomes significant at the highest temperatures, with t_{av} increasing to 0.22, t_{ai} to 0.12 and t_{cv} falling to 0.65 at 949 K.

In the extrinsic region of the S^{2-}-doped samples, t_{cv} is zero and transport is completely dominated by anion vacancies. As the temperature increases, anion vacancy

transport still dominates, however, transport due to the cation vacancies and anion interstitials increases to 25% each at 941 K.

The degree of association, p, was calculated for each cation and anion-doped sample as the fraction of impurities that are complexed with vacancies and were then plotted against temperature (Figures 5-16, 5-17).

The RbCl:Sr^{2+} samples show the expected increase in association with decreasing temperature in all three cases. The association curves for the RbCl:S^{2-} samples however, have a parabolic shape. At temperatures below approximately 800 K the same trend of increasing association with decreasing temperature is observed and the curves lie in order of increasing S^{2-} concentration. At temperatures above these minima though, the association increases with increasing temperature. There is an additional effect observed at high temperatures with the 0.83 ppm curve crossing over the 0.71 ppm curve, resulting in a lower degree of association in the more heavily doped sample.

The minima observed are a result of the rising vacancy concentration from the Schottky equilibrium which outweighs the decrease in the number of complexes due to the thermal dependence of the equilibrium constant, K_{ass}. Thus, at higher impurity concentrations, more vacancies are required to produce the same concentration of the complex defect. As a result, a crossover is observed.

5-3 Diffusion

The movement of atoms through a solid is a result of the mobility of point defects and when there is a gradient in composition, relative mass transport occurs to level out these variations. This transport of material in a concentration gradient is known as diffusion. The general transport law, which says that the flow of any quantity, i, is proportional to the force that drives the flow, applied to diffusion is

$$J_i = -D_i \, dc_i/dx \qquad (5\text{-}17)$$

where J_i is the flow, dc_i/dx is the concentration gradient along the x-axis, and D_i is the diffusion coefficient[49].

An understanding of diffusion at an atomic level can be gained by studying the diffusion coefficients and relating them to the physical properties of the defect mechanisms. This also allows a comparison of diffusion and ionic conductivity using the Nernst-Einstein relation

$$D_r = \sigma_r \, k_B T \, / \, ne^2 \qquad (5\text{-}18)$$

where n is the number of ions per unit volume.

5-3.1 Diffusion Coefficient Calculations

Diffusion occurs as a result of the atoms in a solid jumping from one position to another. If those jumps are

random, the diffusion coefficient of a species r, D_r, is given by

$$D_r = \Gamma_r r^2 / 6 \qquad (5\text{-}19)$$

where Γ_r is the jump frequency, and $r^2=2a^2$ is the mean square displacement. At this point it is necessary to distinguish between a "self-diffusion coefficient" and a "tracer diffusion coefficient"[3]. The former measures the rate of migration of species r relative to the crystal lattice and the latter measures the migration rate of an isotope of species r.

In the former, it is impossible to distinguish between the individual ions. However, for tracer diffusion, the diffusing ions are distinguishable and it is possible to detect their individual movements. In solids, the movement is not necessarily a random walk and in fact, for some mechanisms, such as ionic jumps, the movements are correlated[50].

For example, if a vacancy mechanism holds for tracer diffusion, a tracer having exchanged with a vacancy has a better than random chance of executing the reverse jump. The expression for the tracer diffusion coefficient, D_r^*, must then include a correlation factor, f. This factor depends on the crystal lattice as well as on the mechanism of ionic transport[51]. The correlation factor for vacancies in an fcc lattice is 0.78146, and for interstitials jumping

by the collinear interstitialcy mechanism, is 1/3.

The jump frequencies, υ_r, can be calculated from the defect parameters in Table 5-6 using the expression

$$\upsilon_r = \upsilon_0 \exp(\Delta s_r / k_B) \exp(-\Delta h_r / k_B T) \qquad (5\text{-}20)$$

The jump rate, Γ_r, is the product of the jump frequency and the number of equivalent sites available

$$\Gamma_r = 12\ n_r\ \upsilon_0 \exp(-\Delta g_r / k_B T) \qquad (5\text{-}21)$$

If these relations are substituted into equation (5-19), the following expressions are obtained

$$D_{cv} = 4\ a^2\ f_S\ n_{cv}\ \upsilon_{cv} \qquad (5\text{-}22)$$

$$D_{av} = 4\ a^2\ f_S\ n_{av}\ \upsilon_{av} \qquad (5\text{-}23)$$

$$D_{ci} = 4\ a^2\ f_i\ n_{ci}\ \upsilon_{ci} \qquad (5\text{-}24)$$

$$D_{ai} = 4\ a^2\ f_i\ n_{ai}\ \upsilon_{ai} \qquad (5\text{-}25)$$

Vacancy pair contributions to diffusion must also be considered. At low temperatures, the measured diffusion rate is higher than expected from conductivity results and is a consequence of the mobility of vacancy pairs[3]. The vacancy pairs contribute to the diffusion but not the conductivity because they are electrically neutral. The concentration of vacancy pairs is given by

$$c_p = 6 \exp(-g_p / k_B T) \qquad (5\text{-}26)$$

where, g_p is the pair formation Gibbs energy and is equal to that for the formation of a Schottky defect plus that for the formation of a pair. The factor 6 arises from the orientational entropy.

The jump frequencies are given by

$$\upsilon_{cp} = \upsilon_0 \exp(-\Delta g_{cp} / k_B T) \qquad (5\text{-}27)$$

$$\upsilon_{ap} = \upsilon_0 \exp(-\Delta g_{ap} / k_B T) \qquad (5\text{-}28)$$

and the jump distance is the same as for single vacancies, $\sqrt{2}a$. The correlation factor is a function of the anion and cation jump frequencies, $f_{cp} = \Phi(\upsilon_{ap}/\upsilon_{cp})$ and $f_{ap} = \Phi(\upsilon_{cp}/\upsilon_{ap})$[52]. Thus, the diffusion coefficients for vacancy pairs are

$$D_{cp} = (4/3)\ a^2\ f_{cp}\ n_{cp}\ \upsilon_{cp} \qquad (5\text{-}29)$$

$$D_{ap} = (4/3)\ a^2\ f_{ap}\ n_{ap}\ \upsilon_{ap} \qquad (5\text{-}30)$$

5-3.2 Results of Diffusion Coefficient Calculations

The enthalpy of vacancy pair association and the enthalpies for the cation and anion jumps into the pair were held constant at the 0 K energy determined in the HADES calculations (Table 5-8). The entropies were allowed to vary and converged at the values shown in Table 5-8.

The diffusion coefficients were calculated using the individual parameter sets. In addition to the total cation

and anion contributions, the individual contribution of each species to the diffusion was calculated. Each set of three pure, three cation-doped and three anion-doped samples yielded Arrhenius plots which were similar. The plots for RbCl:pure 2-1, RbCl:Sr^{2+} 2-1, and RbCl:S^{2-} 5 are shown in Figures 5-18 through 5-23.

Arai and Mullen[1] studied the diffusion of Rb^{86} in RbCl crystals and their results for the total cation contribution to diffusion agree extremely well with the results for all three pure samples (e.g. Figure 5-18). In the extrinsic region, cation transport is entirely via cation vacancies but as the temperature rises the cation pair contribution increases to 43% of the cation total at 960 K. This observation emphasizes the temperature dependence of the vacancy pair equilibrium and the higher Gibbs energy of the cation jump into the pair than that for cation vacancy migration by single vacancies.

In the strontium-doped crystals the intrinsic region is absent and the cation contribution is almost due entirely to cation vacancies. An upward curvature is observed at the highest temperatures due to the influence of cation pairs in the transition region (Figure 5-19).

In the sulphide-doped sample 5, the cation vacancies and cation pairs contribute 53% and 46%, respectively, to the total cation transport at 940 K (Figure 5-20). As the temperature decreases, however, the cation vacancy contribution at first increases slightly and then the curve

bends downward at approximately 630 K. This is a result of a decrease in c_{cv}, which drops an order of magnitude between 630 and 600 K. The cation pair contribution is linear throughout the temperature range since the concentration of pairs is independent of the impurity concentration. At the lowest temperatures the cation interstitials contribute the largest proportion to the cation diffusion. This observation is also true in the conductivity analysis--at the lowest temperatures the contribution of the cation interstitials is greater than that of the cation vacancies. This is a result of a decreased concentration of cation vacancies due to temperature, which is further decreased by incorporation into impurity-vacancy complexes and vacancy pairs. At any particular temperature, a decreasing concentration of cation vacancies from doping results in an increased concentration of interstitials through the Frenkel defect equilibrium.

In the extrinsic region, the total anion contribution is due entirely to anion interstitials for both the pure and cation-doped samples. In the cation-doped samples, the anion pairs and anion vacancies do not contribute appreciably to the diffusion until the transition region is reached (Figure 5-22). In the pure samples (Figure 5-21), the pairs and vacancies start to influence the diffusion at approximately 676 K. The anion pair contribution is linear throughout the temperature region analysed. In the cation-doped samples, the presence of Sr^{2+} shifts the Schottky equilibrium and fewer vacancies are formed. In addition,

anion interstitials have a greater mobility in comparison to anion vacancies and thus are the major contributors to anion diffusion. This is true to a lesser extent in the pure samples due to the Ca^{2+}-impurities. Hoodless and Turner[2] measured anion self-diffusion and analysed their data using a single vacancy mechanism with additional contribution from vacancy pairs. The small differences between their diffusion results and the calculated diffusion results in the high temperature region cannot be accounted for by differences in sample purity (Figure 5-21).

In the anion-doped sample 5, the total anion contribution is due entirely to anion vacancies until approximately 760 K ($1.316*10^{-3}$ K^{-1}), at which point the pairs and interstitials start to contribute (Figure 5-23).

Table 5-1: Symbols and units for thermodynamic properties determined during data analysis

Symbol	Units	Description
h_S	eV	Schottky formation enthalpy
s_S	k_B	entropy
Δh_{cv}	eV	cation vacancy migration enthalpy
Δs_{cv}	k_B	entropy
Δh_{av}	eV	anion vacancy migration enthalpy
Δs_{av}	k_B	entropy
h_{Fc}	eV	cation Frenkel formation enthalpy
s_{Fc}	k_B	entropy
Δh_{ci}	eV	cation interstitial migration enthalpy
Δs_{ci}	k_B	entropy
h_{Fa}	eV	anion Frenkel formation enthalpy
s_{Fa}	k_B	entropy
Δh_{ai}	eV	anion interstitial migration enthalpy
Δs_{ai}	k_B	entropy
h_{ck}	eV	cation impurity-vacancy association enthalpy
s_{ck}	k_B	entropy
h_{ak}	eV	anion impurity-vacancy association enthalpy
s_{ak}	k_B	entropy
c_M	ppm	cation impurity mole fraction
c_X	ppm	anion impurity mole fraction
h_{vp}	eV	vacancy pair association enthalpy
s_{vp}	k_B	entropy
Δh_{cp}	eV	cation jump into pair enthalpy
Δs_{cp}	k_B	entropy
Δh_{ap}	eV	anion jump into pair enthalpy
Δs_{ap}	k_B	entropy

Table 5-2: Vacancy concentrations in RbCl:S^{-2} 5 and pure 2-1.

	S^{-2} 5		pure 2-1	
T /K	c_{cv} /ppm	c_{av} /ppm	c_{cv} /ppm	c_{av} /ppm
908	6.95	7.25	8.18	7.77
831	1.44	1.78	2.08	1.59
768	0.24	0.59	0.73	0.25

Table 5-3: Final defect parameters for pure RbCl samples

Property	Sample		
	2-1	4-1	4-2
h_S	2.52	2.52	2.52
S_S	8.723	8.723	8.723
Δh_{cv}^*	0 .661	0.661	0.661
Δs_{cv}	2.078	2.078	2.078
Δh_{av}^*	0.725	0.725	0.725
Δs_{av}	3.013	3.013	3.013
h_{Fc}^*	3.457	3.457	3.457
s_{Fc}^*	7.40	7.40	7.40
Δh_{Fc}^*	0.208	0.208	0.208
Δs_{Fc}^*	5.60	5.60	5.60
h_{Fa}^*	3.484	3.484	3.484
s_{Fa}	9.980	9.980	9.980
Δh_{ai}^*	0.188	0.188	0.188
Δs_{ai}	6.996	6.996	6.996
h_{ck}	-0.956	-0.895	-0.897
s_{ck}	-2.201	-2.201	-2.201
c_M	1.30	1.70	1.90
RSS*10^4	4.88	2.23	5.59
T/K	960.7-641.8	959.3-645.0	960.2-645.0

*indicates parameters held constant during fitting process

Table 5-4: Final defect parameters for RbCl:Sr^{2+} samples

Property	Sample		
	1-1	1-2	6-1
h_S	2.52	2.52	2.52
S_S	9.328	9.216	9.182
$\Delta h_{cv}^{\bullet}$	0 .661	0.661	0.661
Δs_{cv}	1.922	1.868	1.776
$\Delta h_{av}^{\bullet}$	0.715	0.715	0.715
$\Delta s_{av}^{\bullet}$	3.289	3.416	3.289
$h_{Fc}^{\bullet}$	3.457	3.457	3.457
$s_{Fc}^{\bullet}$	7.40	7.40	7.40
$\Delta h_{Fc}^{\bullet}$	0.208	0.208	0.208
$\Delta s_{Fc}^{\bullet}$	5.60	5.60	5.60
$h_{Fa}^{\bullet}$	3.484	3.484	3.484
$s_{Fa}^{\bullet}$	9.062	9.062	9.062
$\Delta h_{ai}^{\bullet}$	0.188	0.188	0.188
$\Delta s_{ai}^{\bullet}$	6.507	6.507	6.507
h_{ck}	-0.607	-0.602	-0.568
s_{ck}	-3 198	-2.915	-2.451
$c_M^{\bullet}$	45.41	49.02	57.06
RSS*10^4	6.53	3.24	2.39
T/K	948.0-527.0	949.0-517.0	949.0-518.0

*indicates parameters held constant during fitting process

Table 5-5: Final defect parameters for RbCl:S^{2-} samples

Property	Sample		
	3-1	5	1-3
h_S^*	2.52	2.52	2.52
S_S	8.365	8.492	8.921
Δh_{cv}^*	0 .661	0.661	0.661
Δs_{cv}	1.816	1.776	1.816
Δh_{av}	0.709	0.724	0.724
Δs_{av}	3.366	3.475	3.215
h_{Fc}^*	3.457	3.457	3.457
s_{Fc}^*	7.40	7.40	7.40
Δh_{Fc}^*	0.208	0.208	0.208
Δs_{Fc}^*	5.60	5.60	5.60
h_{Fa}^*	3.484	3.484	3.484
s_{Fa}	9.557	9.223	9.841
Δh_{ai}^*	0.188	0.188	0.188
Δs_{ai}	6.365	6.461	7.007
h_{ck}^*	-0.592	-0.592	-0.592
s_{ck}^*	-2.850	-2.850	-2.850
h_{ak}	-1.044	-0.835	-0.755
s_{ak}	-5.517	-2.619	-1.017
c_M	0.12	0.25	0.00
c_X	0.83	0.71	1.20
RSS*10^4	6.53	3.24	2.39
T/K	909.0-600.0	909.0-576.0	943.0-523.0

*indicates parameters held constant during fitting process

Table 5-6: Final defect parameters for RbCl, KCl[5] and NaCl[4]

Property	RbCl	KCl	NaCl
h_S	2.52	2.50	2.41
S_S	8.853	7.15	8.896
Δh_{cv}	0.661	0.680	0.626
Δs_{cv}	1.912	2.4	1.065
Δh_{av}	0.720	0.843	0.744
Δs_{av}	3.232	5.65	2.272
h_{Fc}	3.457	3.61	3.32
s_{Fc}	7.40	7.40	**
Δh_{Fc}	0.208	0.38	0.170
Δs_{Fc}	5.60	5.60	**
h_{Fa}	3.484	3.710	3.470
s_{Fa}	9.527	8.15	**
Δh_{ai}	0.188	0.280	0.170
Δs_{ai}	6.705	8.90	**
$h_{ck}(Sr^{2+})$	-0.592	-0.625	-0.643
$s_{ck}(Sr^{2+})$	-2.850	-2.50	-2.326
$h_{ck}(Ca^{2+})$	-0.916	-0.590	-0.612
$s_{ck}(Ca^{2+})$	-2.201	-1.50	-2.508
$h_{ck}(S^{2-})$	-0.872	*	-0.751
$s_{ck}(S^{2-})$	-3.051	*	-1.418

*anion dopant used was SO_4^{2-}

**not available

Table 5-7: Arrhenius energies for NaCl[4], KCl[5] and RbCl

Property	NaCl	KCl	RbCl	
			calculated	experimental
E_{cv}	1.83	1.93	1.92	1.92
E_{av}	1.95	2.09	1.93	1.98
E_{ct}	1.83	2.19	1.94	1.94
E_{at}	1.91	2.14	1.93	1.94

Table 5-8: Vacancy pair energies and entropies for RbCl

Property	Value
u_{vp}	-0.940
s_{vp}	0.700
Δu_{cp}	0.795
Δs_{cp}	1.065
Δu_{ap}	0.808
Δs_{ap}	0.950

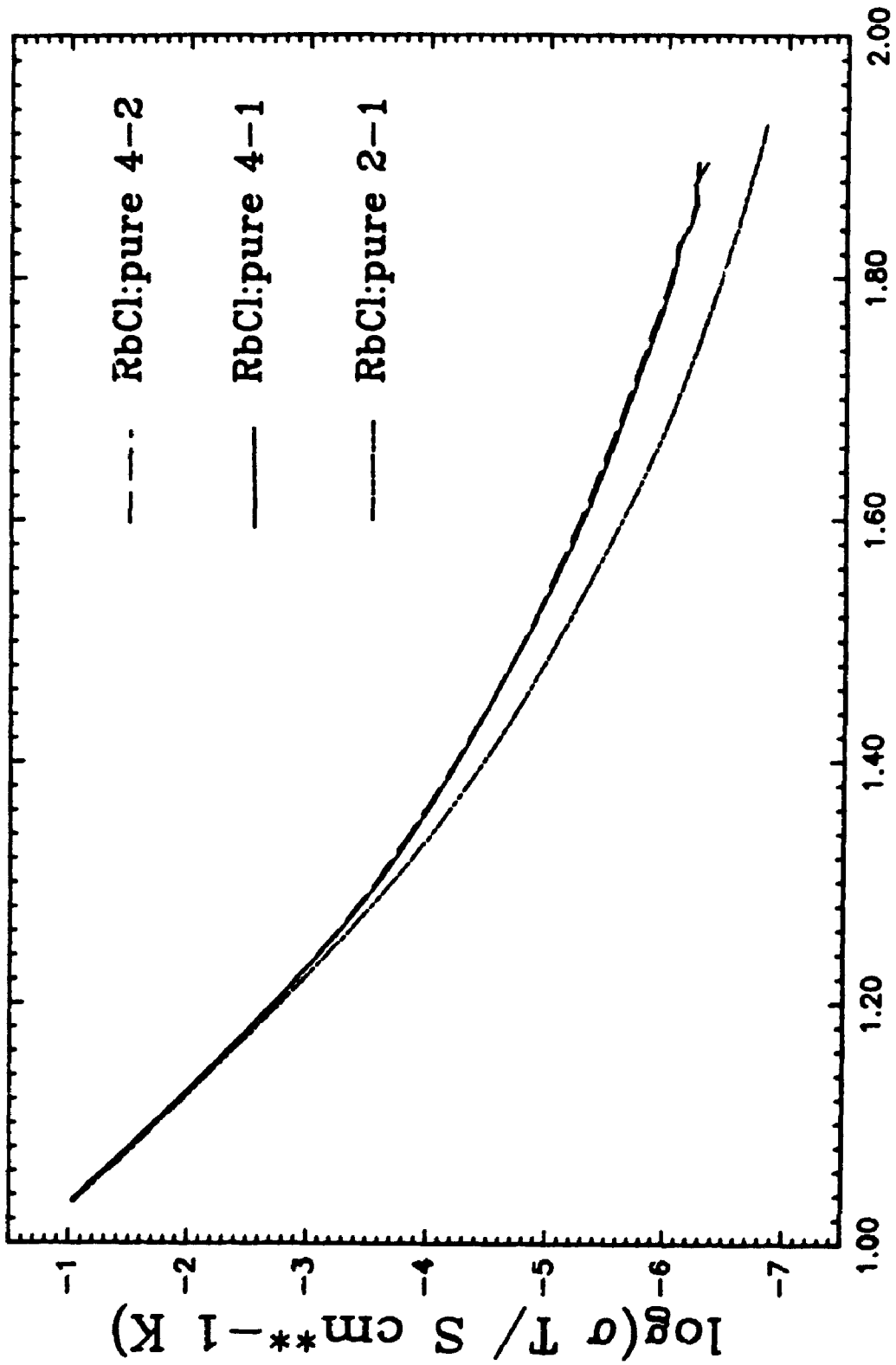

Figure 5-1: Arrhenius plots for RbCl:pure 2-1, 4-1, 4-2

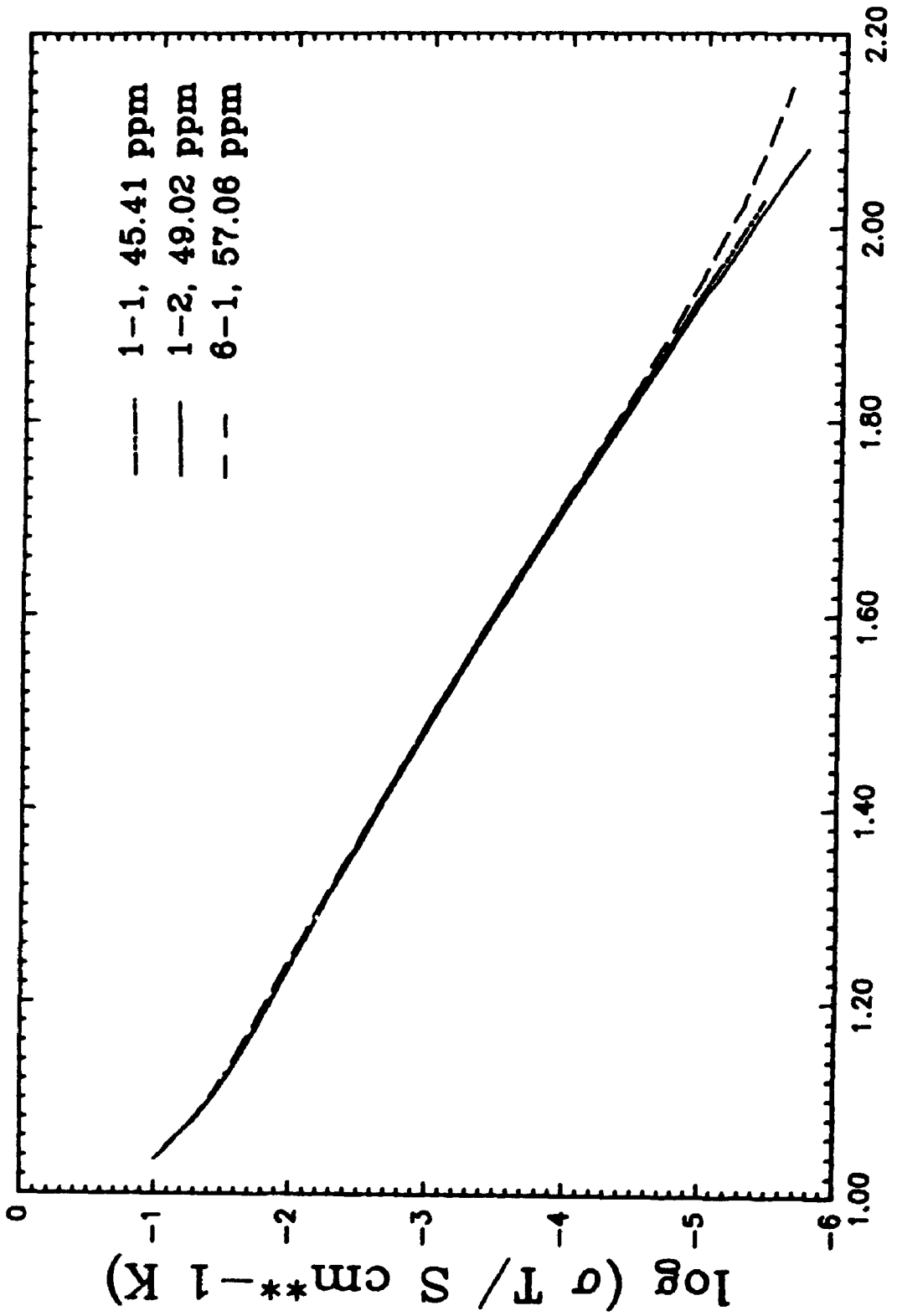

Figure 5-2: Arrhenius plots for $RbCl:Sr^{+2}$ 1-1, 1-2, 6-1

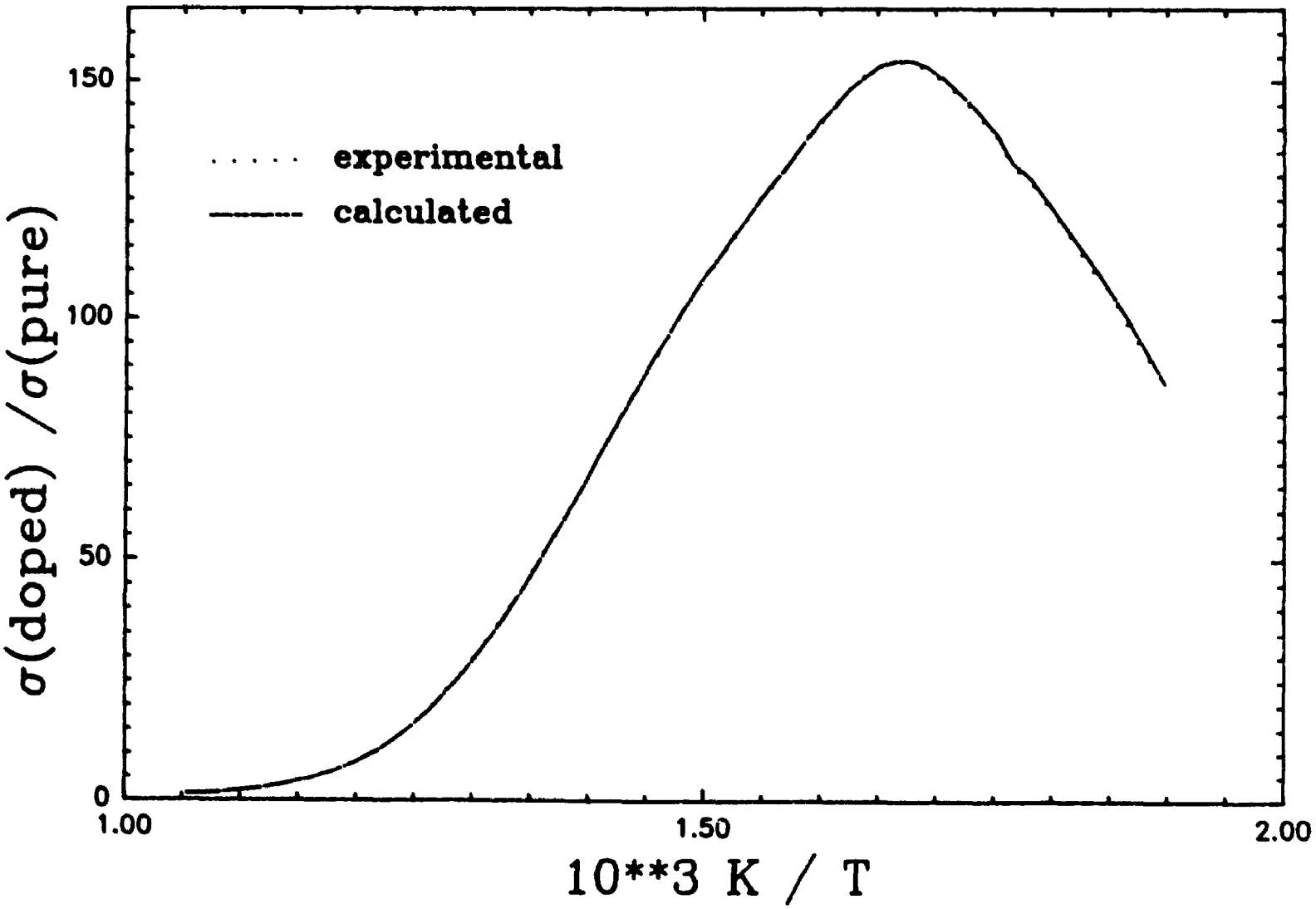

Figure 5–3: Ratio of the conductivities of RbCl:Sr^{+2} 1–1 to RbCl:pure 2–1

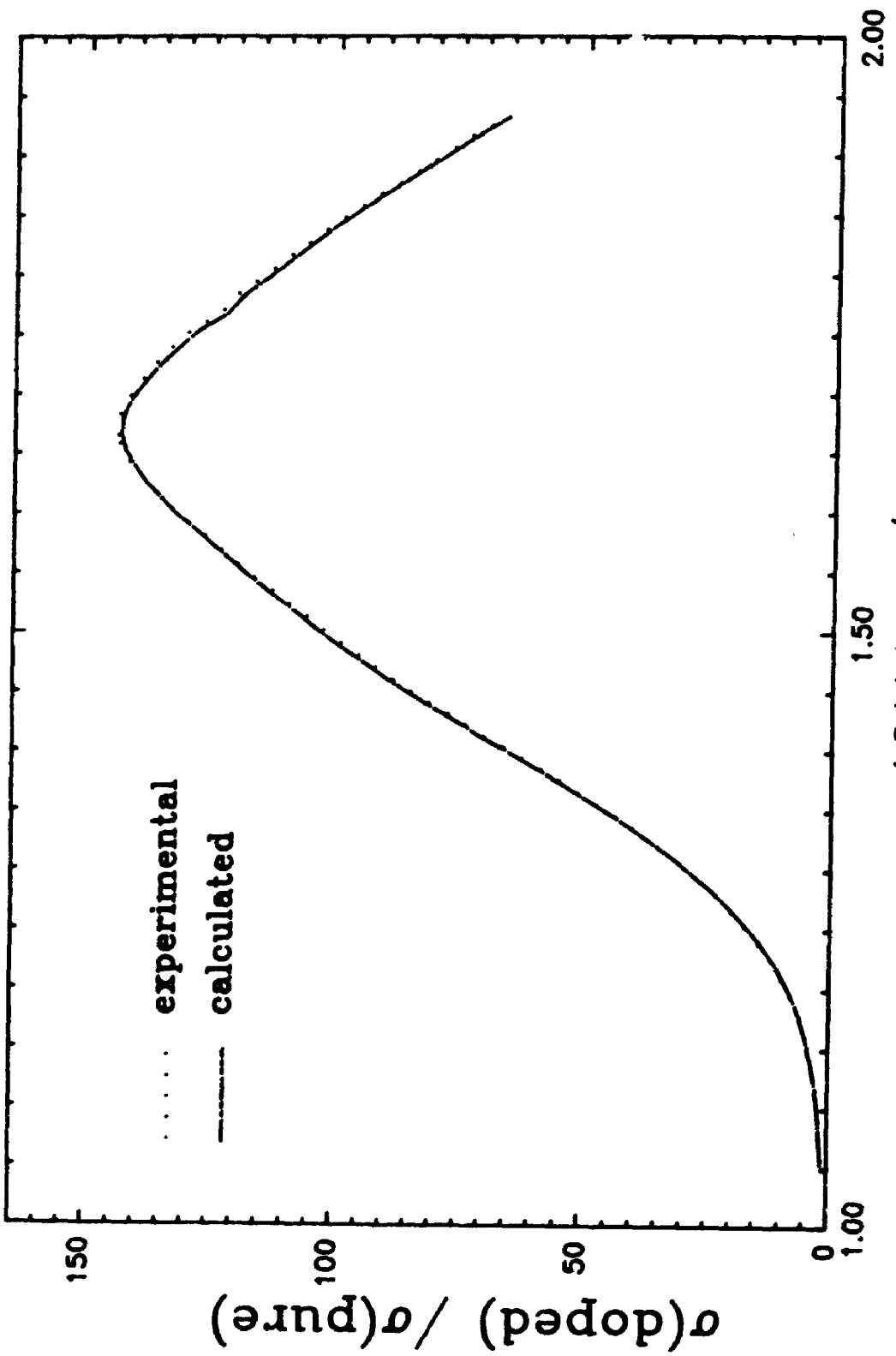

Figure 5–4: Ratio of the conductivities of RbCl:Sr^{+2} 1–2 to RbCl:pure 2–1

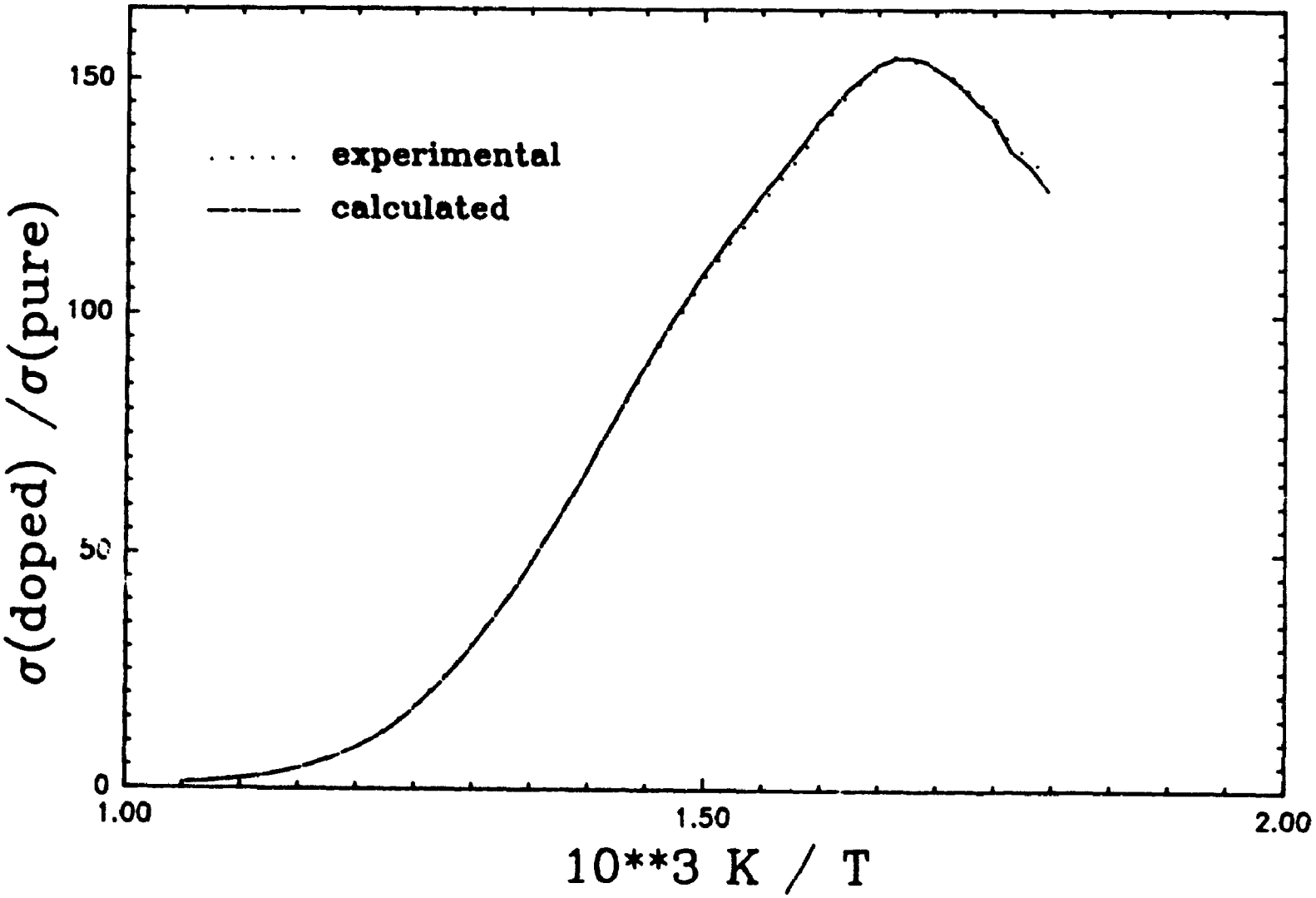

Figure 5–5: Ratio of the conductivities of RbCl:Sr^{+2} 6–1 to RbCl:pure 2–1

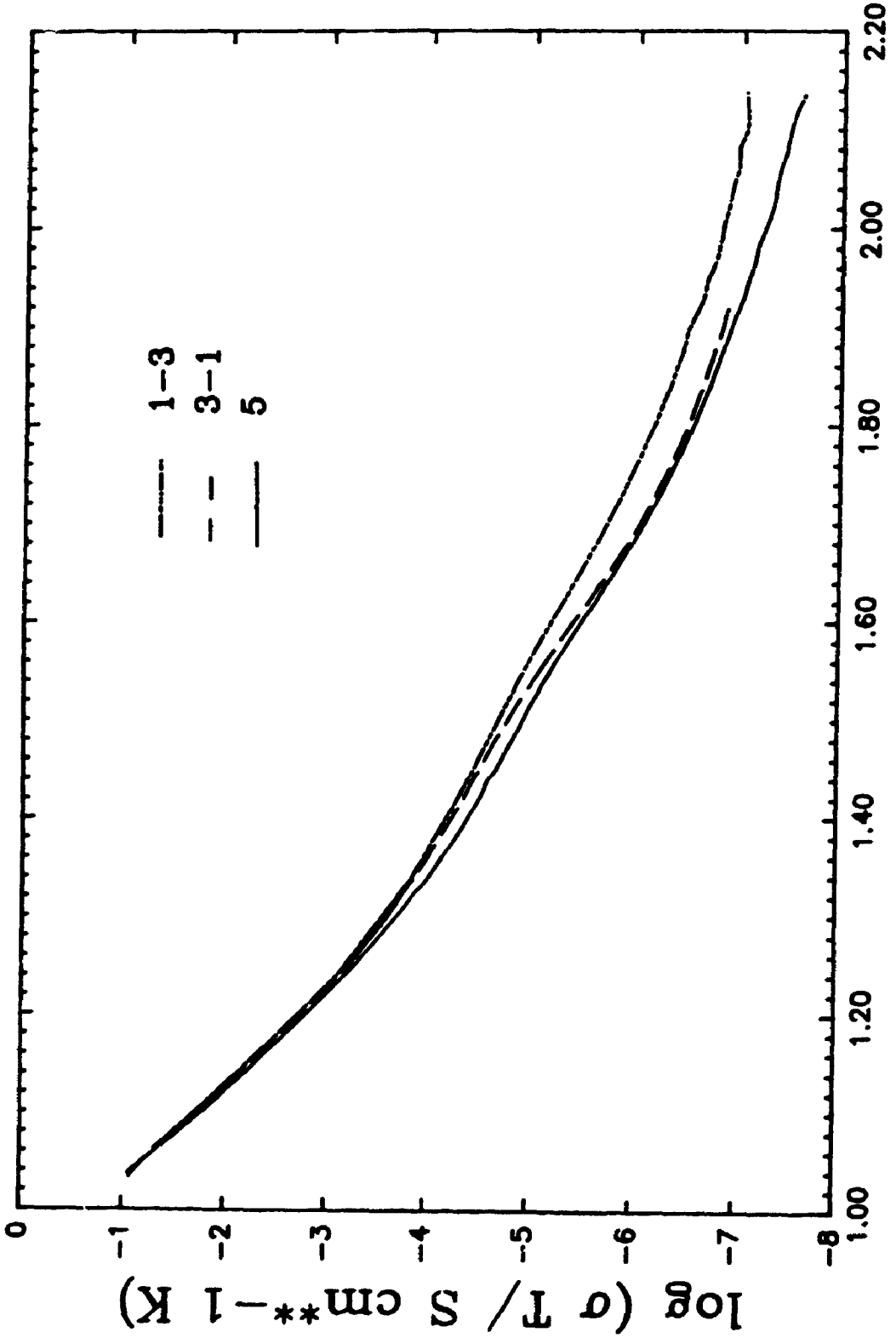

Figure 5-6: Arrhenius plots for RbCl:S^{-2} 1-3, 3-1, 5

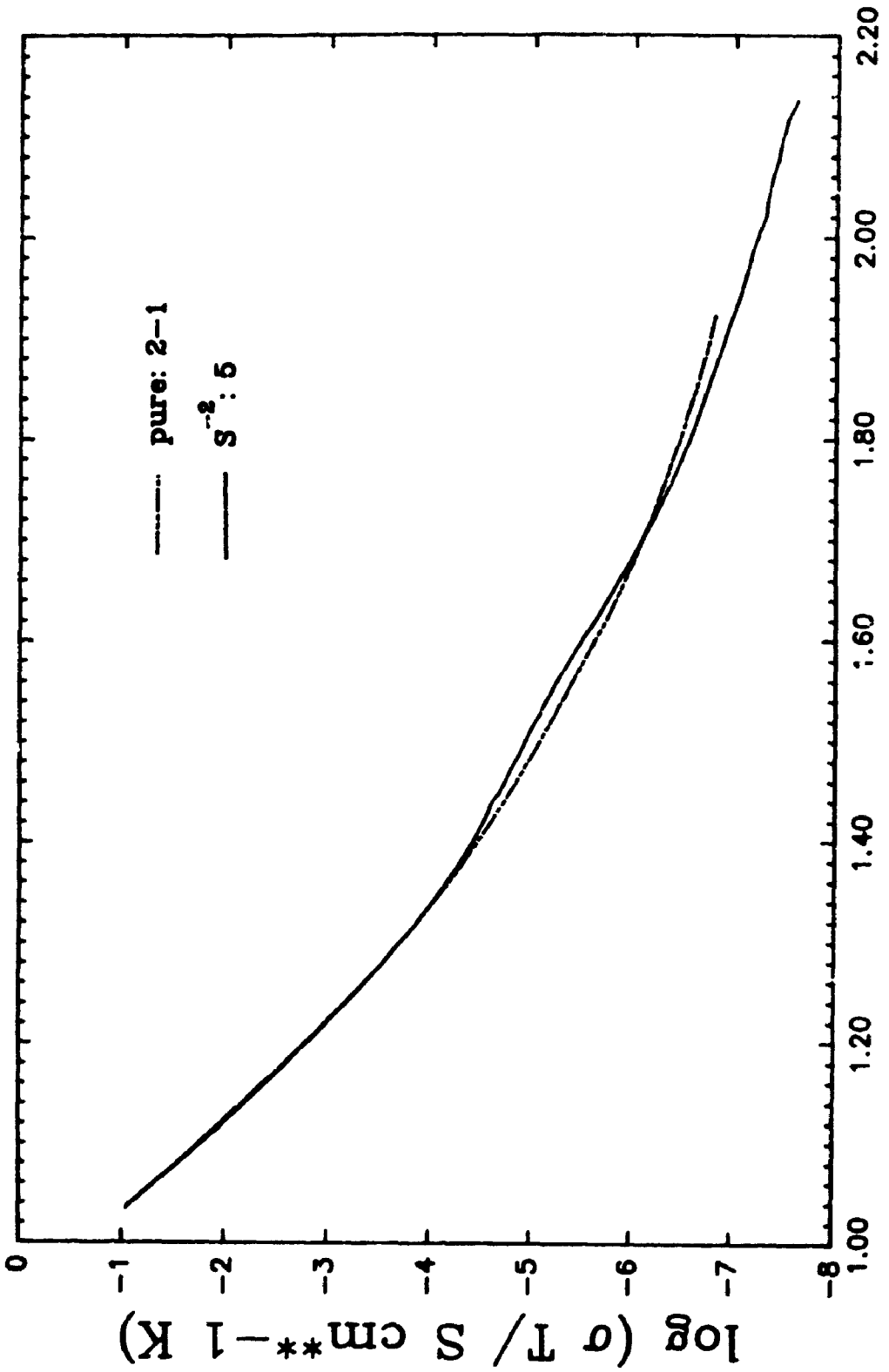

Figure 5-7: Arrhenius plots for RbCl:S^{-2} 5 and RbCl:pure 2-1

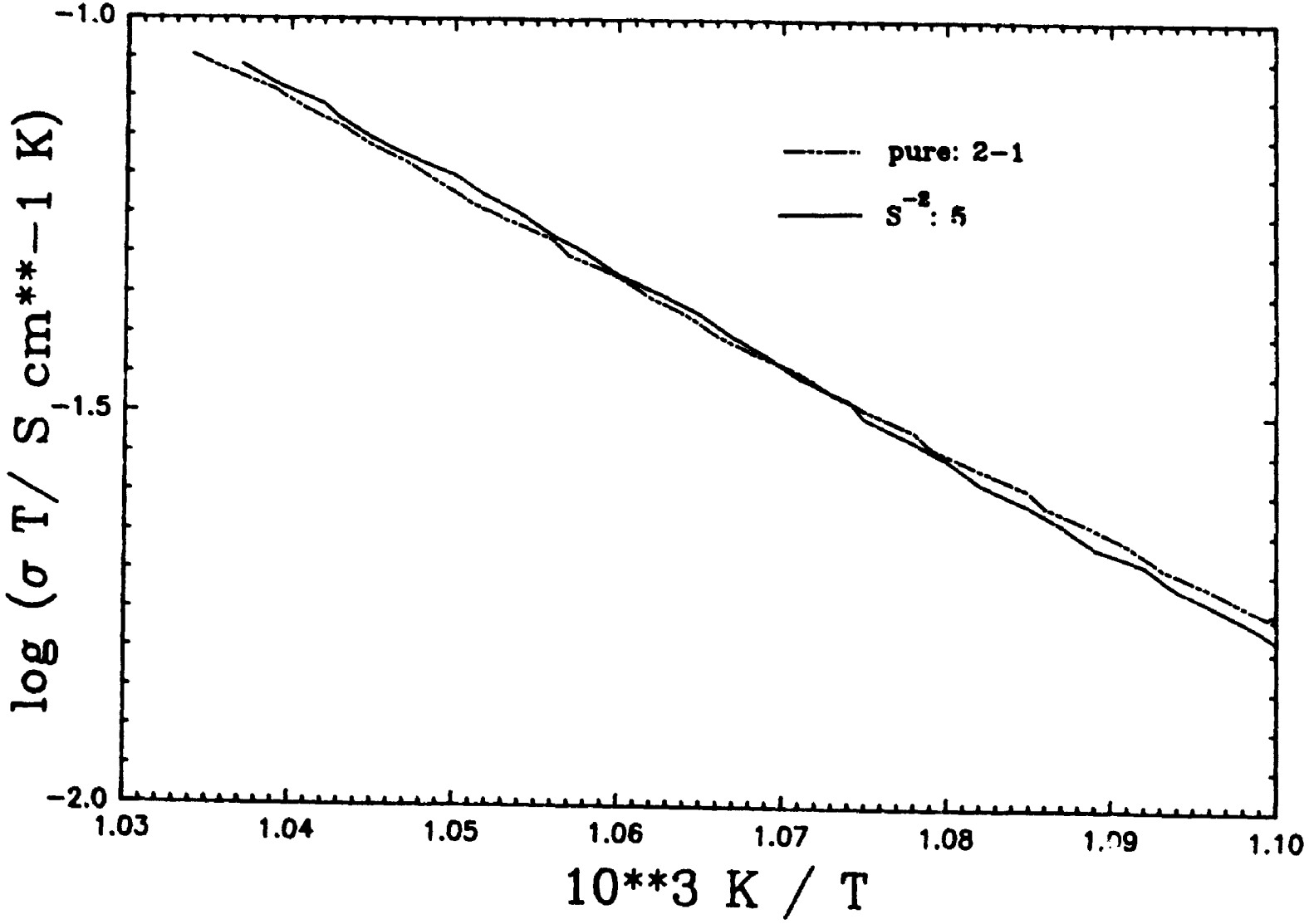

Figure 5−8: Arrhenius plots for RbCl:S^{-2} 5 and RbCl:pure 2−1

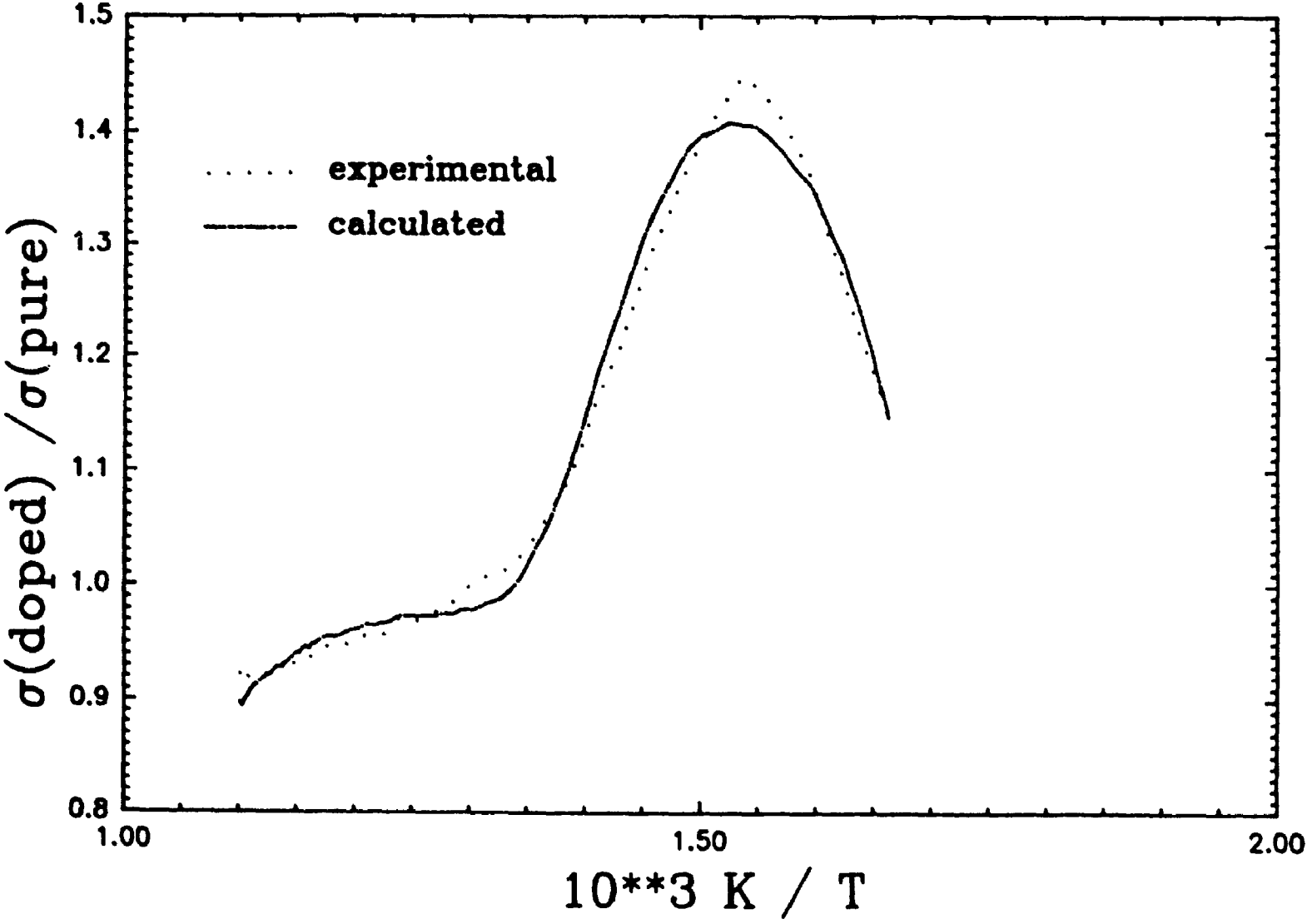

Figure 5–9: Ratio of the conductivities of RbCl:S^{-2} 5 to RbCl:pure 2–1

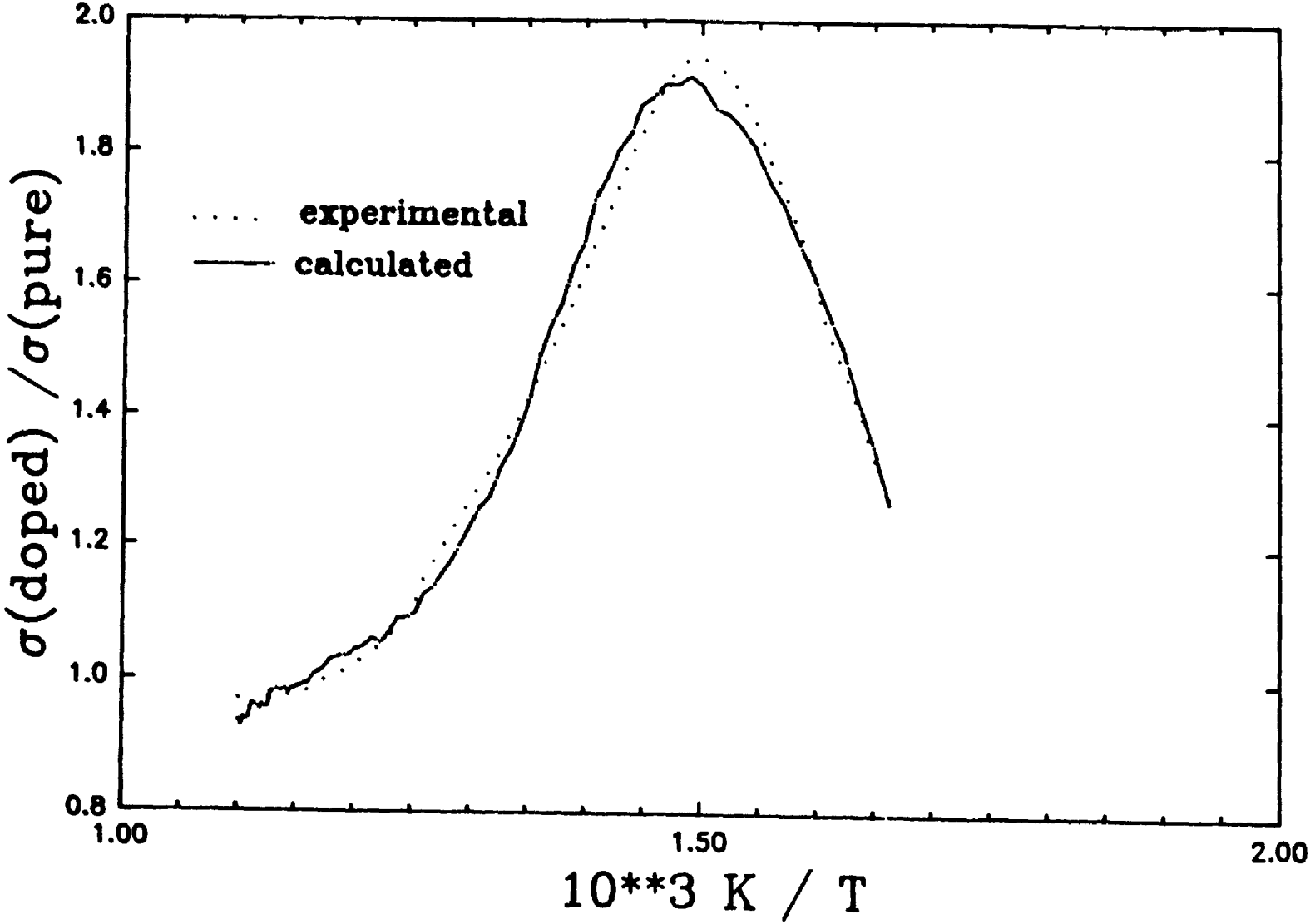

Figure 5–10: Ratio of the conductivities of RbCl:S^{-2} 3–1 to RbCl:pure 2–1

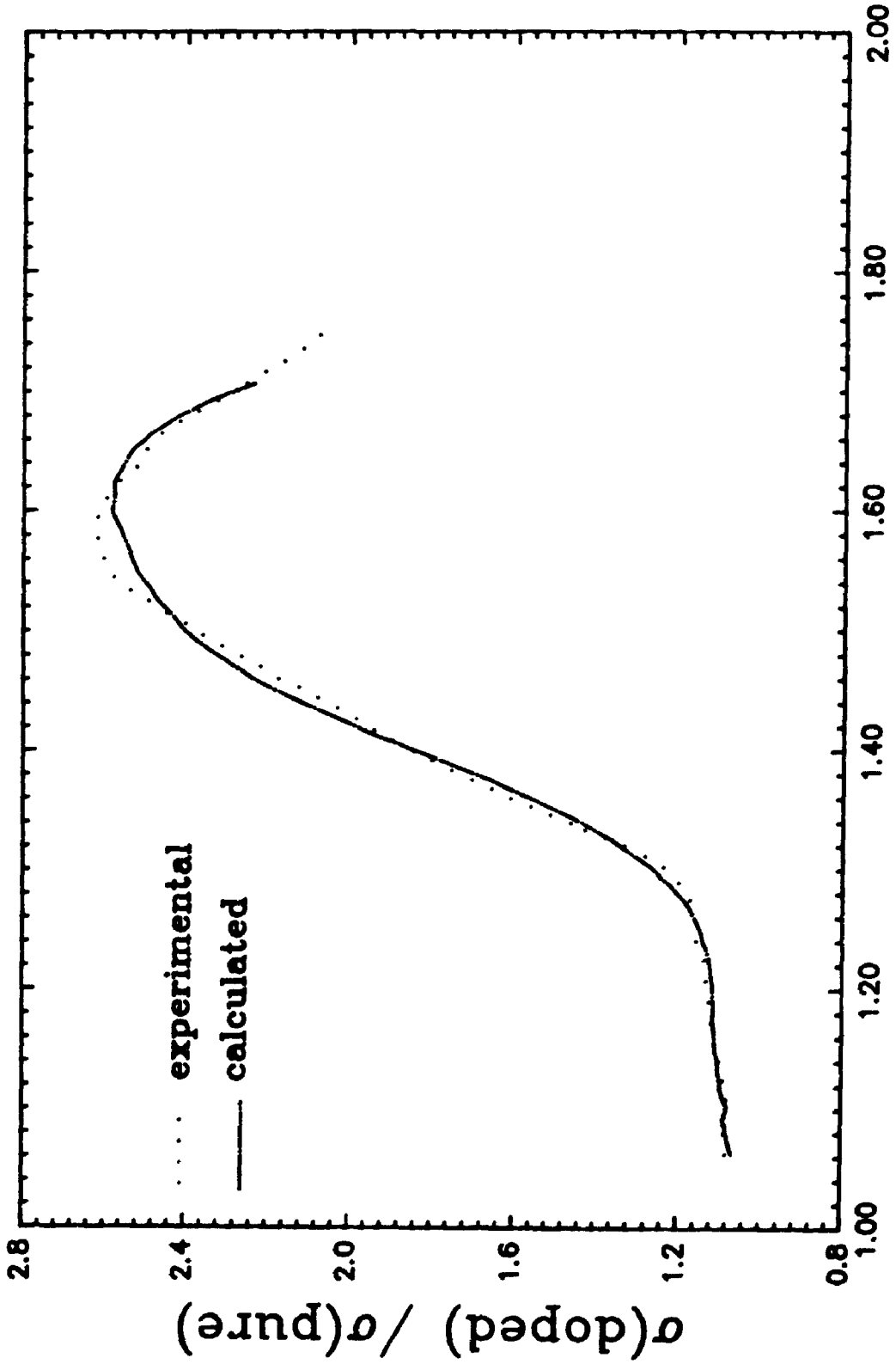

Figure 5-11: Ratio of the conductivities of RbCl:S^{-2} 1-3 to RbCl:pure 2-1

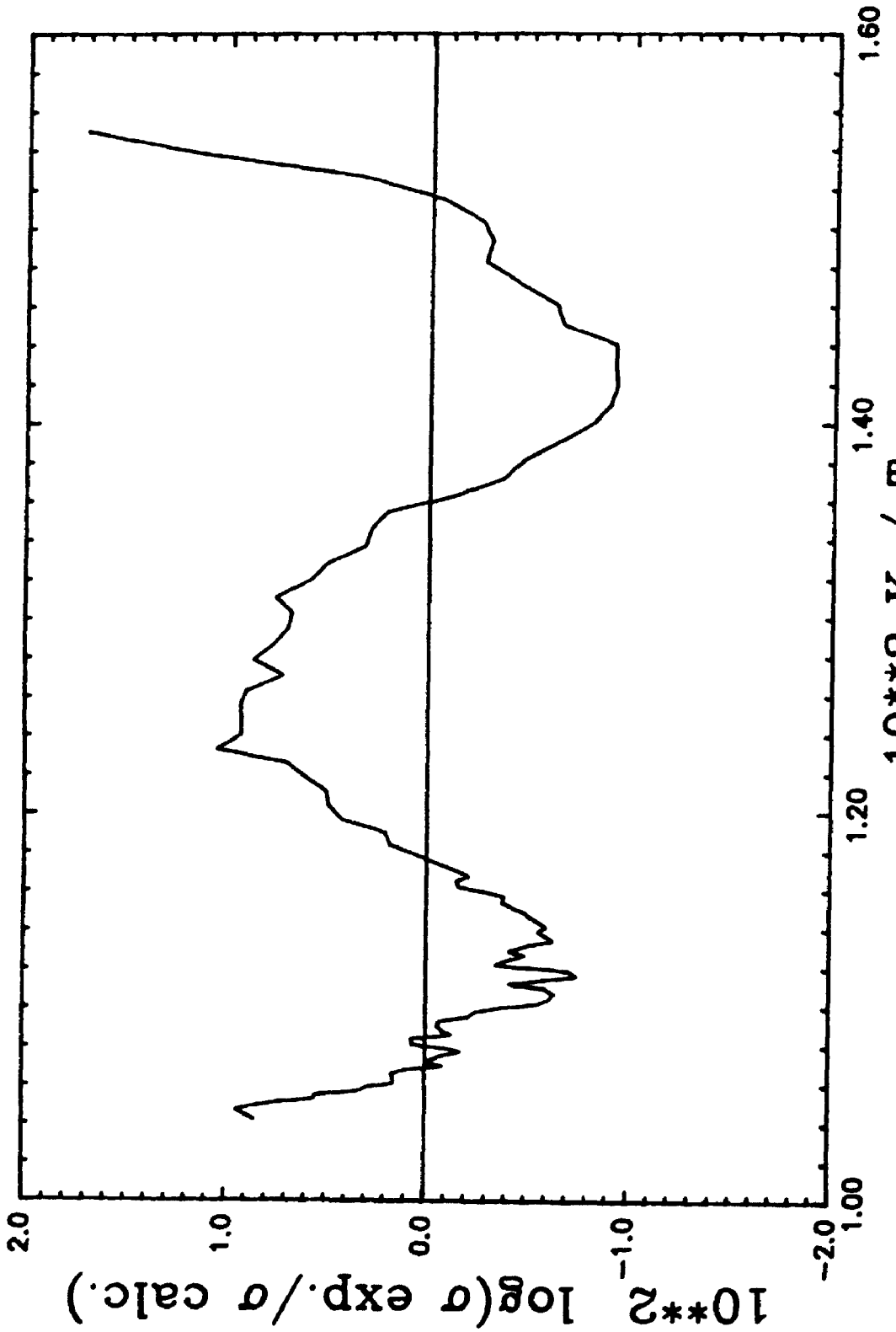

Figure 5-12: Residuals from fitting of RbCl:pure 4-1

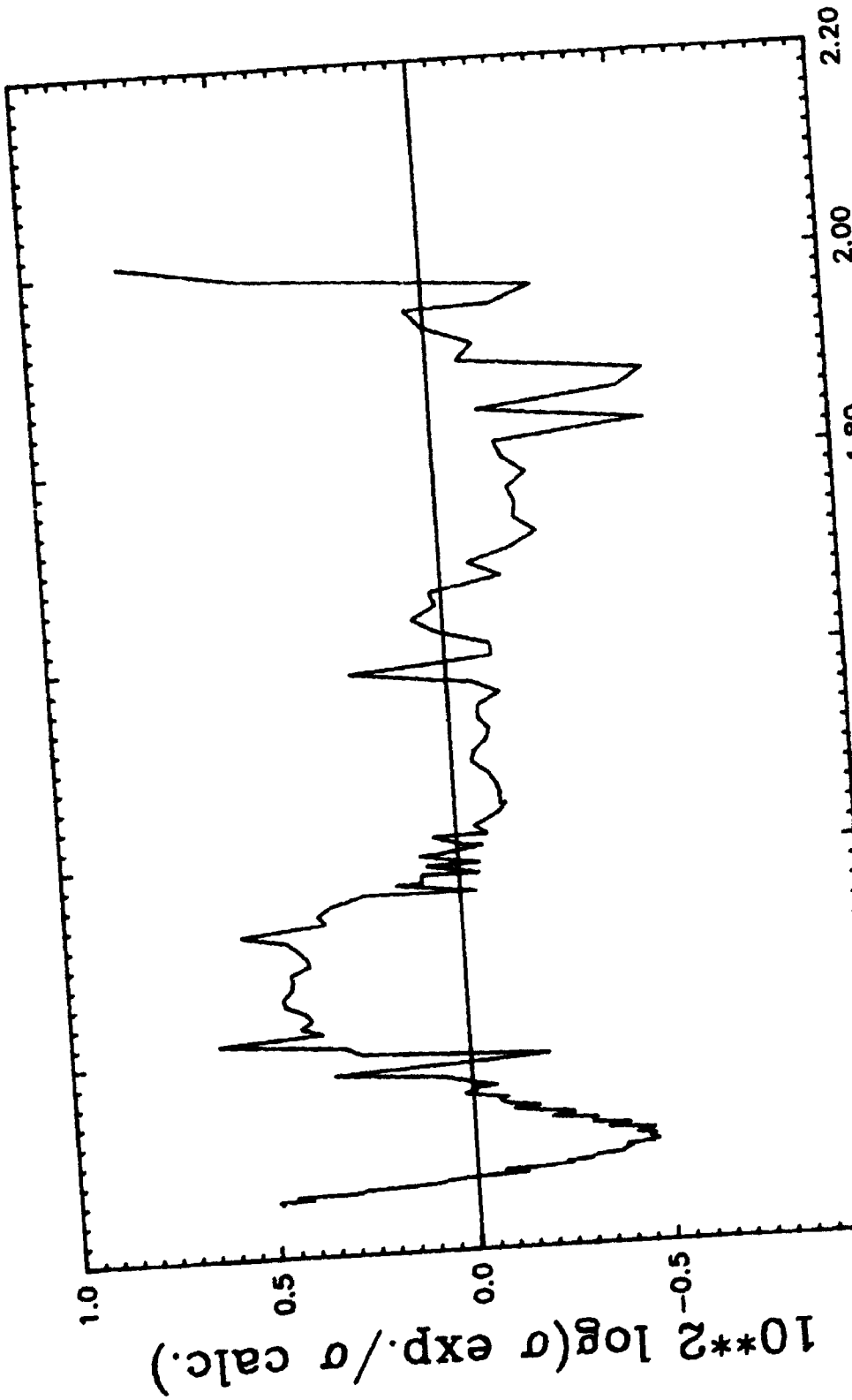

Figure 5–13: Residuals from fitting of RbCl:Sr^{+2} 1–1

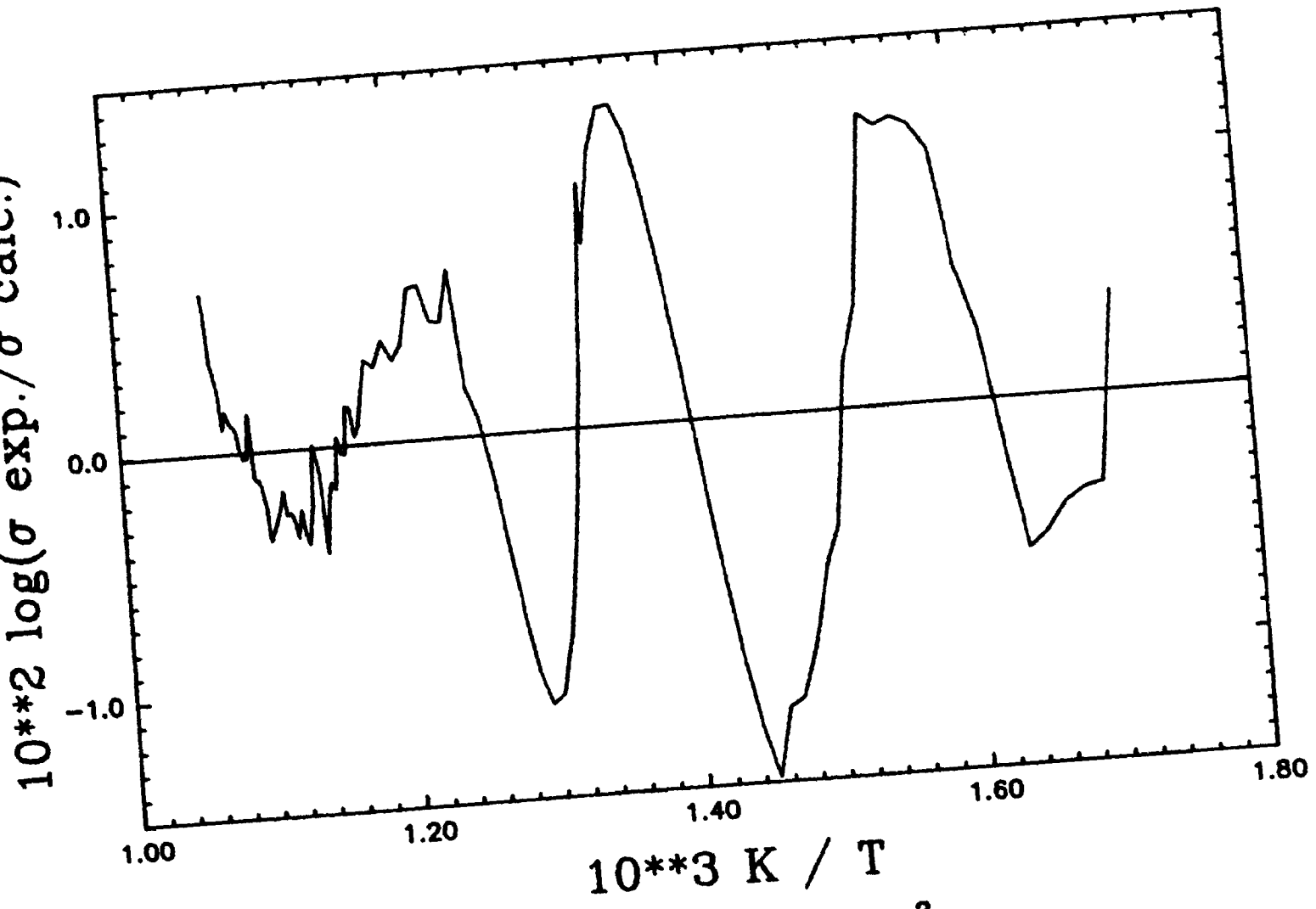

Figure 5–14: Residuals from fitting of RbCl:S^{-2} 1–3

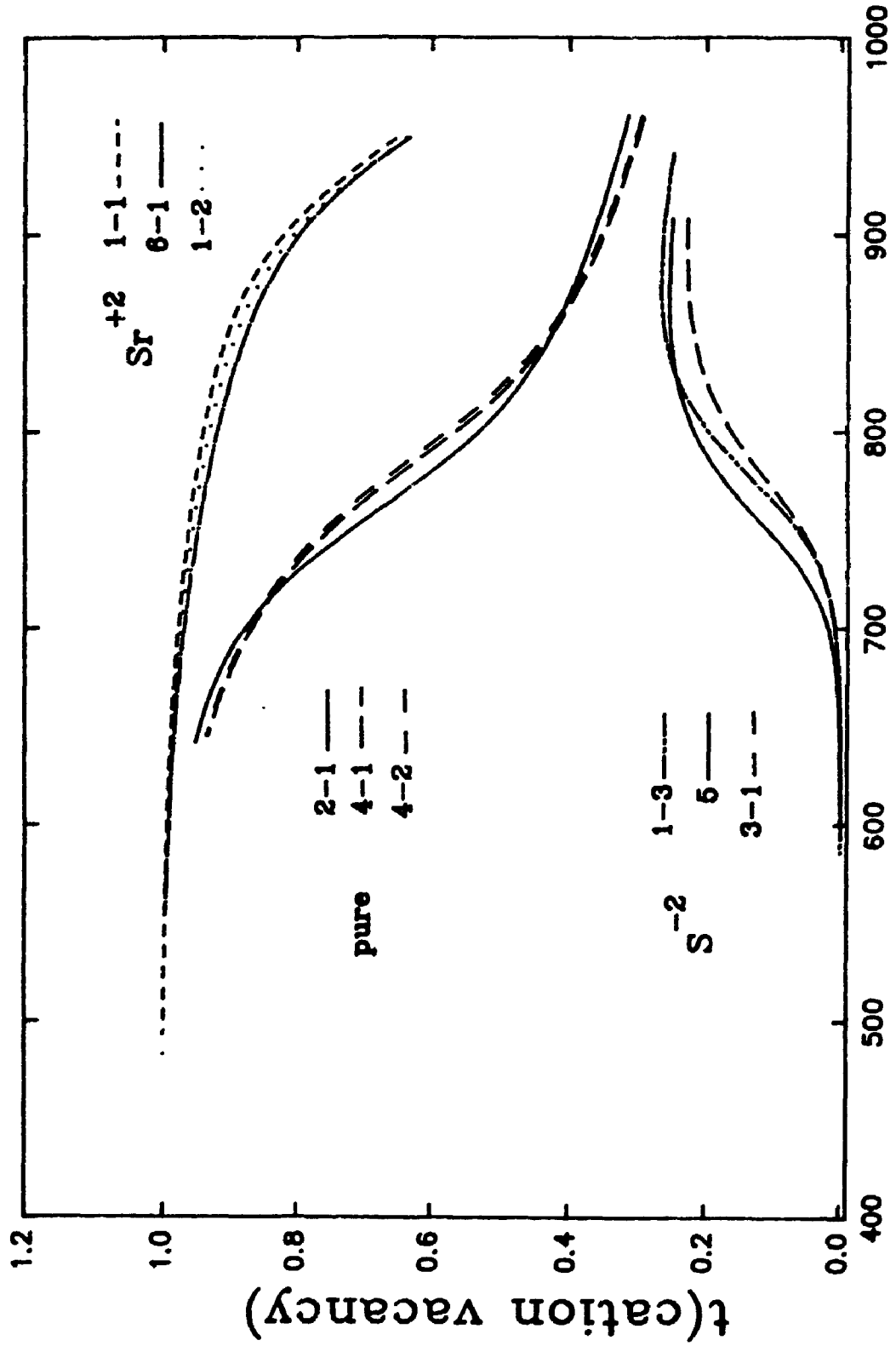

Figure 5–15: Cation vacancy transport numbers for RbCl:pure, Sr^{+2}, S^{-2}

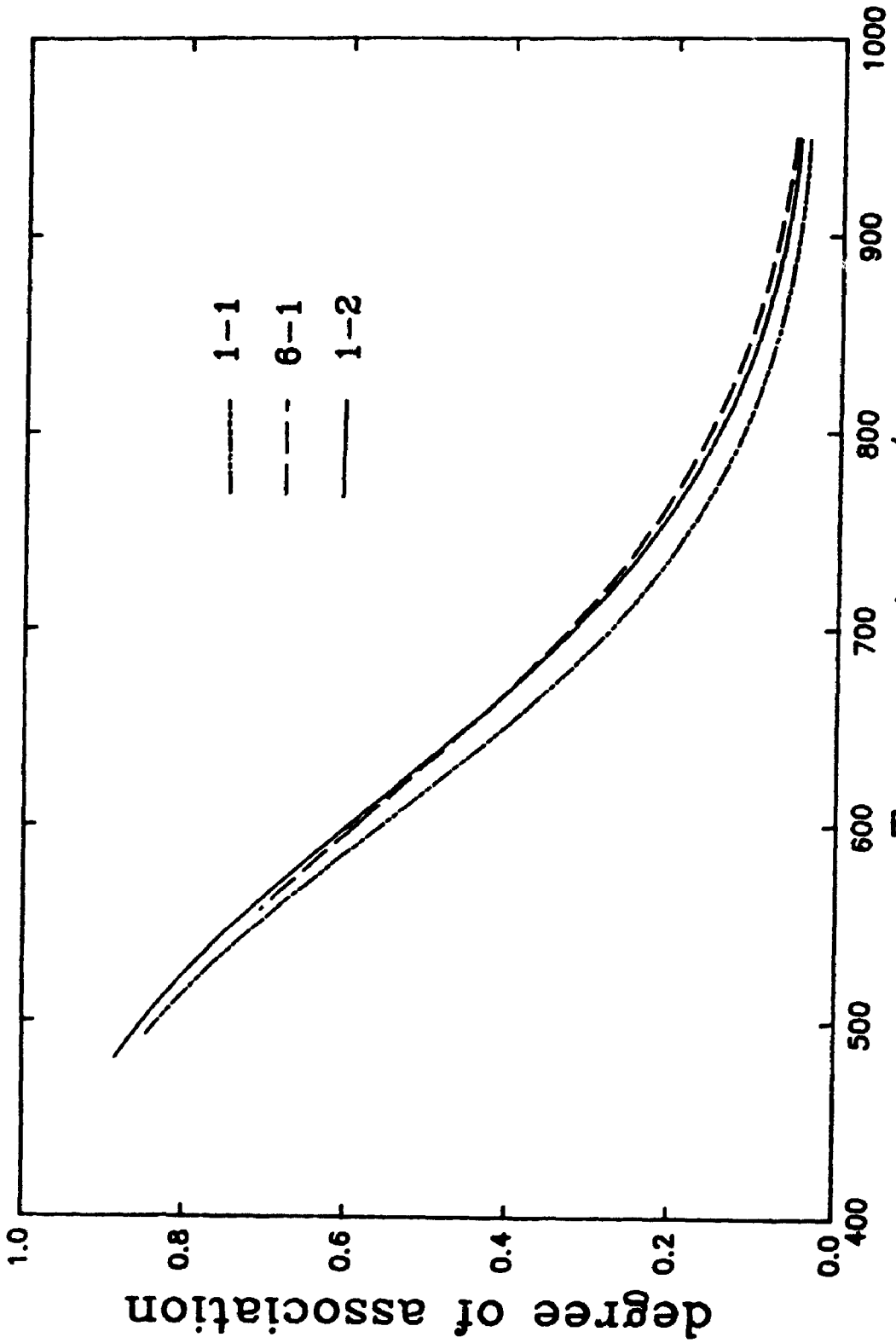

Figure 5-16: Fraction of complexed impurity in RbCl:Sr^{+2}

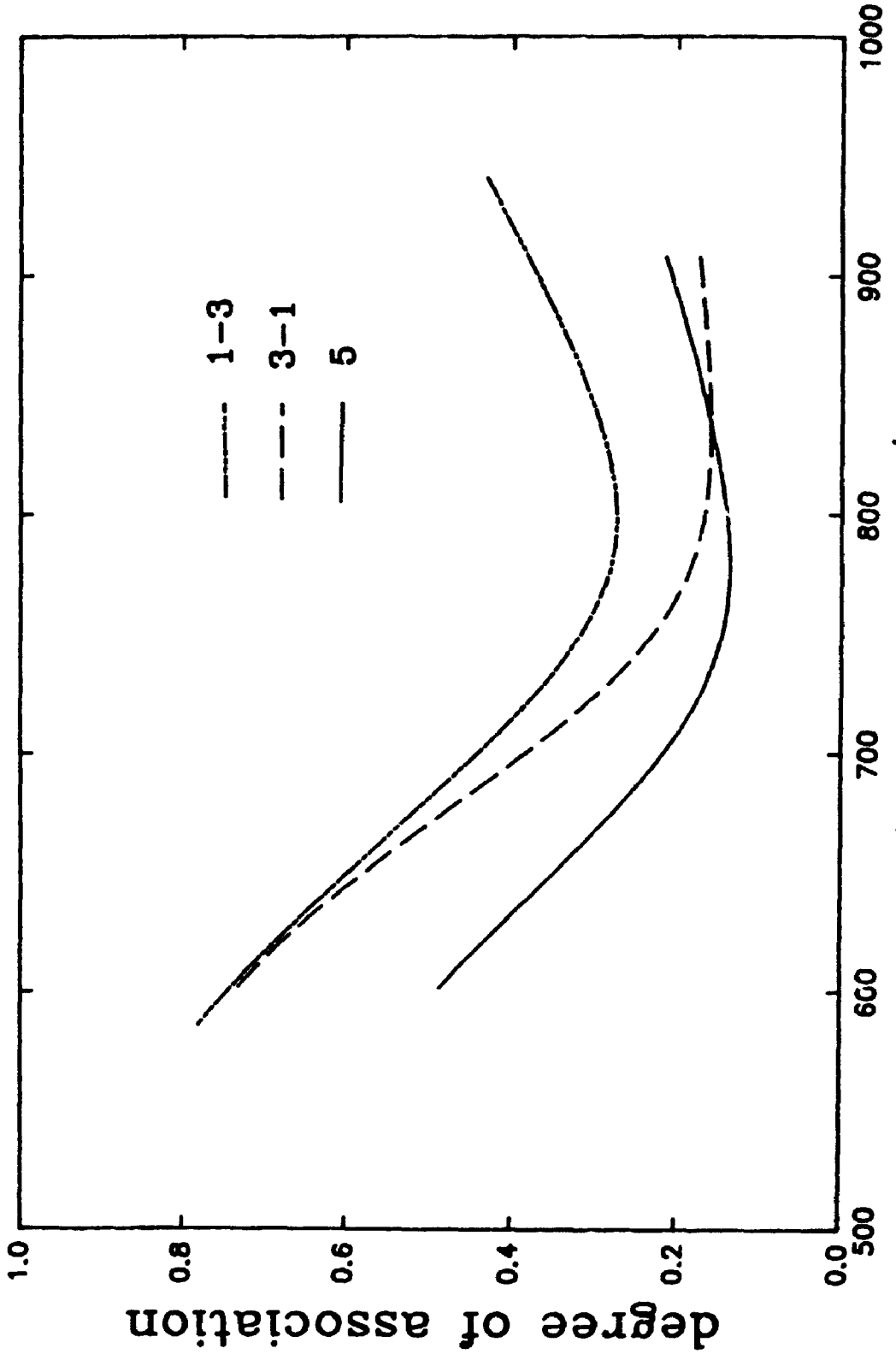

Figure 5-17: Fraction of complexed impurity in RbCl:S^{-2}

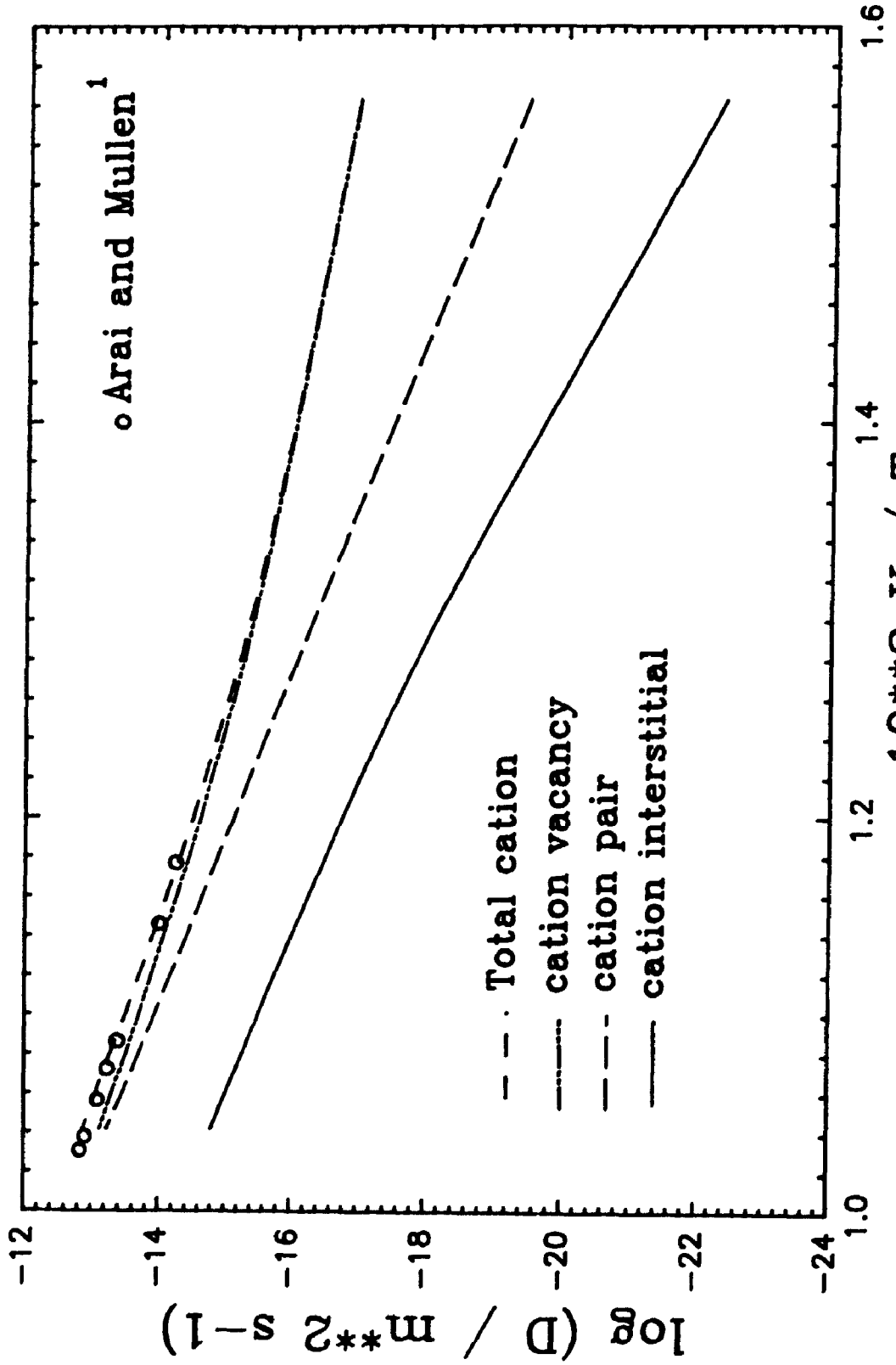

Figure 5-18: Cation diffusion in RbCl:pure 2-1

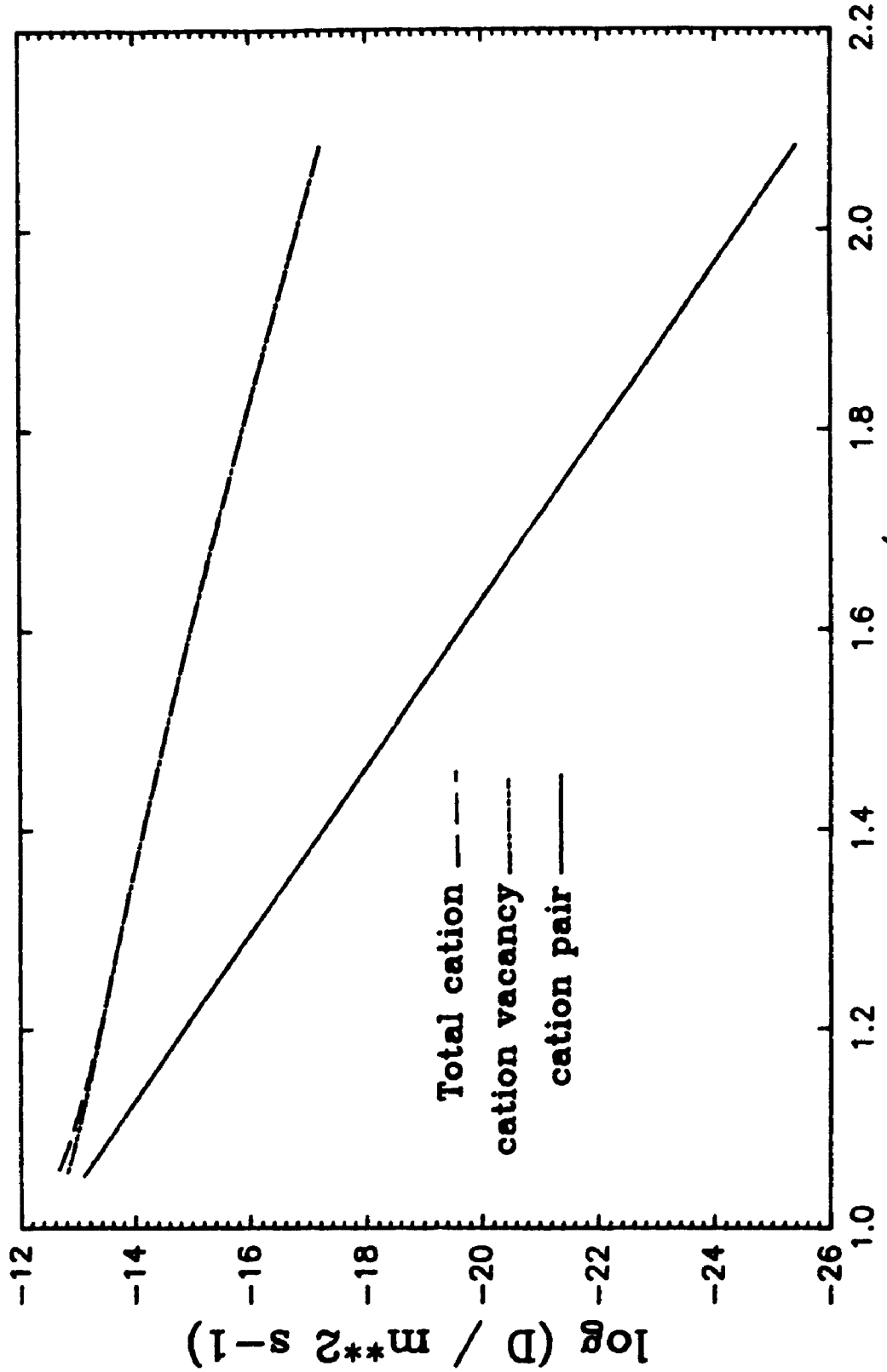

Figure 5-19: Cation diffusion in RbCl:Sr^{+2} 1-1

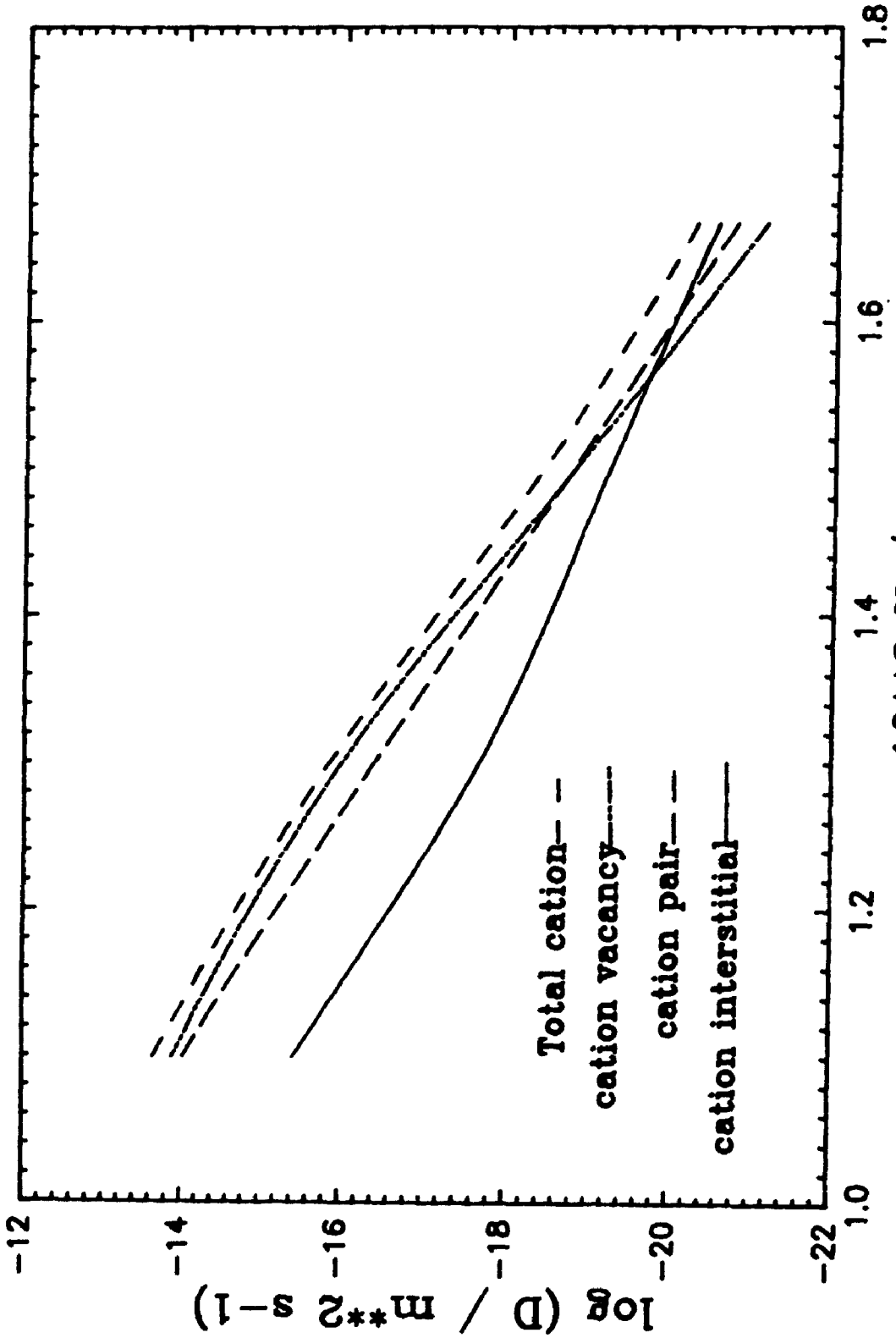

Figure 5-20: Cation diffusion in RbCl:S^{-2} 5

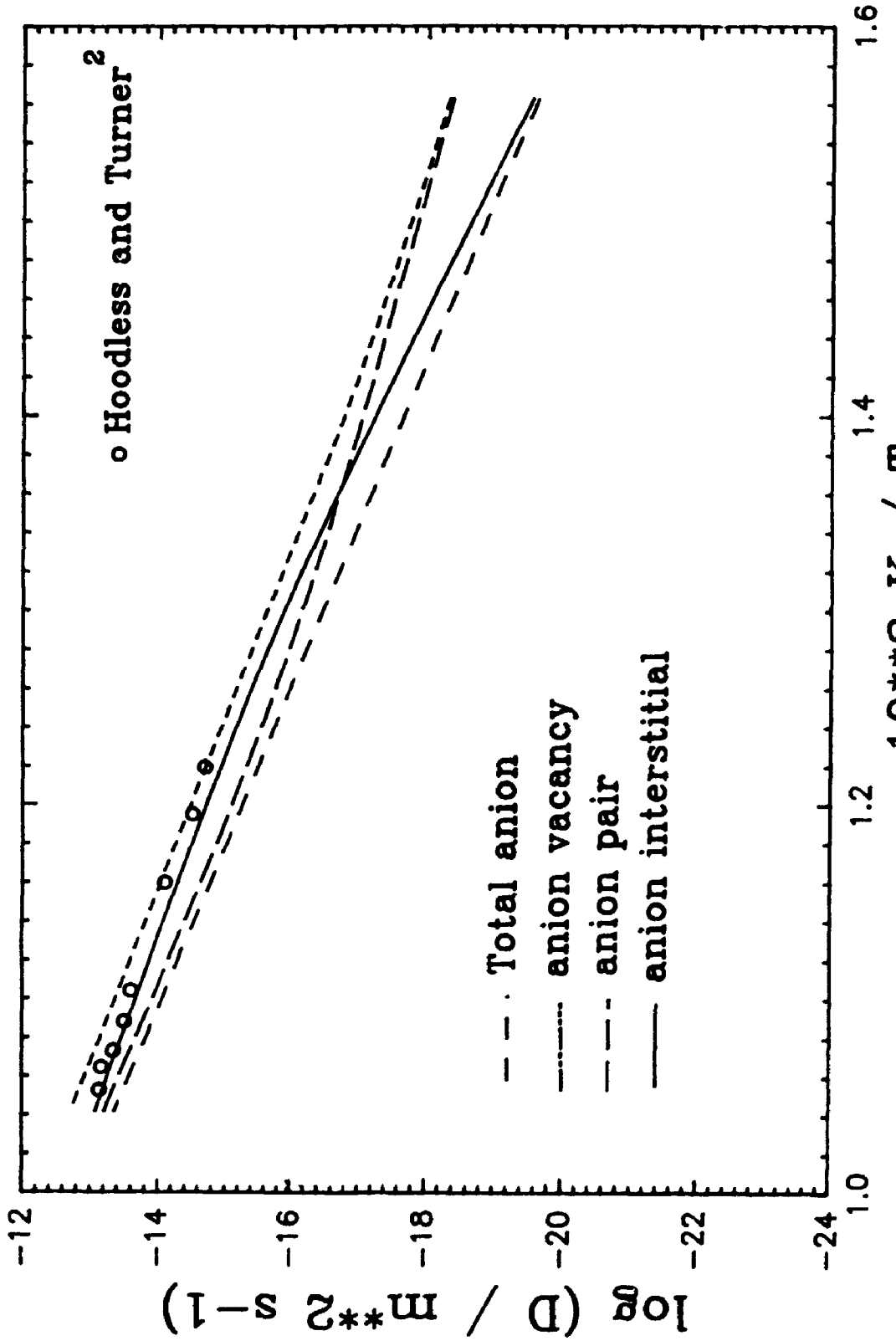

Figure 5-21: Anion diffusion in RbCl:pure 2-1

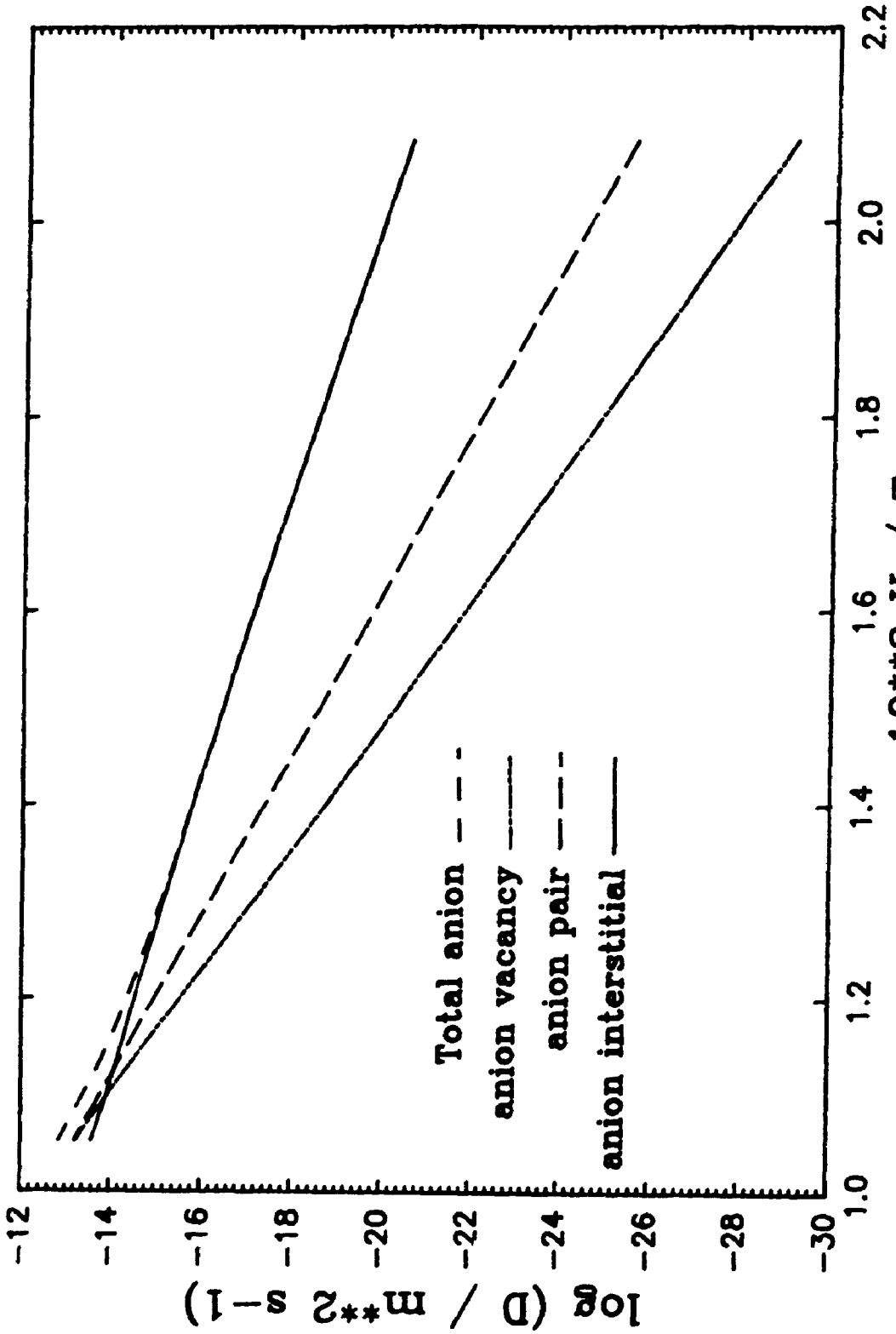

Figure 5-22: Anion diffusion in RbCl:Sr^{+2} 1-1

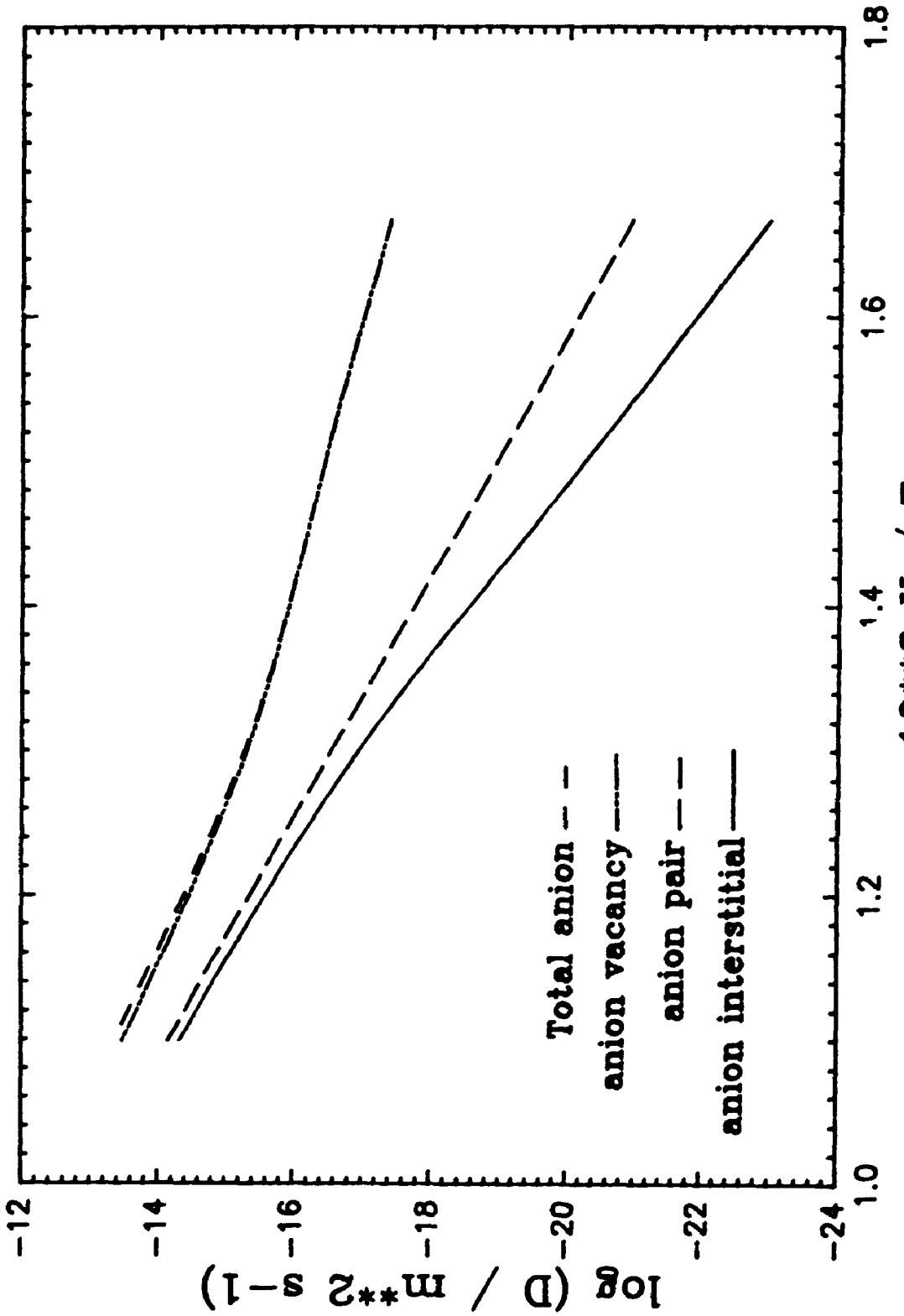

Figure 5-23: Anion diffusion in RbCl:S^{-2} 5

Chapter 6

Conclusions

In this study, the defect properties of rubidium chloride have been determined from theoretical and experimental analyses. The main conclusion of this work is that the Schottky model, which is usually used for alkali halides, is not adequate to explain ionic conductivity in RbCl. The inclusion of Frenkel defects on both sub-lattices is required, with the anion interstitials contributing significantly to transport. The difficulties that Downing and Friauf[34] had in interpreting their diffusion and conductivity data for RbBr would indicate that the inclusion of anion interstitials is also necessary to explain transport in rubidium bromide.

The defect parameters determined from each analysis are compared in Table 6-1 and show excellent agreement. The only exceptions are the anion vacancy migration and the anion association parameters.

The calculated anion vacancy migration energy is lower than the experimentally determined migration enthalpy and is, in fact, predicted to be nearly equal to the cation vacancy migration energy. The similarity in size between cation and anion results in the calculated similarity in migration energies, an effect which is not observed to the same extent experimentally. However, the difference between cation and anion is still much less than that observed in

KCl[5] or NaCl[4], which is expected to be due to size considerations.

The experimental anion association enthalpy, which is the binding enthalpy of a sulphide impurity ion with an anion vacancy, is lower than expected from calculations. This was compensated for in the fitting by an association entropy that was lower than the original estimate from KCl. The anion association parameters were difficult to fix experimentally because of the low concentration of divalent anion impurity.

The calculations done on RbCl, RbBr, and RbI show that although the formation of defects is more easily achieved in RbI, the mobility of the defects is greater in RbCl. This results in an ordering of Arrhenius energies such that, $E(RbCl) > E(RbBr) > E(RbI)$.

A test of the validity of the conclusions drawn regarding the contribution of anion interstitials could be made by measuring anion diffusion in RbCl as a function of the concentration of added Sr^{+2}. The anion diffusion coefficient, D_a, is a sum of the individual contributions of anion vacancies, anion pairs, and anion interstitials, and is at a maximum at zero $[Sr^{+2}]$. As cation dopant is added, D_a should decrease due to the suppression of anion vacancies. But as the concentration of Sr^{+2} further increases, D_a should go through a minimum and then increase due to the increasing contribution from anion interstitials. Thus D_a(concentration) isotherms should display a positive

curvature if anion interstitials contribute to transport.

Further work would involve the calculation of the defect energies of the RbBr:Sr^{+2} and RbI:Sr^{+2} systems and the measurement of the ionic conductivity of RbBr and RbI. The latter would be somewhat difficult due to the hygroscopic nature of RbI and the former would require the resolution of the structures of $SrBr_2$ and SrI_2 with respect to the existing computer codes. However, these investigations would serve to complete the picture of the defect properties of the alkali halides.

Table 6-1: Calculated and experimental defect parameters of RbCl

Parameter	Calculated	Experimental
u_S/h_S	2.520	2.52
$\Delta u_{cv}/\Delta h_{cv}$	0.661	0.661
$\Delta u_{av}/\Delta h_{av}$	0.667	0.720
u_{Fc}/h_{Fc}	3.457	3.457
u_{Fa}/h_{Fa}	3.480	3.484
$\Delta u_{ci}/\Delta h_{ci}$	0.208	0.208
$\Delta u_{ai}/\Delta h_{ai}$	0.188	0.188
u_{ck}/h_{ck}	-0.596	-0.592
u_{ak}/h_{ak}	-0.650	-0.878

APPENDIX 1

AUTOMATED IONIC CONDUCTIVITY EXPERIMENT PROGRAM

```
DECLARE SUB AIN800 CDECL (BYVAL lchan%, SEG erstat%)
DECLARE SUB Average (R0!, R1!, R2!, R3!, R4!, R5!, R6!, R7!,
                     R8!, RV!, A(), B(), C(), t)
DECLARE SUB Bridge (filenum, conductance$)
DECLARE SUB Cycle (R0, R1, R2, R3, R4, R5, R6, R7, R8)
DECLARE SUB Decrease (R0, R1, R2, R3, R4, R5, R6, R7, R8,
                      A(), B(), C(), Sx(), Sy())
DECLARE SUB DELAY CDECL (BYVAL min%, BYVAL sec%, BYVAL hun%)
DECLARE SUB DOTB CDECL (BYVAL lchan%, BYVAL value%, SEG
                        erstat%)
DECLARE SUB DOTB800 CDECL (BYVAL lchan%, BYVAL brd%, BYVAL
                           bitn%, SEG erstat%)
DECLARE SUB INITIALIZE CDECL (SEG erstat%)
DECLARE SUB Plotting (G, t, ht, area, Tm, Tf, ymax, ymin,
                      counter%, Sx(), Sy())
DECLARE SUB Ramp (R0, R1, R2, R3, R4, R5, R6, R7, R8)
DECLARE SUB Ramp700 (R0, R1, R2, R3, R4, R5, R6, R7, R8)
DECLARE SUB TypeR (RV!, R0, R1, R2, R3, R4, R5, R6, R7, R8,
                   t)
DECLARE FUNCTION AIN% CDECL (BYVAL lchan%, SEG erstat%)
DECLARE FUNCTION Filter$ (reading$)
DELCARE FUNCTION Temp! (A0, A1, A2, A3, A4, A5, A6, A7, A8,
                        B!)
DIM Sx(1 TO 300), Sy(1 TO 300)
DIM A(1 TO 2), B(1 TO 2), C(1 TO 2)
REM $STATIC     'sets aside storage for arrays during
                'compilation

'For TypeR thermocouples, these polynomial coefficients are
'valid 'for 0 - 1000 degC.

     R0 = 0.263632917
     R1 = 179075.491#
     R2 = -48840341.37#
     R3 = 1.90002E+10
     R4 = -4.82704E+12
     R5 = 7.62091E+14
     R6 = -7.20026E+16
     R7 = 3.71496E+18
     R8 = -8.03104E+19

OPEN "p200.bas" FOR INPUT AS #1              'heat to 200 degC
OPEN "com1:9600,o,7,1" FOR OUTPUT AS #2
     DO UNTIL EOF(1)
      INPUT #1, Linebuffer$
      PRINT #2, Linebuffer$
      FOR i = 1 TO 40                  'delay between commands
      NEXT i                           'req'd by Watlow
```

```
      NEXT i                              'req'd by Watlow
    LOOP
CLOSE

INPUT "Hold at 200 degC for how many minutes?", x
min% = x
sec% = 0
hun% = 0
CALL DELAY(min%, sec%, hun%)

PRINT "Turn on conductivity bridge and wait 10 minutes."
PRINT "Then press the 'Trim' key on bridge."
PRINT "After trimming completed, press C key to continue"
    DO
      Test$ = UCASE$(INKEY$)
    LOOP UNTIL Test$ = "C"

SHELL "copy wayne com2"      'turns bridge to remote control
SHELL "MSHERC.COM"           'loads the Hercules graphics
                             'routines

INPUT "Hold at 600 degC for how many minutes", y
min% = y

PRINT "Press C key to heat to 600 degC"
    DO
      Test$ = UCASE$(INKEY$)
    LOOP UNITL Test$ = "C"

'Now start to heat to 600 degC slowly.
PRINT "Ramping to 600 degC slowly"
CALL Ramp(R0, R1, R2, R3, R4, R5, R6, R7, R8)
CLOSE

CALL DELAY (min%, sec%, hun%)

'must now cycle between 600 and 630 degC until reproducible
CALL Cycle(R0, R1, R2, R3, R4, R5, R6, R7, R8)

'must now ramp to 700 degC slowly
CALL Ramp700(R0, R1, R2, R3, R4, R5, R6, R7, R8)

'must now take the temp. downwards from 700 degC and measure
CALL Decrease(R0, R1, R2, R3, R4, R5, R6, R7, R8, A(), B(),
              C(), Sx(), Sy())

OPEN "p200.bas" FOR INPUT AS #1          'reduce to 200 degC
OPEN "com1:9600,o,7,1" FOR OUTPUT AS #2
    DO UNTIL EOF(1)
       INPUT #1, Linebuffer$
       PRINT #2, Linebuffer$
        FOR i = 1 TO 40                  'delay between commands
        NEXT i                           'req'd by Watlow
```

```
     LOOP
CLOSE
END


SUB Average (R0, R1, R2, R3, R4, R5, R6, R7, R8, RV!, A(),
             B(), C(), t)
'determines if the temp is constant by averaging temp.
'readings for each channel and comparing them.

70 FOR i = 1 TO 2
    n = 10
    T0 = 0
    T1 = 0
    T2 = 0
FOR J = 1 TO n
m = 2
FOR k = 1 TO m
erstat% = 0
CALL INITIALIZE(erstat%)
IF (erstat% <> 0) GOTO 999
lchan% = k
  brd% = 1
 chan% = k
 gain% = 10

CALL AIN800(lchan%, brd%, chan%, gain%, erstat%)
IF (erstat% <> 0) GOTO 999
  r% = AIN(lchan%, erstat%)
IF (erstat% <> 0) GOTO 999
   GOTO 3300

999 PRINT erstat%
    STOP

'OV is the "output value", 95.54598 is the "gain", and RV
'is the "compensated voltage" in volts.

3300 F% = 4096
    OV! = (r% / F%) * 1

SELECT CASE k
CASE 0
RV! = (((OV!*0.0106708 - .0001418)+ .0001537)/ 1.06351)/
      0.954619
T0 = T0 + Temp!(R0, R1, R2, R3, R4, R5, R6, R7, R8, RV!) +
     273.15
GOTO 30

CASE 1
RV! = (OV! / 95.4619)
T1 = T1 + Temp!(R0, R1, R2, R3, R4, R5, R6, R7, R8, RV!) +
     273.15
```

```
t = Temp!(R0, R1, R2, R3, R4, R5, R6, R7, R8, RV!) + 273.15
GOTO 30

CASE 2
RV! = (((OV!*0.0106261 - .0001434)+ .0001537)/ 1.06351)/
      0.954619
T2 = T2 + Temp!(R0, R1, R2, R3, R4, R5, R6, R7, R8, RV!) +
     273.15
END SELECT

30 NEXT k
   NEXT j

TA0 = T0 / n + 273.15
TA1 = T1 / n + 273.15
TA2 = T2 / n + 273.15

A(i) = TA0
B(i) = TA1
C(i) = TA2
NEXT i

i = 1
IF ABS(A(i)-A(i+1)) < 0.1 AND ABS(B(i)-B(i+1)) < 0.1 AND
ABS(C(i)-C(i+1)) < 0.1 THEN GOTO 80 ELSE GOTO 70
80 PRINT #1, A(1), B(1)
   PRINT #3, B(1), C(1)
END SUB


SUB Bridge (filenum, conductance$)
'takes readings from the Wayne-Kerr bridge

OPEN "cap.bas" FOR APPEND AS #4
'capacitance is written as a check

   ws$ = "M"      'single mode
   wc$ = "CP"
   wg$ = "G"      'conductance
   wf$ = "F1"     '120 Hz
  wff$ = "F2"     '1.02 kHz
 wfff$ = "F3"     '10.2 kHz
wffff$ = "F4"     '300 Hz
   wa$ = "A5"
sec% = 0
hun$ = 0

OPEN "com2:9600,O,7,1" FOR OUTPUT AS #2
PRINT #2, wc$, wg$, wf$, wa$, ws$
CLOSE #2
OPEN "com2:9600,O,7,1" FOR INPUT AS #2
INPUT #2, capacitance$, conductance$
PRINT #filenum, Filter$(conductance$)
```

```
PRINT #4, Filter$(capacitance$)
CLOSE #2
OPEN "com2:9600,O,7,1" FOR OUTPUT AS #2
PRINT #2, wffff$, ws$
CLOSE #2
OPEN "com2:9600,O,7,1" FOR INPUT AS #2
INPUT #2, capacitance$, conductance$
PRINT #filenum, Filter$(conductance$)
PRINT #4, Filter$(capacitance$)
CLOSE #2
OPEN "com2:9600,O,7,1" FOR OUTPUT AS #2
PRINT #2, wff$, ws$
CLOSE #2
OPEN "com2:9600,O,7,1" FOR INPUT AS #2
INPUT #2, capacitance$, conductance$
PRINT #filenum, Filter$(conductance$)
PRINT #4, Filter$(capacitance$)
CLOSE #2
OPEN "com2:9600,O,7,1" FOR OUTPUT AS #2
PRINT #2, wfff$, ws$
CLOSE #2
OPEN "com2:9600,O,7,1" FOR INPUT AS #2
INPUT #2, capacitance$, conductance$
PRINT #filenum, Filter$(conductance$)
PRINT #4, Filter$(capacitance$)
CLOSE #2
CLOSE #4
END SUB

SUB Cycle (R0, R1, R2, R3, R4, R5, R6, R7, R8)
'must cycle between 600 and 630 degC until reproducible
'results are obtained.

CALL INITIALIZE(erstat%)
10 sec% = 0
   hun% = 0
      l = 3
      m = 2
      n = 10
   brd% = 1
FOR h = 1 TO l
FOR i = 1 TO m
lchan% = 4
 bitn% = 4
value% = 1
CALL DOTB800(lchan%, brd%, bitn%, erstat%)
CALL DOTB(lchan%, value%, erstat%)
OPEN "repro.bas" FOR APPEND AS #1

  min% = 2
lchan% = 5
 bitn% = 5
value% = 1
```

```
CALL DOTB800(lchan%, brd%, bitn%, erstat%)
CALL DOTB(lchan%, value%, erstat%)
CALL DELAY(min%, sec%, hun%)

FOR j = 1 TO n
   CALL TypeR(RV!, R0, R1, R2, R3, R4, R5, R6, R7, R8, t)
NEXT j

lchan% = 5
 bitn% = 5
value% = 0
filenum = 1
CALL DOTB800(lchan%, brd%, bitn%, erstat%)
CALL DOTB(lchan%, value%, erstat%)
CALL DELAY(min%, sec%, hun%)
CALL Bridge(filenum, lconductance$)

lchan% = 4
 bitn% = 4
value% = 0
CALL DOTB800(lchan%, brd%, bitn%, erstat%)
CALL DOTB(lchan%, value%, erstat%)
lchan% = 5
 bitn% = 5
value% = 1
filenum = 1
CALL DOTB800(lchan%, brd%, bitn%, erstat%)
CALL DOTB(lchan%, value%, erstat%)
CALL DELAY(min%, sec%, hun%)
CALL Bridge(filenum, uconductance$)

CLOSE
NEXT i
CLOSE

OPEN "p630.bas" FOR INPUT AS #1
OPEN "com:9600,O,7,1" FOR OUTPUT AS #2
DO UNTIL EOF(2)
  INPUT #1, Linebuffer$
  PRINT #2, Linebuffer$
  FOR k = 1 TO 40
  NEXT k
LOOP
CLOSE

min% = 20
CALL DELAY(min%, sec%, hun%)

FOR i = 1 TO m
min% = 2
lchan% = 4
 bitn% = 4
value% = 1
```

```
CALL DOTB800(lchan%, brd%, bitn%, erstat%)
CALL DOTB(lchan%, value%, erstat%)
OPEN "repro.bas" FOR APPEND AS #1
lchan% = 5
 bitn% = 5
value% = 1
CALL DOTB800(lchan%, brd%, bitn%, erstat%)
CALL DOTB(lchan%, value%, erstat%)
CALL DELAY(min%, sec%, hun%)

FOR j = 1 TO n
   CALL TypeR(RV!, R0, R1, R2, R3, R4, R5, R6, R7, R8, t)
NEXT j

lchan% = 5
 bitn% = 5
value% = 0
filenum = 1
CALL DOTB800(lchan%, brd%, bitn%, erstat%)
CALL DOTB(lchan%, value%, erstat%)
CALL DELAY(min%, sec%, hun%)
CALL Bridge(filenum, lconductance$)

lchan% = 4
 bitn% = 4
value% = 0
CALL DOTB800(lchan%, brd%, bitn%, erstat%)
CALL DOTB(lchan%, value%, erstat%)
lchan% = 5
 bitn% = 5
value% = 1
filenum = 1
CALL DOTB800(lchan%, brd%, bitn%, erstat%)
CALL DOTB(lchan%, value%, erstat%)
CALL DELAY(min%, sec%, hun%)
CALL Bridge(filenum, uconductance$)

CLOSE
NEXT i
CLOSE

OPEN "p600.bas" FOR INPUT AS #1
OPEN "com:9600,O,7,1" FOR OUTPUT AS #2
DO UNTIL EOF(2)
  INPUT #1, Linebuffer$
  PRINT #2, Linebuffer$
  FOR k = 1 TO 40
  NEXT k
LOOP
CLOSE

min% = 20
CALL DELAY(min%, sec%, hun%)
```

```
NEXT h
CLOSE
'Send file repro.bas to printer and examine for
'reproducibility.
PRINT, "Press P to print cycling data"
DO
     Test$ = UCASE$(INKEY$)
LOOP UNTIL Test$ = "P"
OPEN "lpt1:" FOR OUTPUT AS #1
OPEN "repro.bas" FOR INPUT AS #2
DO UNTIL EOF(2)
     INPUT #2, Linebuffer$
     PRINT #1, Linebuffer$
LOOP
CLOSE
PRINT "Do you wish to Continue, Repeat or Stop?"
INPUT "Type C, R or S", action$
IF action$ = "R" OR action$ = "r" THEN
   GOTO 10
ELSEIF action$ = "S" OR action$ = "s" THEN
   STOP
ELSEIF action$ = "C" OR action$ = "c" THEN
   RETURN
END IF
END SUB


SUB Decrease(R0, R1, R2, R3, R4, R5, R6, R7, R8, A(), B(),
             C(), Sx(), Sy())
'decreasing the temp. until impurities have precipitated

CALL INITIALIZE(erstat%)
        sec% = 0
        hun% = 0
    counter% = 0
           n = 10
        brd% = 1
Stringlength = 1

INPUT "Name of datafiles for this run; pure, doped"; pfile$,
           dfile$
INPUT "Height of pure crystal in cm"; pht
INPUT "Area of pure crystal in cm"; parea
INPUT "Height of doped crystal in cm"; dht
INPUT "Area of doped crystal in cm"; darea
INPUT "Starting temp., approx. final temp. in Kelvin"; Tm,
           Tf
INPUT "max.log(sigma*T/Scm-1 K), min.log(sigma*T/Scm-1 K)";
           ymax, ymin
INPUT "Press the C key when impurities have precipitated."


DO
```

```
      Test$ = UCASE$(INKEY$)
OPEN "com1:9600,O,7,1" FOR OUTPUT AS #1
OPEN "s2param.bas" FOR INPUT AS #2

FOR j = 1 TO 4
      SEEK #2, Stringlength
      INPUT #2, parameter$
      PRINT #1, parameter$
      FOR i = 1 TO 40
      NEXT i
      Stringlength = Stringlength + LEN(parameter$) + 4
NEXT j
CLOSE
lchan% = 4
 bitn% = 4
value% = 1
CALL DOTB800(lchan%, brd%, bitn%, erstat%)
CALL DOTB(lchan%, value%, erstat%)
lchan% = 5
 bitn% = 5
value% = 1
CALL DOTB800(lchan%, brd%, bitn%, erstat%)
CALL DOTB(lchan%, value%, erstat%)
min% = 15
CALL DELAY(min%, sec%, hun%)
OPEN pfile$ FOR APPEND AS #1
OPEN dfile$ FOR APPEND AS #3
CALL Average(R0, R1, R2, R3, R4, R5, R6, R7, R8, RV!, A(),
             B(), C(), t)
FOR k = 1 TO 2
lchan% = 5
 bitn% = 5
value% = 0
CALL DOTB800(lchan%, brd%, bitn%, erstat%)
CALL DOTB(lchan%, value%, erstat%)
min% = 2
filenum = 1
CALL DELAY(min%, sec%, hun%)
CALL Bridge(filenum, lconductance$)

lchan% = 4
 bitn% = 4
value% = 0
CALL DOTB800(lchan%, brd%, bitn%, erstat%)
CALL DOTB(lchan%, value%, erstat%)
lchan% = 5
 bitn% = 5
value% = 1
filenum = 3
CALL DOTB800(lchan%, brd%, bitn%, erstat%)
CALL DOTB(lchan%, value%, erstat%)
CALL DELAY(min%, sec%, hun%)
CALL Bridge(filenum, uconductance$)
```

```
lchan% = 4
 bitn% = 4
value% = 1
CALL DOTB800(lchan%, brd%, bitn%, erstat%)
CALL DOTB(lchan%, value%, erstat%)
CALL DELAY(min%, sec%, hun%)
CALL Average(R0, R1, R2, R3, R4, R5, R6, R7, R8, RV!, A(),
             B(), C(), t)
NEXT k

lG = VAL(Filter(lconductance$))  'converts filtered string
uG = VAL(Filter(uconductance$))  'to a number
counter% = counter% + 1
CALL Plotting(lG, t, pht, parea, Tm, Tf, ymax, ymin,
              counter%, Sx(), Sy())
counter% = counter% + 1
CALL Plotting(uG, t, dht, darea, Tm, Tf, ymax, ymin,
              counter%, Sx(), Sy())
CLOSE
LOOP UNTIL Test$ = "C"
END SUB


FUNCTION Filter$ (reading$)
'filters the non-numerical characters from the Wayne-Kerr
'bridge readings

Valtemp$ = ""
Stinglength = LEN(reading$)
FOR i% = 1 TO Stinglength
     Char$ = MID$(reading$, i%, 1)
     IF INSTR(".0123456789-E", Char$) > 0 THEN
     Valtemp$ = Valtemp$ + Char$
NEXT i%
Filter$ = Valtemp$
END FUNCTION


SUB Plotting(G, t, ht, area, Tm, Tf, ymax, ymin, counter%,
             Sx(), Sy())
'plots log(sigma*T) vs. 1/T during the experiment

xmin = 1 / Tm
xmax = 1 / Tf
SCREEN 3
sigma = (G / area) * ht
x = 1 / t
y = LOG(sigma* t) / LOG(10)
Sx(counter%) = (x - xmin) / ((xmax - xmin) / 720)
Sy(counter%) = 300 - (y - ymin) / ((ymax - ymin) / 300)
LINE (0, 300)-(720, 300)   'drawing the x-axis
LINE (0, 0)-(0, 300)       'drawing the y-axis
n = 72
```

```
FOR k = 1 TO 9
LINE (n * k, 300)-(n * k, 297)  'drawing the axis markings
NEXT k
n = 30
FOR k = 1 TO 9
LINE (0, n * k)-(3, n * k)
NEXT k
FOR i = 1 TO counter%
PSET (Sx(i), Sy(i))
NEXT i
END SUB


SUB Ramp(R0, R1, R2, R3, R4, R5, R6, R7, R8)
'Slowly ramping the temp. to 600 degC.
'This will take 10 hours.

min% = 15
sec% = 0
hun% = 0

OPEN "com:9600,O,7,1" FOR OUTPUT AS #2
INPUT "Initial setpoint to start ramping-200,290,390,490
       degC";sp
IF sp = 200 THEN
     GOTO 200
ELSEIF sp = 290 THEN
     GOTO 290
ELSEIF sp = 390 THEN
     GOTO 390
ELSEIF sp = 490 THEN
     GOTO 490
ENDIF

200 k = 200
    DO UNTIL k = 280
     k = k + 10
     PRINT #2, "= sp1"; k
     CALL DELAY(min%, sec%, hun%)
    LOOP
290 k = 290
PRINT #2, "= sp1"; k
  FOR i = 1 TO 40
  NEXT i
PRINT #2, "= pb1% 1.2"
  FOR i = 1 TO 40
  NEXT i
PRINT #2, "= it1 50.0"
  FOR i = 1 TO 40
  NEXT i
PRINT #2, "= de1 2.39"
CALL DELAY(min%, sec%, hun%)
     DO UNTIL k = 380
```

```
      k = k + 10
      PRINT #2, "= sp1"; k
      CALL DELAY(min%, sec%, hun%)
     LOOP
390 k = 390
PRINT #2, "= sp1"; k
  FOR i = 1 TO 40
  NEXT i
PRINT #2, "= pb1% 1.1"
  FOR i = 1 TO 40
  NEXT i
PRINT #2, "= it1 33.3"
  FOR i = 1 TO 40
  NEXT i
PRINT #2, "= de1 1.50"
CALL DELAY(min%, sec%, hun%)
      DO UNTIL k = 480
      k = k + 10
      PRINT #2, "= sp1"; k
      CALL DELAY(min%, sec%, hun%)
     LOOP
490 k = 490
PRINT #2, "= sp1"; k
  FOR i = 1 TO 40
  NEXT i
PRINT #2, "= pb1% 0.9"
  FOR i = 1 TO 40
  NEXT i
PRINT #2, "= it1 20.0"
  FOR i = 1 TO 40
  NEXT i
PRINT #2, "= de1 0.97"
CALL DELAY(min%, sec%, hun%)
      DO UNTIL k = 590
      k = k + 10
      PRINT #2, "= sp1"; k
      CALL DELAY(min%, sec%, hun%)
     LOOP

OPEN "p600.bas" FOR INPUT AS #1
      DO UNTIL EOF(1)
        INPUT #1, Linebuffer$
        PRINT #2, Linebuffer$
        FOR i = 1 TO 40
        NEXT i
      LOOP
CLOSE
END SUB


SUB Ramp700(R0, R1, R2, R3, R4, R5, R6, R7, R8)

min% = 15
```

```
sec% = 0
hun% = 0
k = 600
OPEN "com1:9600,O,7,1" FOR OUTPUT AS #2
     DO UNTIL k = 700
       k = k + 10
       PRINT #2, "= sp1"; k
       CALL DELAY(min%, sec%, hun%)
     LOOP
CLOSE
END SUB


FUNCTION Temp!(A0, A1, A2, A3, A4, A5, A6, A7, A8, B!)

Temp! = A0+ A1*B+ A2*(B^2)+ A3*(B^3)+ A4*(B^4)+ A5*(B^5)+
            A6*(B^6)+ A7*(B^7)+ A8*(B^8)
END FUNCTION


SUB TypeR(RV!, R0, R1, R2, R3, R4, R5, R6, R7, R8, t)
'reads the temp. of the TypeR thermocouples

m = 2
FOR k = O TO m
erstat% = 0
CALL INITIALIZE(erstat%)
IF (erstat% <> 0 ) GOTO 888
lchan% = k
  brd% = 1
 chan% = k
 gain% = 10
CALL AIN800(lchan%, brd%, chan%, gain%, erstat%)
IF (erstat% <> 0) GOTO 888
r% = AIN(lchan%, erstat%)
IF (erstat% <> 0) GOTO 888
GOTO 2200

888 PRINT erstat%
    STOP

2200 F% = 4096
    OV! = (r% / F%) * 1
SELECT CASE k
CASE 0
RV! = (((OV!*0.0106708 - .0001418)+ .0001537)/ 1.06351)/
      0.954619
PRINT #1, Temp!(R0, R1, R2, R3, R4, R5, R6, R7, R8, RV!),
t = Temp!(R0, R1, R2, R3, R4, R5, R6, R7, R8, RV!) + 273.15
GOTO 20

CASE 1
RV! = (OV! / 95.4619)
```

```
PRINT #1, Temp!(R0, R1, R2, R3, R4, R5, R6, R7, R8, RV!)
GOTO 20

CASE 2
RV! = (((OV!*0.0106261 - .0001434)+ .0001537)/ 1.06351)/
      0.954619
PRINT #1, Temp!(R0, R1, R2, R3, R4, R5, R6, R7, R8, RV!)
END SELECT
20 NEXT k
END SUB
```

References

1. G. Arai and J. Mullen, Phys. Rev. 143, 663, 1966.

2. I.M. Hoodless and R.G. Turner, Phys. Stat. Sol. A, 11, K55, 1972.

3. A.B. Lidiard, Handbuch der Physik, Springer-Verlag, Berlin, 20, 1957.

4. I.E. Hooton, Ph.D. Thesis (UWO), London, Canada, 1988.

5. L.A. Acūna, Ph.D. Thesis (UWO), London, Canada, 1979.

6. L.W. Barr and A.B. Lidiard, "Physical Chemistry - An Advanced Treatise", ed. H. Eyring, D. Henderson and W. Jost, Academic Press, New York, 10, 151, 1970.

7. P.W.M. Jacobs, Proceedings NATO ASI, Diffusion in Materials, eds. A.L. Lasker, J.L. Bocquet, G. Brebec, and C. Monty, 203, 1990.

8. P.W.M. Jacobs, and M.L. Vernon, J.Chem.Soc. Faraday Trans., 86, 1233, 1990

9. R.G. Gordon and Y.S. Kim, J.Chem.Phys., 56, 3122, 1972.

10. R. Ahlrichs, R. Penco and G. Scoles, Chem.Phys., 19, 119, 1977.

11. C.R.A. Catlow and M.J. Norgett, "Lattice Structure and Stability of Ionic Materials", Tech. report M2936, AERE Harwell, 1976.

12. B.G. Dick and A.W. Overhauser, Phys.Rev., 112, 90, 1958.

13. C.R.A. Catlow and J.R. Mackrodt, Computer Simulation of Solids, eds. C.R.A. Catlow and J.R. Mackrodt, 1, 1982.

14. C.R.A. Catlow, K.M. Diller and M.J. Norgett, J.Phys.C, 10, 1395, 1977.

15. G.G. Agarwal, O.P. Sharma, J.C. Sharma, H.P. Sharma and J. Shanker, J.Inorg.Nuclear Chem., 39, 2131, 1977.

16. V.K. Jain and J. Shanker, Phys.Stat.Sol.B, 114, 271, 1982.

17. E.W. Pearson, M.D. Jackson and R.G. Gordon, J.Phys.Chem., 88, 119, 1984.

18. M.J. Norgett, Tech. report R765, AERE Harwell, 1974.

19. P.B. Ghate, Phys.Rev. A, 139, 1666, 1965.

20. M.P. Tosi, Solid State Physics, 16, 1, 1964.

21. J.T. Lewis, A. Lehoczky and C.V. Briscoe, Phys.Rev., 161, 877, 1967.

22. R.P. Lowndes and D.H. Martin, Proc.Roy.Soc., A308, 473, 1969.

23. R.P. Lowndes and D.H. Martin, Proc.Roy.Soc., A316, 351, 1970.

24. R.W.G. Wyckoff, "Crystal Structures", Interscience Pub., New York, 1, 1963.

25. D.H. Kuhner, H.V. Lauer and W.E. Bron, Phys.Rev. B, 5, 4112, 1972.

26. G. Raunio and S. Rolandson, J.Phys. C, 3, 1013, 1970.

27. G. Raunio and S. Rolandson, J.Phys. C, 4, 958, 1971.

28. G. Raunio and S. Rolandson, Phys.Stat.Solidi, 40, 749, 1970.

29. A. Sadoc, F. Moussa and G. Pepy, J.Phys.Chem.Solids, 37, 197, 1976.

30. N.F. Mott and M.J. Littleton, Trans.Faraday Soc., 34, 485, 1938.

31. C.N.R. Rao and S. Ramdas, "Modern Aspects of Solid State Chemistry", ed. C.N.R. Rao, Plenum Press, New York, 107, 1970.

32. D.K. Rowell and M.J.L. Sangster, J.Phys.C, 14, 2909, 1981.

33. M.K. Uppal, C.N.R. Rao and M.J.L. Sangster, Phil.Mag.A, 38, 341, 1978.

34. H.L. Downing and R.J. Friauf, Phys.Rev.B, 12, 5981, 1975.

35. S. Chandra and J. Rolfe, Can.J.Phys., 51, 236, 1973.

36. M.P. Tosi and F.G. Fumi, J.Phys.Chem.Solids, 25, 45, 1964.

37. N.M. Bannon, C.R.A. Catlow, J. Corish, W.J. Fredericks and P.W.M. Jacobs, Physica B, 131, 126, 1985.

38. J. Corish, B.M.C. Parker and P.W.M. Jacobs, Can.J.Chem, 54, 3839, 1976.

39. S.P. Sanyal, N. Agnihotri and R.K. Singh, Phil.Mag.A, 57, 661, 1988.

40. C.R.A. Catlow, J. Corish, K.M. Diller, P.W.M. Jacobs and M.J. Norgett, J.Phys.C, 12, 451, 1979.

41. I.M. Boswarva and J.H. Simpson, Can.J.Phys., 51, 1923, 1973.

42. Y.S. Touloukian, R.K. Kirby, R.E. Taylor and T.Y.R. Lee, "Thermophysical Properties of Matter", 13, 990, 1970.

43. S. Chandra and J. Prakash, Can.J.Phys., 50, 1053, 1972.

44. R.G. Fuller and M.H. Reilly, Phys.Rev.Letters, 19, 113, 1967.

45. A.K. Shukla and C.N.R. Rao, J.Chem.Soc. Faraday Trans., 71, 1628, 1975.

46. P. Jurczak and D.H. Whitmore, Mater.Sci.Res., 6, 49, 1973.

47. N.L. Peterson and S.J. Rothman, Phys.Rev., 177, 1329, 1969.

48. S.J. Rothman and N.L. Peterson, Bull.Am.Phys.Soc., 13, 466, 1968.

49. G.W. Castellan, "Physical Chemistry", Addison-Wesley, Mass., 746, 1983.

50. A.D. LeClaire, "Treatise on Solid State Chemistry", ed. N.B. Hannay, Plenum Press, New York, 4, 1976.

51. K. Compaan and Y. Haven, Trans.Faraday Soc., 52, 786, 1956.

52. R.E. Howard, Phys.Rev., 144, 650, 1966.